Growth of nanostructures by cluster deposition: Experiments and simple models

Pablo Jensen*

Département de Physique des Matériaux, Université Claude Bernard Lyon-1, F-69622 Villeurbanne Cédex, France

This paper presents simple models useful in analyzing the growth of nanostructures obtained by cluster deposition. After a brief survey of applications and experimental methods, the author describes the Monte Carlo techniques for simulating nanostructure growth. Simulations of the first stages, the submonolayer regime, are reported for a wide variety of experimental situations: complete condensation, growth with reevaporation, nucleation on defects, and total or null cluster-cluster coalescence. [Note: Software for all these simulation programs, which are also useful for analyzing growth from *atomic* beams, is available on request from the author.] The aim of the paper is to help experimentalists, in analyzing their data, to determine which processes are important and to quantify them. Experiments on growth from cluster beams are discussed, as is the measurement of cluster mobility on the surface. Surprisingly high mobility values are found. An important issue for future technological applications of cluster deposition is the relation between the size of the incident clusters and the size of the islands obtained on the substrate, which is described by an approximate formula depending on the melting temperature of the deposited material. Finally, the author examines the atomic mechanisms that can explain the diffusion of clusters on a substrate and their mutual interaction, to aggregate keeping their integrity or to coalesce. [S0034-6861(99)00405-5]

CONTENTS

I. INTRODUCTION

Growth of new materials with tailored properties is one of the most active research directions for physicists. As pointed out by Silvan Schweber in his brilliant analysis of the evolution of physics after World War II, ''An important transformation has taken place in physics: As had previously happened in chemistry, an ever larger fraction of the efforts in the field [are] being devoted to the study of novelty [creation of new structures, new objects, and new phenomena] rather than to the elucidation of fundamental laws and interactions. ... Condensed matter physics has indeed become the study of systems that have never before existed'' (Schweber, 1993).

Among these new materials, those presenting a structure controlled down to the nanometer scale are being

*Electronic address: jensen@dpm.univ-lyon1.fr

extensively studied.[1] There are different ways to build up nanostructured systems (Edelstein and Cammarata, 1996): atomic deposition (Bunshah, 1994; Glocker, 1995; Arthur, 1997), mechanical milling (Koch, 1991), chemical methods (Shalaev and Moskovits, 1997; Fendler, 1998), and gas-aggregation techniques (Granqvist and Buhrman, 1976; Siegel, 1991; Melinon *et al.*, 1995; Siegel, 1996; Perez *et al.*, 1997). Each of these techniques has its own advantages, but, as happens with atomic-deposition techniques, the requisites of *control* (in terms of characterization and flexibility) and *efficiency* (in terms of quantity of matter obtained per second) are generally incompatible. As a physicist wishing to understand the details of the processes involved in the building of these nanostructures, I shall focus in this review on a carefully *controlled* method: low-energy cluster deposition (Melinon *et al.*, 1995; Perez *et al.*, 1997).

Clusters are large ''molecules'' containing typically from 10 to 2000 atoms. They have been studied for their specific physical properties (mostly due to their large surface-to-volume ratio), which are size dependent and different from both the atoms and the bulk material (Sugano *et al.*, 1987; Joyes, 1990; Averback, 1991; de Heer *et al.*, 1993; Rubinstien, 1996). By depositing preformed clusters on a substrate, one can build nanostructures of two types: in the submonolayer range, separated (and hopefully ordered) nanoislands, and for higher thicknesses, thin films or cluster-assembled materials (CAM). The main advantage of the cluster-deposition technique is that one can carefully control the building block (i.e., the cluster) and characterize the growth mechanisms. By changing the size of the incident clusters one can change the growth mechanisms (Fuchs *et al.*, 1991; Bréchignac *et al.*, 1997, 1998; Yoon, 1997) and the characteristics of the materials. For example, it has been shown that by changing the mean size of incident carbon clusters, one can modify the properties of carbon film, from graphitic to diamondlike (Paillard *et al.*, 1993).

This review is organized as follows. First, I discuss briefly the interest of nanostructures, both in the domain of nanoislands arranged on a substrate and as nanostructured, continuous films. I also review different strategies employed to deposit clusters on a substrate—by accelerating them or by achieving their soft-landing. The intent of this section is to convince the reader that cluster deposition is a promising technique for nanostructure growth in a variety of domains and therefore deserves careful study. In Sec. III, models for cluster deposition are introduced. These models can also be useful for atomic deposition in some simple cases, namely, when aggregation is irreversible. The models are adapted here to the physics of cluster deposition. In this case, reevaporation from the substrate can be important (as opposed to the usual conditions of molecular-beam epitaxy), cluster-cluster aggregation is always irreversible [as opposed to the possibility of bond breaking for atoms (Zhdanov and Norton, 1994; Bartelt *et al.*, 1995; Ratsch *et al.*, 1995)], and particle-particle coalescence is possible. After a brief presentation of kinetic Monte Carlo (KMC) simulations, I show how the submonolayer regime can be studied in a wide variety of experimental situations: complete condensation, growth with reevaporation, nucleation on defects, and formation of two- and three-dimensional islands. Since I want these models to be useful for experimentalists, Sec. V is entirely devoted to the presentation of a strategy for analyzing experimental data and extracting microscopic parameters, such as diffusion and evaporation rates. I remind the reader that simple software simulating all these situations is available on request from the author. Section VI analyzes in detail several cluster deposition experiments. These studies serve as examples of the approaches presented in Sec. V for analyzing the data and also demonstrate that clusters can have surprisingly large mobilities (comparable to atomic mobilities) on some substrates. A first interpretation of these intriguing results at the atomic level is given in Sec. VII, where the kinetics of cluster-cluster coalescence are also studied. The main results of this section are that high cluster mobilities can be achieved provided the cluster does not find an epitaxial arrangement on the substrate and that cluster-cluster coalescence can be much slower than predicted by macroscopic theories.

A note on terminology: The structures formed on the surface by aggregations of clusters are called islands. This is to avoid possible confusion with the terms usually employed for atomic deposition, where islands are formed by aggregations of atoms on the surface. Here the clusters are preformed in the gas phase before deposition. I use the terms *coverage* for the actual portion of the surface covered by the islands and *thickness* for the total amount of matter deposited on the surface (see also the list of symbols).

II. INTEREST IN NANOSTRUCTURES AND THEIR CONSTRUCTION

Before turning to the heart of this paper—the growth of nanostructures by cluster deposition—I think it is appropriate to show why one wants to obtain nanostructures at all and how these can be prepared experimentally. A tremendous amount of both experimental and theoretical work has been carried out in this field, and it is impossible to summarize every aspect of it here. For a recent and rather thorough review, see the collection edited by Edelstein and Cammarata (1996), in which the possible technological impact of nanostructures is also addressed. It is also interesting to read the proceedings of conferences on this topic (Averback, 1991; Suzuki *et al.*, 1996; Anderson, 1997). Several journals such as Nanostructured Materials or Physica E are entirely devoted to this field. The reader is also referred to the enormous number of World Wide Web pages (about

[1]See, for example, Siegel, 1991 1996; Gleiter, 1992; Edelstein and Cammarata, 1996; Rubinstein, 1996; Sattler, 1996; Palmer, 1997; Fendler, 1998.

6000 on nanostructures).[2] A short summary of the industrial interest in nanostructures appeared recently in Europhys. News (Fecht, 1997), and introductory reviews on the appeal of ''Nanoscale and ultrafast devices'' (Physics Today, 1990) or ''Optics of nanostructures'' (Physics Today, 1993) are also available.

There are two distinct (though related) domains where nanostructures can be interesting for applications. The first stems from the desire to miniaturize electronic devices. Specifically, one would like to grow organized nanometer-size islands with specific electronic properties. As a consequence, an impressive number of deposition techniques have been developed to grow carefully controlled thin films and nanostructures from atomic deposition (Bunshah, 1994; Glocker, 1995; Arthur, 1997). While most of these techniques are complex and keyed to specific applications, molecular-beam epitaxy (MBE) (Herman and Sitter, 1989; Cho, 1994) has received much attention from physicists (Lagally, 1993), mainly because of its relative simplicity. The second subfield is that of nanostructured materials (Edelstein and Cammarata, 1996), as thin or thick films, which show mechanical, catalytic, and optical properties different from their microcrystalline counterparts (Siegel, 1991, 1996; Hadjiapanayis and Siegel, 1994; Jena *et al.*, 1996; Sattler, 1996; Shalaev and Moskovits, 1997).

I shall now briefly review the two subfields, since cluster deposition can be used to build both types of nanostructures. Moreover, some of the physical processes studied below (such as cluster-cluster coalescence) are of interest for both types of structure.

A. Organized nanoislands

There has been growing interest in the fabrication of organized islands of nanometer dimensions. One of the reasons is the obvious advantage of miniaturizing electronic devices both for device speed and for density on a chip (for a simple and enjoyable introduction to the progressive miniaturization of electronics devices, see the book by Turton, 1995). But it should be noted that, at these scales, shrinking the size of the devices also changes their properties, owing to quantum confinement effects. Specifically, semiconductor islands that are smaller than the Bohr diameter of the bulk material (from several nm to several tens of nm) show an interesting property: as their size decreases, their effective band gap increases. The possiblity of tailoring the electronic properties of a given material by controlling the island size has generated a high level of interest in the field of these *quantum dots* (Weisbuch and Binter, 1991; Banyai and Koch, 1993; Alivisiatos, 1996; Mater. Res. Soc. 1998). But quantum dots are not the only incentive for obtaining organized nanoislands. Isolated nanoparticles are also interesting as model catalysts (Freund *et al.*, 1997; Henry *et al.*, 1997; Besenbacher, 1998; Henry, 1998; Chapter 12 of Edelstein and Cammarata, 1996). Clearly, using small particles increases the specific catalytic area for a given volume. More interesting, particles smaller than 4–5 nm in diameter might show specific catalytic properties, different from the bulk (Che and Benett, 1989; Henry, 1998), although the precise mechanisms are not always well identified (Chapter 12 of Edelstein and Cammarata, 1996). One possibility is an increase, for small particle sizes, in the proportion of low-coordination atoms (corners, kinks) whose electronic (and therefore catalytic) properties are expected to be different from those of bulk atoms. For even smaller particles (1–2 nm), interaction with the substrate can significantly alter their electronic properties (Pacchioni and Roesch, 1994). Recently, there have been attempts at organizing isolated islands to test the consequences for their catalytic properties (Jacobs *et al.*, 1997). Obtaining isolated clusters on a surface can also be interesting for a study of their properties. For example, Schaefer *et al.* (1995) have obtained isolated gold clusters on a variety of substrates in order to investigate the elastic properties of single nanoparticles by atomic force microscopy (AFM).

Let me now briefly turn to the possible ways of obtaining such organized nanoislands. Deposition of atoms on carefully controlled substrates is the main technique used presently by physicists trying to obtain a periodic array of nanometer islands of well-defined sizes. A striking example (Brune, 1998) of organized nanoislands is shown in Fig. 1. These triangular islands were grown on the dislocation network formed by the second Ag atomic layer on Pt(111). Beautiful as these triangles are, they have to be formed by nucleation and growth on the substrate, and therefore the process is highly dependent on the interaction of the adatoms with the substrate (energy barriers for diffusion, possibility of exchange of adatoms and substrate atoms, etc.). This drastically limits the range of possible materials that can be grown by this method. However, the growth of strained islands by heteroepitaxy is under active study, since stress is a force that can lead to order, and even a tunable order, as observed, for example, in the system $PbSe/Pb_{1-x}Eu_xTe$ (Springholz *et al.*, 1998).[3]

In this review, I shall focus on an alternative approach to forming nanoislands on substrates: instead of growing them by atom-atom aggregation *on* the substrate, a process that dramatically depends on the idiosyncrasies of the substrate and its interaction with the deposited atoms, one can prepare the islands (as free clusters) *before* deposition and then deposit them. It should be noted that the cluster structure can be extensively characterized prior to deposition by several in-flight techniques,

[2]Especially useful are the following sites: http://www.metallurgy.nist.gov/; http://nanoweb.mit.edu/; http://www.amtexpo.com/nano/; http://molecule.ecn.purdue.edu./~cluster/. A more extensive list is available at the author's web page, http://dpm.univ-lyon1.fr/~jensen/.

[3]For further details on stress, see also (Eaglesham and Cerullo, 1990; Leonard *et al.* 1993; Moison *et al.*, 1994; Brune *et al.*, 1995; Mater. Res. Soc. Bull, 1996b; Brune and Kern, 1997 and the review by Ibach, 1997).

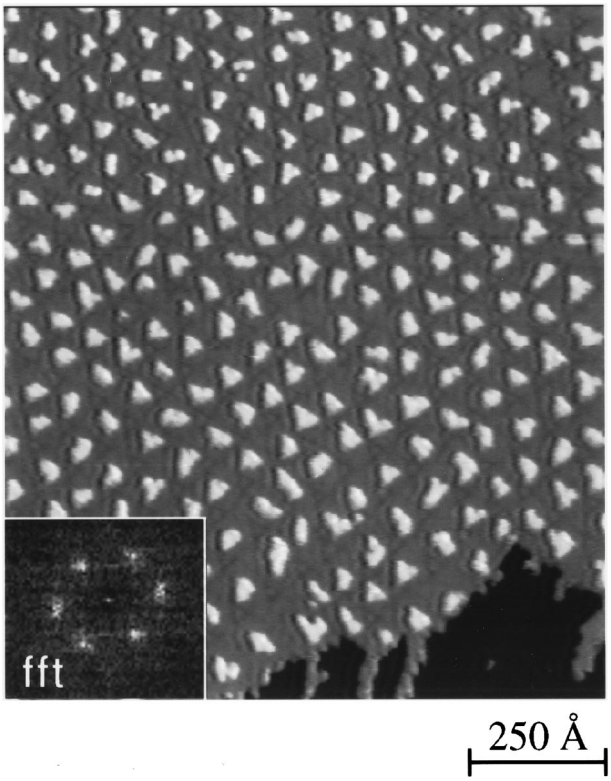

FIG. 1. Ag nanoislands grown on two monolayers of Ag deposited on Pt(111) and annealed at 800 K. The inset shows a fast Fourier transform of the spatial distribution. From Brune (1998).

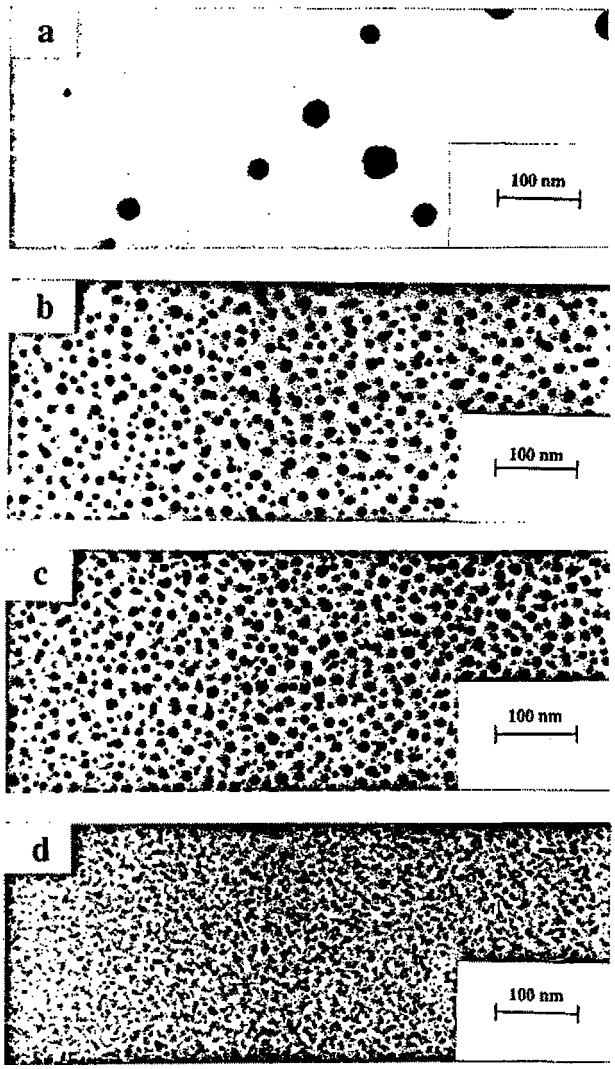

FIG. 2. By changing the mean size of the incident antimony clusters, one can dramatically change the morphology of the submonolayer film. The four micrographs have been obtained for the same thickness (1 nm) and deposition rate (5×10^{-3} nm s^{-1}). The mean sizes are (a) Sb_4, (b) Sb_{16}, (c) Sb_{36}, (d) Sb_{240}. The changes in morphology are interpreted by the different mobilities of the clusters as a function of their size, as well as their different coalescence dynamics and sensitivity to surface defects. From Fuchs *et al.* (1991).

such as time-of-flight spectrometry, photoionization, or fragmentation (Vialle *et al.*, 1997). Moreover, the properties of these building blocks can be adjusted by changing their size, which also affects the growth mechanisms and therefore the film morphology (Fuchs *et al.*, 1991; Bréchignac *et al.*, 1997, 1998; Yoon, 1997). A clear example of the ability to change film morphology by varying only the mean cluster size was given a few years ago by Fuchs *et al.* (1991; Fig. 2), and this study was extended recently by Bréchignac's group to larger cluster sizes (Bréchignac *et al.*, 1997, 1998; Yoon, 1997).

There are several additional motivations for depositing clusters. First, these are grown in extreme nonequilibrium conditions, which allows one to obtain metastable structures or alloys. It is true that islands grown on a substrate are not generally in equilibrium, but the quenching rate is very high in a beam, and the method is more flexible, since one avoids the effects of nucleation and growth on a specific substrate. For example, PdPt alloy clusters—which are known to have interesting catalytic properties—can be prepared with a precise composition (corresponding to the composition of the target rod, see below) and variable size and then deposited on a surface (Rousset *et al.*, 1995, 1996). The same is true for SiC clusters, where one can modify the electronic properties of the famous C_{60} clusters by introducing, in a controlled way, Si atoms before deposition (Ray *et al.*, 1998). This allows one to tune within a certain range the properties of the films by choosing the preparation conditions for the preformed clusters. It might also be anticipated that cluster nucleation is less sensitive to impurities than atomic nucleation. Atomic island growth can be dramatically affected by impurities, as exemplified by the celebrated case of the different morphologies of Pt islands grown on Pt(111) (Michely *et al.*, 1993), which were actually the result of CO contamination at an incredibly low level: 10^{-10} mbar (Kalff *et al.*, 1998). Clusters, being larger entities than atomic islands, might interact less specifically with the substrate and its impurities. Unfortunately, there is still no systematic way of organizing the clusters on a surface. One could try to pin them on selected sites, such as defects, or to encapsulate them with organic molecules before deposition in order to obtain ordered arrays on a substrate (Andres *et al.*, 1996).

B. Nanostructured materials

Although the main focus in this review is the understanding of the first stages of growth, it is worth pointing out the appeal of thicker nanostructured films (for a recent review of this field, see Edelstein and Cammarata, 1996). It is known (Siegel, 1991, 1996; Hadjiapanayis and Siegel, 1994; Sattler, 1996) that the magnetic, optical, and mechanical properties of these films can be intrinsically different from their macrocrystalline counterparts. The precise reasons for this are currently being investigated, but one can cite the presence of a significant fraction (more than 10%) of atoms in configurations different from the bulk configuration, for example, in grain boundaries (Gleiter, 1992). It is reasonable to suppose that both dislocation generation and mobility may become significantly difficult in nanostructured films (Siegel, 1991, 1996). For example, recent studies of the mechanical deformation properties of nanocrystalline copper (Schiotz *et al.*, 1996) have shown that high levels of strain can be reached before the appearance of plastic deformation. However, recent computer simulations of the deformation of nanocrystalline copper show the opposite effect: a softening with decreasing grain size for the smallest sizes (Schiotz *et al.*, 1998). A review of the effects of nanostructuration on the mechanical response of solids is given by Weertman and Averback in Chapter 13 of Edelstein and Cammarata (1996). Another interesting property of these materials is that their crystalline order is intermediate between that of the amorphous materials (first-neighbor order) and of crystalline materials (long-range order). It is given by the size of the crystalline cluster, which can be tuned. For example, for random magnetic materials, by varying the size of the clusters, and consequently of the ferromagnetic domain, one can study the models of amorphous magnetic solids (Perez *et al.*, 1995).

C. How can one deposit clusters on surfaces?

After considering the potential appeal of nanostructures, I now address the practical preparation methods by cluster deposition. Two main variants have been explored. Historically, the first idea was to produce beams of accelerated (ionized) clusters and take advantage of the incident kinetic energy to enhance atomic mobility even at low substrate temperatures. This method does not lead, in general, to nanostructured materials, but to films similar to those obtained by atomic deposition, with sometimes better properties. A more recent approach is to deposit neutral clusters, with low energy to preserve their peculiar properties (characteristic of the free, isolated clusters) when they reach the surface. The limit between the two methods is roughly at a kinetic energy of 0.1 to 1 eV/atom.

1. Accelerated clusters

The group of Yamada at Kyoto University was the first to explore the idea of depositing clusters with high kinetic energies (typically a few keV) to form thin films (Yamada and Takaoka, 1993; Yamada, 1996). The basic idea of the ionized cluster beam (ICB) technique is that the cluster breaks upon arrival and its kinetic energy is transferred to the adatoms, which then have high lateral (i.e., parallel to the substrate) mobilities on the surface. This allows one, in principle, to achieve epitaxy at low substrate temperatures, which is desirable for avoiding diffusion at interfaces or other activated processes. Several examples of good epitaxy by ionized cluster beam have been obtained by the Kyoto group, including Al/Si (Yamada *et al.*, 1984), which has a large mismatch and many other pairings of metals and ceramics on various crystalline substrates, such as Si(100), Si(111). Molecular-dynamics (MD) simulations have supported this idea of epitaxy by cluster spreading (Biswas *et al.*, 1988). The reader is referred to Yamada's reviews (Yamada and Takaoka, 1993; Yamada, 1996) for an exhaustive list of ionized cluster beam applications, which also includes high-energy-density bombardment of surfaces to achieve sputter yields significantly higher than those obtained from atomic bombardment (Insepov and Yamada, 1995).

However, the physics behind these technological successes is not clear. In fact, the very presence of a significant fraction of large clusters in the beam seems uncertain (McEachern *et al.*, 1991; Turner and Shanks, 1991). There is some experimental evidence (Yamada and Takaoka, 1993; Yamada, 1996) offered by the Kyoto group to support the effective presence of a significant fraction of large clusters in the beam, but the evidence is not conclusive. In short, it is difficult to make a definite judgement about the ionized cluster beam technique. There is no clear proof of the presence of clusters in the beam and the high energy of the incident particles renders difficult any attempt at modeling. The Kyoto group has clearly shown that the ionized cluster beam does lead to good-quality films in many cases, but it is not clear how systematic the improvement is when compared to atomic-deposition techniques.

Haberland's group in Freiburg has recently developed a different technique called energetic cluster impact (ECI), in which a better-controlled beam of energetic clusters is deposited on surfaces (Haberland *et al.*, 1992). The Freiburg group has shown that accelerating the clusters leads to improvements in some properties of the films: depositing slow clusters (energy per atom of 0.1 eV) produces metal films that can be wiped off easily, but accelerating them before deposition (up to 10 eV per atom) results in strongly adhering films (Haberland *et al.*, 1995). Molecular-dynamics simulations of cluster deposition (Haberland *et al.*, 1995) have explained this behavior qualitatively: while low-energy clusters tend to pile up on the substrate, leaving large cavities, energetic clusters lead to a compact film (Fig. 3). It is interesting to note that, even for the highest energies explored in the MD simulations (10 eV per atom), no atoms were ejected from the cluster upon impact. The effect of film smoothening is only due to the flattening of the cluster when it touches the substrate. Some caution on the interpretation of these simulations is needed because of

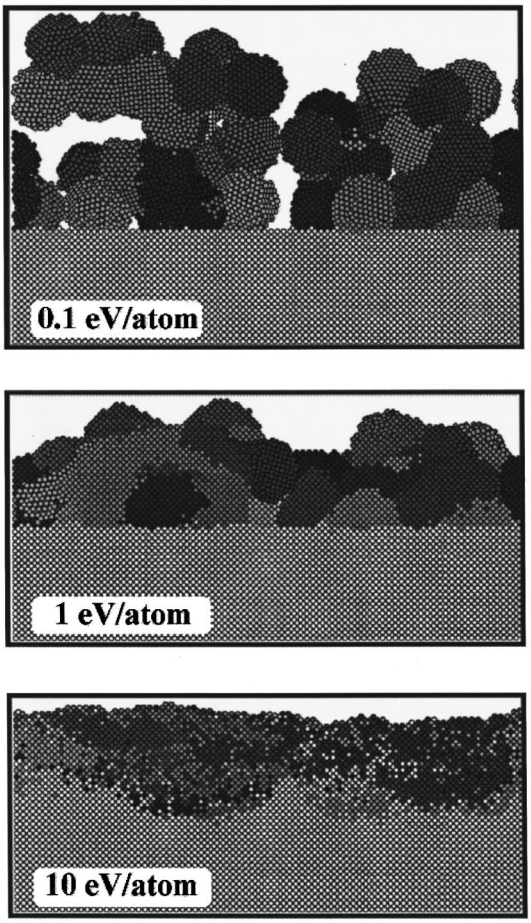

FIG. 3. Molecular-dynamics simulations of the morphology of films obtained by Mo_{1043} cluster deposition for increasing incident kinetic energies per atom (as indicated in the figures) onto a Mo(001) substrate. From Haberland *et al.* (1995).

the very short time scales that can be simulated (a few ps). Similar MD simulations of the impact of a cluster with a surface at higher energies have also been performed (Massobrio and Nacer, 1997). Recently, Palmer's group (Carroll *et al.*, 1998) has studied the interaction of Ag clusters on graphite for various incident kinetic energies (between 15 and 1500 eV). They have shown that, for *small* (Ag_3) clusters, the probability of a cluster's penetrating the substrate critically depends on its orientation relative to the substrate.

2. Low-energy clusters

Another strategy for growing nanostructures with cluster beams consists in depositing low-energy particles.[4] Ideally, by depositing the clusters with low kinetic energies, one would like to conserve the memory of the free-cluster phase (Melinon *et al.*, 1995; Perez *et al.*, 1997) to form thin films with their original properties. Since the kinetic energy is of the order of 10 eV per cluster (Roux *et al.*, 1994), i.e., a few meV per atom, which is negligible compared to the binding energy of an atom in the cluster, no fragmentation of the clusters is expected upon impact on the substrate. Figure 3 suggests that the films are porous (Haberland *et al.*, 1995; Kelchner and De Pristo, 1997), which is desirable for retaining one of the peculiarities of the clusters—their high surface/volume ratio, which affects all their physical (structural, electronic) properties as well as their chemical reactivity (catalysis). Concerning deposition of carbon clusters, experiments (Melinon *et al.*, 1995; Paillard *et al.*, 1993; Perez *et al.*, 1997), as well as simulations (Canning *et al.*, 1997), have shown that the carbon clusters preserve their identity in the thick film.

Another interesting type of nanostructured film grown by cluster deposition is the cermet produced by combining a cluster beam with an atomic beam of the encapsulating material (Kay, 1986; Roux *et al.*, 1997). The size of the metallic particles is determined by the incident cluster size and the concentration by the ratio of the two fluxes. Then these two crucial parameters can be varied independently, in contrast to the cermets grown from atomic beams and precipitation upon annealing. This property has recently allowed a detailed analysis of the size dependence of the optical response of cermet films (Palpant *et al.*, 1998)

Cluster beams are generated by different techniques: multiple-expansion cluster source (MECS, Schaefer *et al.*, 1995) and gas aggregation (Granqvist and Buhrman, 1976; Sattler *et al.*, 1980; Rayane *et al.*, 1989; Melinon *et al.*, 1995; Goldby *et al.*, 1996; Perez *et al.*, 1997). These techniques produce a beam of clusters with a distribution of sizes, with a dispersion of about half the mean size. For simplicity, I shall always refer to this mean size. In gas-aggregation techniques, an atomic vapor obtained from a heated crucible is mixed with an inert gas (usually Ar or He) and the two are cooled by adiabatic expansion, resulting in supersaturation and cluster formation. The mean cluster size can be monitored by the different source parameters (such as the inert-gas pressure) and can be measured by a time-of-flight mass spectrometer. For further experimental details on this technique, see Melinon *et al.*, 1995; Samy El-Shall and Edelstein, 1996; Perez *et al.*, 1997. To produce clusters of refractory materials, a different evaporation technique, vaporization is needed: (Milani and de Heer, 1990, Melinon *et al.*, 1995; Samy El-Shall and Edelstein, 1996; Perez *et al.*, 1997). A plasma created by the impact of a laser beam focused on a rod is thermalized by injection of a high-pressure He pulse (typically, 3–5 bars during 150 to 300 μs), which permits the cluster growth. The mean cluster size is governed by several parameters, such as the helium flow, the laser power, and the delay time between the laser shot and the helium pulse. As a consequence of the pulsed laser shot, the cluster flux reaching the surface is not continuous but chopped. Typical values for the chopping param-

[4]Work in this area includes that of Ganz *et al.*, 1989; Hagena, 1992; Hagena *et al.*, 1994; Ma *et al.*, 1994; Wang *et al.*, 1994; Melinon *et al.*, 1995; Andres *et al.*, 1996; Francis *et al.*, 1996; Goldby *et al.*, 1996; Wawro *et al.*, 1996; Bréchignac *et al.*, 1997, 1998; Perez *et al.*, 1997; Yoon, 1997.

eters are (a) active portion of the period, $\simeq 100\,\mu$s, and (b) chopping frequency, $f=10$ Hz.

3. Other approaches

Alternatively, one can deposit accelerated clusters onto a buffer layer, which acts as a ''mattress'' to dissipate the kinetic energy. This layer is then evaporated, which leads to a soft landing of the cluster on the substrate (Cheng and Landman, 1993; Vandoni *et al.*, 1994). The advantage of this method is that it is possible to select the mass of the ionized clusters before deposition. However, it is difficult with this technique to reach high enough deposition rates to grow films in reasonable times. Vitomirov (1990) deposited atoms onto a rare-gas buffer layer, the atoms first clustered on top and within the layer, which was afterwards evaporated, allowing the clusters to reach the substrate. Finally, deposition of clusters from a scanning tunneling microscope (STM) tip has been shown to be possible, both theoretically (Luedtke and Landman, 1991) and experimentally (Pascual *et al.*, 1993).

III. MODELS OF PARTICLE DEPOSITION

In this section I describe simple models that allow us to understand the first stages of film growth by low-energy cluster deposition. These models can also be useful for understanding the growth of islands from atomic beams in the submonolayer regime in simple cases, namely, (almost) perfect substrates, irreversible aggregation, etc., and they have allowed us to understand and quantify many aspects of the growth. For a discussion of atomic deposition with this kind of model, see Lagally, 1993; the review by Barabási and Stanley, 1995; Jensen, 1996; Zhang and Lagally, 1997; Brune, 1998; Pimpinelli and Villain, 1998. The models described below are similar to earlier models of diffusing particles that aggregate, but such ''cluster-cluster aggregation'' (CCA) models (Kolb *et al.*, 1983; Meakin, 1983; for a comprehensive review, see Herrmann, 1986) do not incorporate the possibility of continual injection of new particles via deposition, an essential ingredient for thin-film growth.

Given an experimental system (substrate and cluster chemical nature), how can one predict the growth characteristics for a given set of parameters (substrate temperature, incoming flux of clusters, etc.)?

A first idea—the ''brute-force'' approach—would be to run a molecular-dynamics (MD) simulation with *ab initio* potentials for the particular system one wants to study. It should be clear that such an approach is bound to fail, since the calculation time is far too large for present-day computers. Even using empirical potentials (such as Lennard-Jones, embedded atom, or tight binding) will not do because there is an intrinsically large time scale in the growth problem, the mean time needed to fill a significant fraction of the substrate with the incident particles. An estimate of this time is fixed by t_{ML}, the time needed to fill a monolayer: $t_{ML}\simeq 1/F$ where F is the particle flux expressed in monolayers per second (ML/s). Typically, the experimental values of the flux are lower than 1 ML/s, leading to $t_{ML}\geqslant 1$ s. Therefore there is a time span of about 13 decades between the typical vibration time (10^{-13} s, the lower time scale for the simulations) and t_{ML}, rendering hopeless any ''brute-force'' approach.

There is a rigorous way (Voter, 1986) of circumventing this time-span problem: the idea is to ''coarsen'' the description by defining elementary processes, an approach somewhat reminiscent of the usual (length, energy) renormalization of particle physics (Schweber, 1993). One sums up all the short-time processes (typically, atomic thermal vibrations) in effective parameters (transition rates) valid for a higher-level (longer-time) description. I shall now briefly describe this rigorous approach and then proceed to show how it can be adapted to cluster deposition.

A. Choosing the elementary processes

Voter (1986) showed that the interatomic potential for any system can be translated into a finite set of parameters, which then provides the exact dynamic evolution of the system. Recently, the same idea has been applied to Lennard-Jones potentials (Schroeder *et al.*, 1997) by using only two parameters. This coarse-grained, lattice-gas approach requires orders of magnitude less computer power than the MD simulation described above. One can understand the basic idea by the following simple example: for the MD description of the diffusion of an atom by hopping, one has to follow in detail its motion at the picosecond scale, where the atom mainly oscillates in the bottom of its potential well. Only rarely at this time scale will the atom jump from site to site, which is what one is interested in. Voter showed that, provided some conditions are met concerning the separation of these two time scales, and restricting the motion to a regular (discrete) lattice (see Voter, 1986 for more details), one could replace this ''useless'' information by an effective parameter taking into account all the detailed motion of the atom within the well (including the correlations between the motions of the atom and its neighbors) and allowing a rapid evaluation of its diffusion rate.

Unfortunately, this rigorous approach is not useful for cluster deposition, because the number of atomic degrees of freedom (configurations) is too high. Instead, one chooses—from physical intuition—a ''reasonable'' set of elementary processes, whose magnitudes are used as free parameters. This allows one to understand the role of each of these elementary processes during the growth and then to fit their value from experiments (Fig. 4). These are the models that I shall study in this paper, with precise examples of parameter fit (see Sec. VI). Examples of such fits from experimental data for atomic deposition include homoepitaxial growth of GaAs(001) (Shitara *et al.*, 1992), of Pt(100) (Linderoth *et al.*, 1996) or of several metal (100) surfaces (Evans and Bartelt, 1994). Of course, fitting is not very reliable when there are too many almost free parameters. Interesting alter-

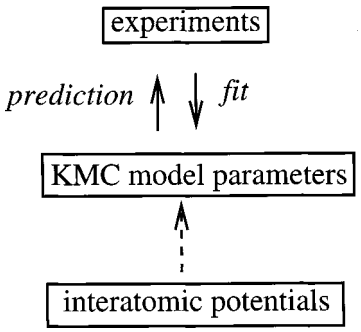

FIG. 4. Principle of a kinetic Monte Carlo simulation (see text).

natives are intermediate cases, where parameters are determined from known potentials but with a simplified fitting procedure taking into account what is known experimentally of the system under study (see Mottet *et al.*, 1998 for a clear example of such a possibility).

B. Predicting the growth from the selected elementary processes

To be able to adjust the values of the elementary processes from experiments, one must first predict the growth from these processes. The oldest way is to write "rate equations," which describe in a mean-field way the effect of these processes on the number of isolated particles moving on the substrate (called monomers) and islands of a given size. The first author to attempt such an approach for growth was Zinsmeister (1966, 1968, 1969, 1971) in 1966, but the general approach is similar to the rate equations first used by Smoluchovsky for particle aggregation (Smoluchovsky, 1916). In the 1970s, many papers dealing with better mean-field approximations and applications of these equations for the interpretation experimental systems were published. The reader is referred to the classical reviews by Venables and co-workers (Venables, 1973; Venables *et al.*, 1984) and Stoyanov and Kaschiev (1981) for more details on this approach. More recently, there have been two interesting improvements. The first is by Villain and coworkers, who simplified enormously the mathematical treatment of the rate equations, allowing one to understand easily the results obtained in a variety of cases (Villain *et al.*, 1992; Villain, Pimpinelli and Wolf, 1992; Villain and Pimpinelli, 1995). Pimpinelli *et al.* (1997) have recently published a summary of the application of this simplified treatment to many practical situations using a unified approach. The second improvement is due to Bales and Chrzan (1994), who developed a more sophisticated self-consistent rate-equations approach that gives better results and allows justification of many of the approximations made in the past. However, these analytical approaches are mean field in nature and cannot reproduce all the characteristics of the growth. Two known examples are the island morphology and the island size distribution (Bales and Chrzan, 1994).

The alternative approach to predicting the growth is that of kinetic Monte Carlo (KMC) simulations. Kinetic Monte Carlo simulations are an extension of the usual Monte Carlo (Metropolis *et al.*, 1953; Binder, 1986, 1994; 1997) algorithm and provide a rigorous way of calculating the dynamical evolution of a complicated system where a large but finite number of random processes occur at given rates. Kinetic Monte Carlo simulations are useful when one chooses to deal with only the slowest degrees of freedom of a system, these variables being only weakly coupled to the fast ones, which act as a heat bath (Binder, 1994, 1997). The "coarsened" description of film growth (basically, diffusion) given above is a good example,[5] but other applications (Binder, 1994, 1997) of kinetic Monte Carlo simulations include interdiffusion in alloys, slow phase separations, and pinning/depinning transitions in dislocation diffusion (Chrzan and Daw, 1997). The principle of kinetic Monte Carlo simulations is straightforward: one uses a list of all the possible processes together with their respective rates ν_{pro} and generates the time evolution of the system from these processes, taking into account the random character of the evolution. For the simple models of film growth described below, systems containing up to 4000 $\times$4000 lattice sites can be simulated in a reasonable time (a few hours), which limits the finite-size effects usually observed in this kind of simulation. Let me now discuss in some detail the way kinetic Monte Carlo simulations are implemented to reproduce the growth, once a set of processes has been defined, with their respective rates ν_{pro} taking arbitrary values or being derived from known potentials.

There are two main points to discuss here: the physical correctness of the dynamics and the calculation speed. Concerning the first point, it should be noted that, originally (Metropolis *et al.*, 1953), Monte Carlo simulations aimed at the description of the equations of state of a system. Then, "the MC method performs a time averaging of a model with (often artificial) stochastic kinetics . . . : time plays the role of a label characterizing the sequential order of states, and need not be related to the physical times" (Binder, 1986). One should be cautious, therefore, about the precise Monte Carlo scheme used for the simulation when attempting to describe the kinetics of a system, as in kinetic Monte Carlo simulations. For example, there are doubts (Kang and Weinberg, 1989; Bogicevic *et al.*, 1998) about some simulation work (Khare *et al.*, 1995; Khare and Einstein, 1996) carried out using Kawasaki dynamics. This point is discussed in detail by Kang and Weinberg (1989).

Let us now address the important problem of the calculation speed. One could naively think of choosing a time interval Δt smaller than all the relevant times in the problem, and then repeat the following procedure:

(1) choose one particle randomly,

[5]See Voter, 1986; Tang, 1993; Bales and Chrzan, 1994; Jensen *et al.*, 1994a, 1994b, 1994c; Barabási and Stanley, 1995; Evans and Bartelt, 1996.

(2) choose randomly one of the possible processes for this particle,

(3) calculate the probability p_{pro} of this process happening during the time interval Δt ($p_{pro}=\nu_{pro}\Delta t$),

(4) throw a random number p_r and compare it with p_{pro}: if $p_{pro}<p_r$ perform the process, if not go to the next step.

(5) increase the time by Δt and go to (1).

This procedure leads to the correct kinetic evolution of the system but might be extremely slow if there were a large range of probabilities p_{pro} for the different processes (and therefore some $p_{pro}\ll 1$). The reason is that a significant fraction of the loops leads to rejected moves, i.e., to no evolution at all of the system.

Instead, Bortz *et al.* (1975) have proposed a clever approach to eliminate *all* the rejected moves and thus reduce dramatically the computational times. This is to choose not the particles but the processes, according to their respective rate and the number of possible ways of performing a process (called Ω_{pro}). This procedure can be represented schematically as follows:

(1) update the list of the possible ways of performing the processes Ω_{pro},

(2) randomly select one of the process, weighting the probability of selection by the process rate ν_{pro} and Ω_{pro}: $p_{pro}=(\nu_{pro}\Omega_{pro})/(\Sigma_{processes}\Omega_{pro}\nu_{pro})$,

(3) randomly select a particle for performing this process,

(4) move the particle,

(5) increase the time by $dt=(\Sigma_{processes}\Omega_{pro}\nu_{pro})^{-1}$,

(6) go to (1).

A specific example of such a scheme for cluster deposition is given below (Sec. III. C). Note that the new procedure implies a less intuitive increment of time, and that one has to create (and update) a list of all the Ω_{pro} constantly, but the acceleration of the calculations is worth the effort.

A serious limitation of kinetic Monte Carlo approaches is that one has to assume a finite number of local environments (to obtain a finite number of parameters): this confines kinetic Monte Carlo approaches to regular lattices, thus preventing a rigorous consideration of elastic relaxation, stress effects, or anything that affects not only the *number* of first or second nearest neighbors but also their precise position. Indeed, considering the precise position as in MD simulations introduces a continuous variable and leads to an infinite number of possible configurations or processes. Stress effects can be introduced approximately in kinetic Monte Carlo simulations, for example, (Ratsch *et al.*, 1994) by allowing a variation of the bonding energy of an atom to an island as a function of the island size (the stress depending on the size), but it is unclear how meaningful these approaches are (see also Nosho *et al.*, 1996; Schroeder and Wolf, 1997). I should mention here a recent proposition (Hamilton, 1997) inspired by the old Frenkel-Kontorova model (Frenkel and Kontorova, 1938), which allows incorporation of some misfit effects in rapid simulations. It remains to be explored whether such an approach could be adapted to the kinetic Monte Carlo scheme.

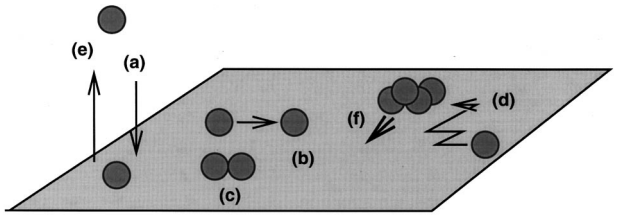

FIG. 5. Main elementary processes considered in this paper for the growth of films by cluster deposition: (a) adsorption of a cluster by deposition; (b) and (d) diffusion of the isolated clusters on the substrate; (c) formation of an island of two monomers by juxtaposition of two monomers (nucleation); (d) growth of a supported island by incorporation of a diffusing cluster; (e) evaporation of an adsorbed cluster. I also briefly consider the influence of island diffusion (f).

C. Basic elementary processes for cluster growth

What is likely to occur when clusters are deposited on a surface? I present here the elementary processes that will be used in cluster deposition models: deposition, diffusion, and evaporation of the clusters and their interaction on the surface (Figs. 5 and 6). The influence of surface defects that could act as traps for the particles is also addressed.

A simple physical rationale for choosing only a limited set of parameters is the following (see Fig. 7). For any given system, there will be a hierarchy of time scales, and the relevant ones for a growth experiment are those much lower than $t_{ML}\simeq 1/F$. The others are too slow to act and can be neglected. The hierarchy of time scales (and therefore the relevant processes) depends, of course, on the precise system under study. It should be noted that for cluster deposition the situation is somewhat simpler than for atom deposition (Jensen, 1998a) since many elementary processes are very slow. For example, diffusion of clusters on top of an already formed island is very low (Bardotti *et al.*, 1995, 1996), cluster detachment from the islands is insignificant, and edge diffusion is not an elementary process at all, since the cluster cannot move as an entity over the island edge (as I shall discuss in Sec. VII. B, the equivalent process is cluster-cluster coalescence by atomic motion). Let us

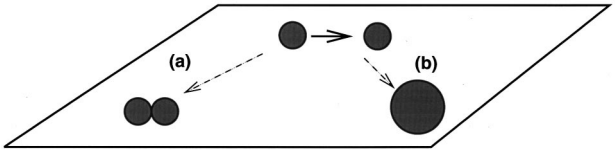

FIG. 6. Possible interaction of two clusters touching on the surface: (a) pure juxtaposition, (b) total coalescence. Intermediate cases (partial coalescence) are possible and will be described later.

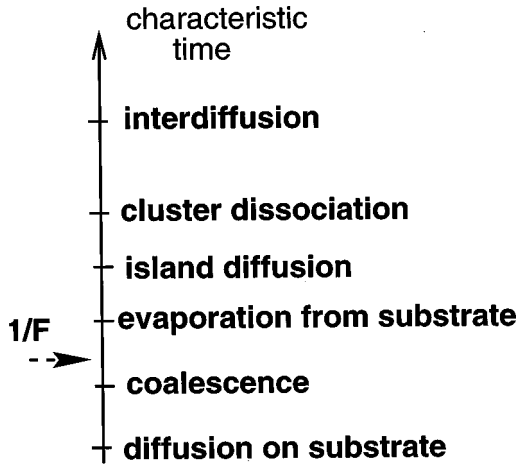

FIG. 7. Arbitrary example of the time scales of some elementary processes considered in this paper for the growth of films by cluster deposition. The relevant processes are those whose time scales are smaller than the deposition time scale shown by the arrow in the left. In this case, models including only cluster diffusion on the substrate and cluster-cluster coalescence are appropriate. "Island diffusion" refers to the motion of islands of clusters as a whole, "cluster dissociation" to the evaporation of atoms from the cluster, and "interdiffusion" to the exchange of atoms in the cluster with substrate atoms.

now consider in detail each of the elementary processes useful for cluster deposition.

The first ingredient *deposition*, is quantified by the flux F, i.e., the number of clusters that are deposited on the surface per unit area and unit time. The flux is usually uniform in time, but in some experimental situations it can be pulsed, i.e., change from a constant value to 0 over a given period. Chopping the flux can affect the growth of the film significantly (Jensen and Niemeyer, 1997), and I shall take this into account when needed (Sec. VI. B. 3).

The second ingredient is the *diffusion* of clusters that have reached the substrate. I assume that the diffusion is Brownian, i.e., the particle undergoes a random walk on the substrate. To quantify the diffusion, one can use either the usual diffusion coefficient D or the diffusion time τ, i.e., the time needed by a cluster to move by one diameter. These two quantities are connected by $D=d^2/(4\tau)$, where d is the diameter of the cluster. Experiments show that the diffusion coefficient of a cluster can be surprisingly large, comparable to the atomic diffusion coefficients. The diffusion is here supposed to occur on a perfect substrate. Real surfaces always present some defects such as steps, vacancies, or adsorbed chemical impurities. The presence of these defects on the surface could significantly alter the diffusion of the particles and therefore the growth of the film. I shall include here one simple kind of defect, a perfect trap for the clusters that definitively prevents them from moving.

A third process that could be present in growth is *re-evaporation* of the clusters from the substrate after a time τ_e. It is useful to define $X_S=\sqrt{D\tau_e}$, the mean diffusion length on the substrate before desorption.

The last simple process I shall consider is the *interaction* between clusters. The simplest case is when aggregation is irreversible and particles simply remain juxtaposed upon contact. This occurs at low temperatures. At higher temperatures, cluster-cluster coalescence will be active (Fig. 6). Thermodynamics teaches us that coalescence should always happen but without specifying the kinetics. Since many clusters are deposited on the surface per unit time, kinetics is here crucial to determine the shape of the islands formed on the substrate. Complete understanding of the kinetics is still lacking, for reasons that I shall discuss later (Sec. VII. B). I note that the shape of the clusters and the islands on the surface need not be perfectly spherical, even in the case of total coalescence. Their interaction with the substrate can lead to half spheres or even flatter shapes, depending on the contact angle. Contrary to what happens for atomic deposition, a cluster touching an island forms a huge number of atom-atom bonds and will not detach from it. Thus models including reversible particle-particle aggregation (Zhdanov and Norton, 1994; Bartelt *et al.*, 1995; Ratsch *et al.*, 1995) are not useful for cluster deposition.

The specific procedure for performing a rapid kinetic Monte Carlo simulation of a system (linear size L) when deposition, diffusion, and evaporation of the monomers are included is the following. The processes are deposition of a particle [$\nu_{depo}=F$, $\Omega_{depo}=L^2$ (it is possible to deposit a particle on each site of the lattice)], diffusion of a monomer ($\nu_{diff}=1/\tau$, $\Omega_{diff}=\rho L^2$ where ρ is the monomer density on the surface), and evaporation of a monomer ($\nu_{evap}=1/\tau_e$, $\Omega_{evap}=\rho L^2$). For each loop, one calculates two quantities,

$$p_{drop}=F\Big/\left[F+\rho\left(\frac{1}{\tau_e}+\frac{1}{\tau}\right)\right]$$

and

$$p_{diff}=(\rho/\tau)\Big/\left[F+\rho\left(\frac{1}{\tau_e}+\frac{1}{\tau}\right)\right].$$

Then one throws a random number p $(0<p<1)$ and compares it to p_{drop} and p_{diff}. If $p<p_{drop}$, a particle is deposited in a random position; if $p>p_{drop}+p_{diff}$, a monomer (randomly selected) is removed, otherwise we just move a randomly chosen monomer. After each of these possibilities, one checks whether an aggregation has taken place (which modifies the number of monomers on the surface, and therefore the number of possible diffusion or evaporation moves), increases the time by

$$dt=1\Big/\left[FL^2+\rho L^2\left(\frac{1}{\tau_e}+\frac{1}{\tau}\right)\right],$$

and goes to the next loop.

The usual game for theoreticians is to combine these elementary processes and predict the growth of the film. However, experimentalists are interested in the reverse strategy: from (a set of) experimental results, they wish to understand which elementary processes are actually present in their growth experiments and in what magni-

tudes, what physicists call understanding a phenomenon. The problem, of course, is that with so many processes, many combinations will reproduce the same experiments (see specific examples below). Then some clever guesses are needed to identify which processes are present. For example, if the saturation island density does not change when flux (or substrate temperature) is changed, one can guess that nucleation is mostly occurring on defects of the surface.

In view of these difficulties, the next section is devoted to predicting the growth when the microscopic processes (and their values) are known. After this, in Sec. V, I propose a detailed procedure for identifying and quantifying the microscopic process from the experiments. Finally, Sec. VI reviews the experimental results obtained for cluster deposition.

IV. PREDICTING GROWTH WITH COMPUTER SIMULATIONS

The aim of this section is to find formulas or graphs to deduce the values of the microscopic processes (diffusion, evaporation, etc.) from the observed experimental quantities (island density, island size histograms, etc.). The classic studies (Venables, 1973; Stoyanov and Kaschiev, 1981; Venables *et al.*, 1984) focused on the evolution of the concentration of islands on the surface as a function of time, and especially on the saturation island density, i.e., the maximum island density observed before reaching a continuous film. The reason is that this quantity can be calculated from the rate equations and measured experimentally by conventional microscopy. I shall show other interesting quantities such as island size distributions that are measurable experimentally and have been recently calculated by computer simulations (Stroscio and Pierce, 1994; Jensen *et al.*, 1995, 1996, 1997; Ratsch *et al.*, 1995; Evans and Bartelt, 1996).

I shall study separately the two limiting cases of pure juxtaposition and total coalescence (which are similar to two- and three-dimensional growth in atomic-deposition terminology). Experimentally, the distinction between the two cases can be made by looking at the shape of the supported islands: if they are circular (and larger than the incident clusters) they have been formed by total coalescence; if ramified, by pure juxtaposition (see several examples below, Sec. VI).

In both cases, I analyze how the growth proceeds when different processes are at work: diffusion, evaporation, defects acting as traps, and island mobility. In the simulations, I often take the diffusion time τ to be the unit time: in this case, the flux is equivalent to the normalized flux ϕ (see the List of Symbols) and the evaporation time corresponds to τ_e/τ. The growth is characterized by the kinetics of island formation, the value of the island concentration at saturation N_{sat} (i.e., the maximum value reached before island-island coalescence becomes important), and the corresponding values of the thickness e_{sat} and condensation coefficient C_{sat}, useful when evaporation is important [the condensation coefficient is the ratio of matter actually present on the substrate to the the total number of particles sent on to the surface (also called the thickness $e=Ft$); see the List of Symbols].

I also give the island size distributions corresponding to each growth hypothesis. These have proven useful as a tool for experimentalists to distinguish between different growth mechanisms (Stroscio and Pierce, 1994; Bardotti *et al.*, 1995, 1996; Evans and Bartelt, 1996). By size of an island, I mean the surface it occupies on the substrate. For ''two-dimensional'' islands (i.e., formed by pure juxtaposition), this is the same as the island mass, i.e., its number of monomers. For ''three-dimensional'' islands (formed by total coalescence), their projected surface is the easiest quantity to measure by microscopy. It should be noted that for three-dimensional islands, their projected surface for a given mass depends on their shape, which is assumed here to be pyramidal (close to a half sphere). It has been shown (Evans and Bartelt, 1994; 1997) that by normalizing the size histograms, one obtains a universal size distribution independent of the coverage, the flux, or the substrate temperature for a large range of their values.

A. Pure juxtaposition: Growth of one-cluster-thick islands

I first study island formation in the limiting case of pure juxtaposition. This is done for several growth hypotheses. The rate-equations treatment is given in Appendix A.

1. Complete condensation

Let us start with the simplest case, in which only diffusion takes place on a perfect substrate (no evaporation). Figure 8(a) shows the evolution of the monomer (i.e., isolated clusters) and island densities as a function of deposition time.

We see that the monomer density rapidly grows, leading to a rapid increase of island density by monomer-monomer encounter on the surface. This goes on until the islands occupy a small fraction of the surface, roughly 0.1% [Fig. 9(a)]. Then islands capture efficiently the monomers, whose density decreases. As a consequence, the creation of more islands becomes less probable, and their number increases more slowly. When the coverage reaches a value close to 15% [Fig. 9(b)], coalescence will start to decrease the number of islands. The maximum number of islands at saturation N_{sat} is thus reached for coverages around 15%. Concerning the dependence of N_{sat} as a function of the model parameters, it has been shown that the maximum number of islands per unit area formed on the surface scales as $N_{sat} \simeq (F/D)^{1/3}$ (Venables, 1973; Stoyanov and Kaschiev, 1981). Recent simulations (Bales and Chrzan, 1994; Bardotti *et al.*, 1995, 1996) and theoretical analyses (Villain *et al.*, 1992; Villain, Pimpinelli, and Wolf, 1992; Barabási and Stanley, 1995) have shown that the precise relation is $N_{sat}=0.53(F\tau)^{0.36}$ for the ramified islands produced by pure juxtaposition (Fig. 10).

It should be noted that if cluster diffusion is vanishingly small, the above relation does not hold: instead,

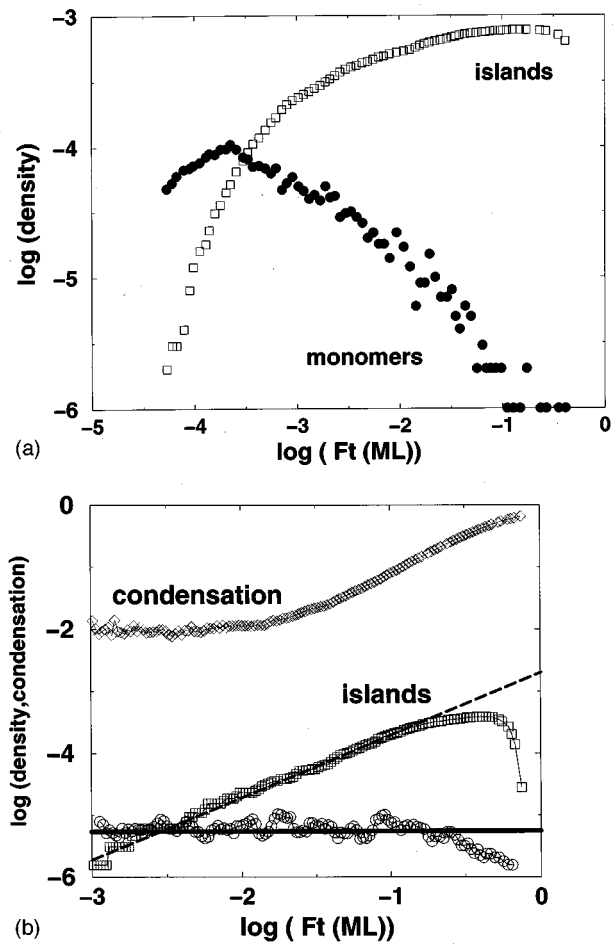

FIG. 8. Evolution of the monomer and island densities as a function of the thickness (in monolayers), for islands formed by pure juxtaposition: (a) complete condensation, $F=10^{-8}$, $\tau_e=10^{10}$ ($\tau=1$). These values mean $X_S=10^5$ and $\ell_{CC}=22$ (b) important evaporation, $F=10^{-8}$, $\tau_e=600$ ($\tau=1$) ($X_S=25$ and $\ell_{CC}=22$). ℓ_{CC} represents the mean island separation at saturation for the given fluxes when there is no evaporation (Jensen *et al.*, 1997). The length units correspond to the incident cluster (monomer) diameter. In (b) the "condensation" curve represents the total number of particles actually present on the surface divided by the total number of particles sent on to the surface (Ft). It would be 1 for the complete condensation case, neglecting the monomers that are deposited on top of the islands. The solid line represents the constant value expected for the monomer concentration, while the dashed line corresponds to the *linear* increase of the island density (see text).

film growth proceeds as in the percolation model (Stauffer and Aharony, 1992), by random paving of the substrate. An experimental example of such a situation has been given by Melinon *et al.* (1991).

2. Evaporation

What happens when evaporation is also included? Figure 8(b) shows that now the monomer density becomes roughly a constant, since it is now mainly determined by the balancing of deposition and evaporation.

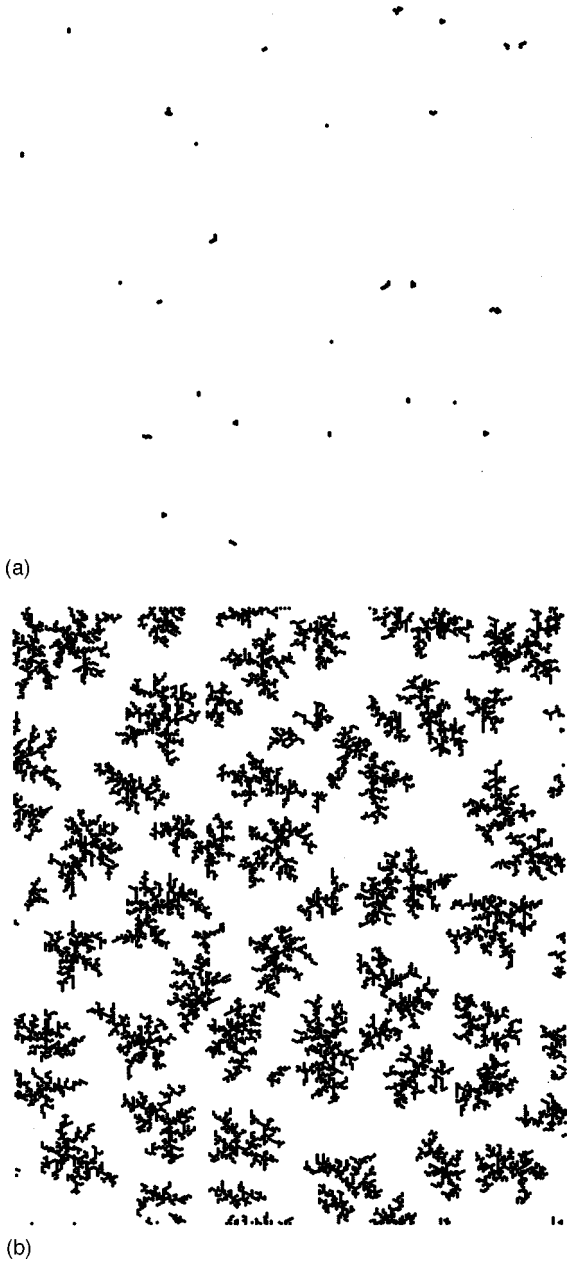

FIG. 9. Morphology of a submonolayer deposit in the case of growth with complete condensation and pure juxtaposition: (a) $\theta=0.1\%$; (b) $\theta=15\%$. The values of the parameters are $F=10^{-8}ML/s$, $\tau=1$, and $L=300$.

As expected, the constant concentration equals $F\tau_e$ (solid line). Then the number of islands increases linearly with time (the island creation rate is roughly proportional to the square monomer concentration; see Appendix A). One can also notice that only a small fraction (1/100) of the monomers effectively remain on the substrate, as shown by the low condensation coefficient value at early times. This can be understood by noting that the islands grow by capturing only the monomers that are deposited within their "capture zone" (comprised between two circles of radius R and $R+X_S$). The other monomers evaporate before reaching the islands. When the islands occupy a significant fraction of the surface, they rapidly capture the monomers. This has two

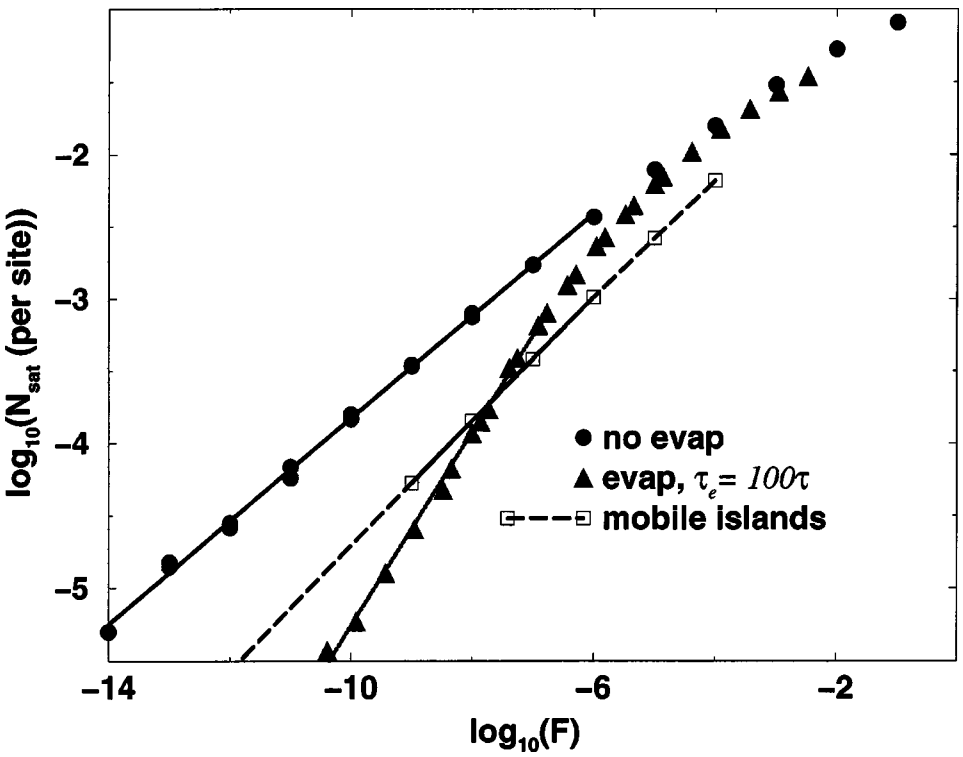

FIG. 10. Saturation island density as a function of the normalized flux ($\tau=1$) for different growth hypotheses indicated on the figure, always in the case of island growth by pure juxtaposition: ●, "*no evap*" means complete condensation, immobiles islands; ▲, densities obtained if there is evaporation, for $\tau_e=100$, immobile islands; □, mobile islands where island mobility is supposed to decrease as the inverse island size (Jensen *et al.*, 1994b), no evaporation; dashed line, an extrapolation of the data for the low normalized fluxes. Fits of the different curves in the low-flux region: (solid line) "*no evap*": $N_{sat}=0.53(F\tau)^{0.36}$; dotted line evap: $N_{sat}=0.26F^{0.67}\tau^{-1/3}\tau_e$ (for the τ and τ_e exponents, see Jensen *et al.*, 1997 and Appendix A) (dashed line, mobile islands: $N_{sat}=0.33(F\tau)^{0.42}$.

effects: the monomer density starts to decrease, and the condensation coefficient starts to increase. Shortly after, the island density saturates and starts to decrease because of island-island coalescence. Figure 10 shows the evolution of the maximum island density in the presence of evaporation. A detailed analysis of the effect of monomer evaporation on the growth is given by Jensen *et al.* (1997), who also discuss the regime of "direct impingement" that arises when $X_S \leqslant 1$: islands are formed by direct impingement of incident clusters as first neighbors of previously adsorbed clusters, and grow by direct impingement of clusters on the island boundary. A summary of the results obtained in the various regimes spanned as the evaporation time τ_e decreases is given in Appendix A. It is interesting to note that these recent results contradict the "classical" predictions by Venables *et al.* (1984).

3. Defects

Now let us consider the influence of a very simple kind of defect: a perfect trap for the diffusing particles. If a particle enters such a defect site, it becomes trapped at this site forever. If such defects are present on the surface (Robins and Rhodin, 1964; Lewis and Anderson, 1978; Larralde *et al.*, 1997) they will affect the growth of the film only if their number is higher than the number of islands that would have been created without defects (for the same values of the parameters). If this is indeed the case, monomers will be trapped by the defects at the very beginning of growth and the number of islands will equal the number of defects, whatever the diffusivity of the particles. The kinetics of island formation is dramatically affected by the presence of defects, the saturation density being reached almost immediately (Fig. 11).

4. Island mobility

The consequences of small-island mobility have not received much attention. One reason is that it is difficult to include island mobility in the rate-equations treatments. A different (though related) reason is that (atomic) islands are expected to be almost immobile in most homoepitaxial systems. However, several studies have shown the following consequences of island mobility for the pure juxtaposition case and in the absence of evaporation. First, the saturation island density is changed (Villain *et al.*, 1992; Villain, Pimpinelli, and Wolf, 1992; Jensen *et al.*, 1994b; Liu *et al.*, 1995a; Kuipers and Palmer, 1996; Furman and Biham, 1997): one obtains $N_{sat}=0.3(F/D)^{0.42}$ (Fig. 10) if all islands are mobile, with a mobility inversely proportional to their size (Jensen *et al.*, 1994a, 1994b). Second, the saturation island density is reached for very low coverages (Fig. 11

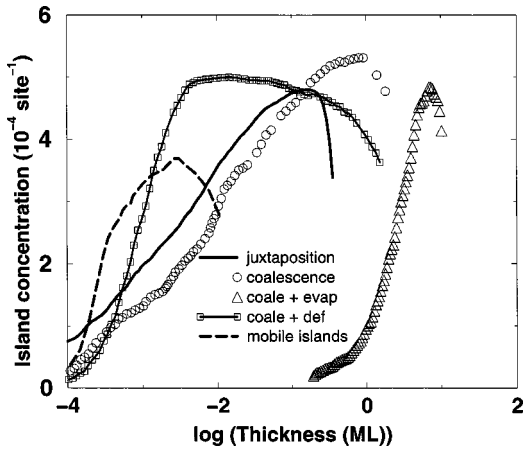

FIG. 11. Evolution of the island density as a function of the thickness for different growth hypotheses. This figure shows that the same saturation density can be obtained for films grown in very different conditions: △, growth with coalescence and evaporation, $\tau_e=100\tau$ and $F\tau=1.2\times10^{-8}$; ○, growth with coalescence but without evaporation ($F\tau=3\times10^{-10}$); solid line, growth with pure juxtaposition without evaporation ($F\tau=2.5\times10^{-9}$); □, growth with coalescence on defects (defect concentration: 5×10^{-4} per site) and $F\tau=10^{-14}$ (no evaporation); dashed line, growth with pure juxtaposition without evaporation but with mobile islands, $F\tau=10^{-8}$.

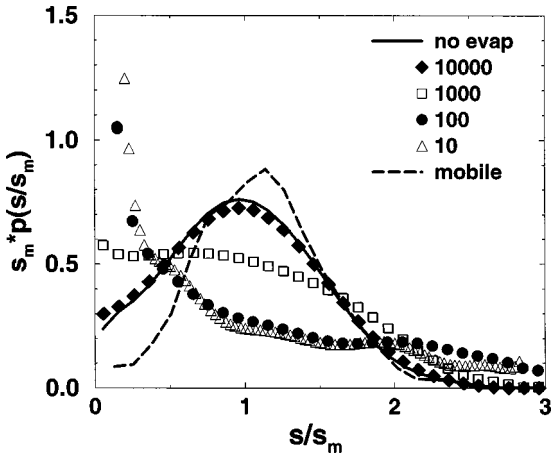

FIG. 12. Normalized island size distributions for $F=10^{-8}$, $\tau=1$, and different values of τ_e for islands formed by pure juxtaposition (no coalescence). The size distributions were obtained for different coverages θ between 0.05 and 0.2: solid line, size distribution obtained without evaporation; dashed line, size distribution obtained with mobile dimers. The numbers show the different values of τ_e. The size distributions shown here were obtained with $F\tau=10^{-8}$, but the same distributions are obtained where F, τ, and τ_e are changed but the parameter $\epsilon=(1+X_S)X_S^5(F\tau)$ is kept fixed (Jensen *et al.*, 1997).

and Jensen *et al.*, 1994b). This can be explained by a dynamical equilibrium between island formation and coalescence taking place at low coverages, thanks to island diffusion. If only monomers are able to move, islands can coalesce (static coalescence) only when the coverage is high enough [roughly 10–15 % (Villain *et al.*, 1992; Villain, Pimpinell, and Wolf, 1992; Jensen *et al.*, 1997)]. Then, the saturation island density is reached for those coverages. When, instead, islands can move, the so-called dynamical coalescence starts from the beginning of the growth and a balance is established at very low coverages (Jensen *et al.*, 1994b). Third, the island size distribution is sharpened by the mobility of the islands (Jensen *et al.*, 1995, 1996; Kuipers and Palmer, 1996; Furman and Biham, 1997). To my knowledge, there is no prediction concerning the growth of films with evaporation when islands are mobile.

5. Island size distributions

Figure 12 shows the evolution of the rescaled (Stroscio and Pierce, 1994; Evans and Bartelt, 1997) island size distributions as a function of evaporation time for islands formed by juxtaposition (Jensen *et al.*, 1996). Size distributions are normalized by the mean island size in the following way: one defines $p(s/s_m)=n_s/N_t$ as the probability that a randomly chosen island has a surface s when the average surface per island is $s_m=\theta/N_t$, where n_s stands for the number of islands of surface s, N_t is the total number of islands, and θ for the coverage of the surface. It is clear that the distributions are significantly affected by evaporation, smaller islands becoming more numerous when evaporation increases. This trend can be qualitatively understood by noting that new islands are created continuously when evaporation is present, while nucleation rapidly becomes negligible in the complete condensation regime. The reason is that islands are created (spatially) homogeneously in the last case, because the positions of the islands are correlated (through monomer diffusion), leaving virtually no room for further nucleation once a small portion of the surface is covered ($\theta\sim0.05$). In the limit of strong evaporation, islands are nucleated randomly on the surface, the fluctuations leaving large regions of the surface uncovered. These large regions can host new islands even for relatively large coverages, which explains why there is a high proportion of small ($s<s_m$) islands in this regime.

B. Total coalescence: Growth of three-dimensional islands

If clusters coalesce when touching, the results are slightly different from those given in the preceding section, mainly because the islands occupy a smaller portion of the substrate at a given thickness. Therefore, in the case of complete condensation, for example, saturation arises at a higher thickness (Fig. 11), even if the coverage is approximately the same (matter is "wasted" in the dimension perpendicular to the substrate). However, the main qualitative characteristics of the growth correspond to those detailed in the preceding section. Figure 13 shows the evolution of the maximum island density in that case, where the three-dimensional islands are assumed to be roughly half spheres [actually, pyramids were used in these simulations, which were originally intended for atomic deposition (Meunier and

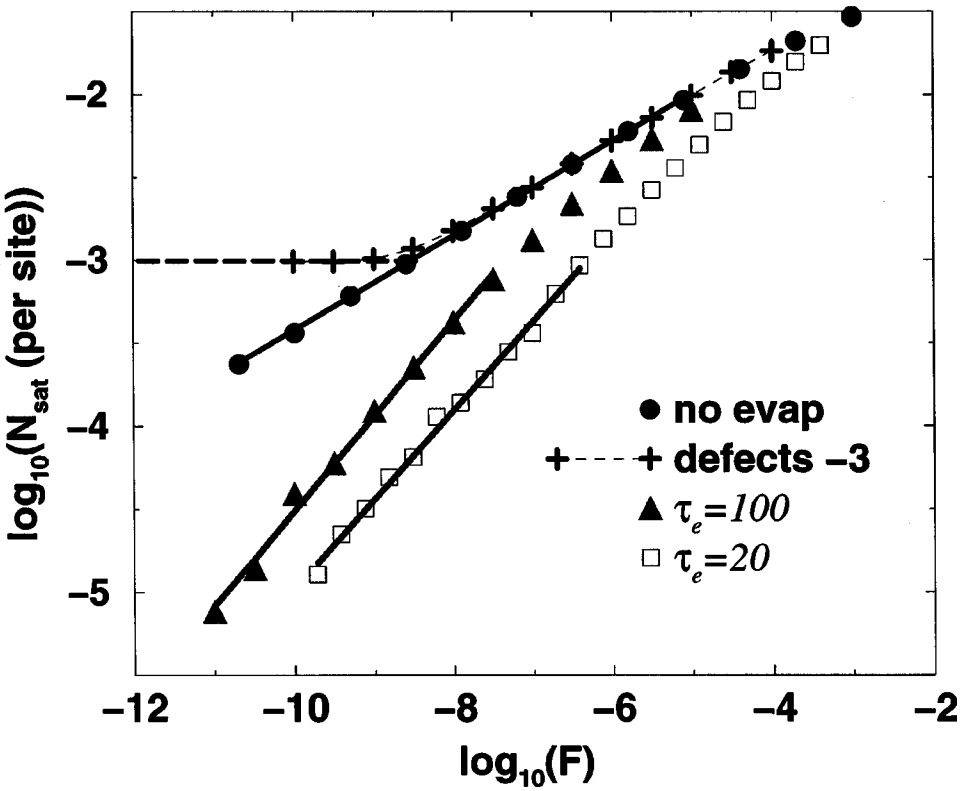

FIG. 13. Saturation island density as a function of the normalized flux ($\tau=1$) for different growth hypotheses in the case of growth by total coalescence (3D islands): ●, densities obtained for the complete condensation case; ▲, evaporation time: $\tau_e=100$; □, $\tau_e=20$ The label *defects* means growth in the presence of defects that act as nucleation centers. Their concentration is 10^{-3} per site. The dashed line is an extrapolation of the defect data for the low normalized fluxes. Fitting the simulation data leads to the following numerical relations: $N_{sat}=0.27(F\tau)^{0.286}$ when there is no evaporation (solid line); $N_{sat}\sim 0.039F^{0.55}\tau^{-2/3}\tau_e^{4/3}$ when evaporation is significant (from an approximation for the two dotted curves): the exponents for τ and τ_e were derived from a rate-equations treatment (Appendix B).

Henry, 1994; Meunier, 1995)]. The analytical results obtained from a rate-equations treatment are given in Appendix B. If the islands are more spherical (i.e., the contact angle is higher), a simple way to adapt these results on the kinetic evolution of island concentration (Fig. 11) is to multiply the thickness by the appropriate form factor, 2 for a sphere, for example. Indeed, if islands are spherical, the same coverage is obtained for a thickness double that obtained for the case of half spheres (there are two identical half spheres). This is a slight approximation, since one has to assume that the capture cross section (which governs the growth) is identical for the two shapes, which is not exactly true (Jensen *et al.*, 1997) but is a very good approximation.

Figure 14 shows the evolution of the rescaled island size distributions for three-dimensional islands (pyramids) in the presence of evaporation. Recall that size means here the projected surface of the island, a quantity that can be measured easily by electron microscopy. We note the same trends as for the pure juxtaposition case (Fig. 12).

Figure 15 shows the evolution of the rescaled island size distributions for pyramidal islands nucleating on defects. Two main differences can be noted. First, the histograms are significantly narrower than in the preceding case, as had already been noted in experimental studies (Harsdorff, 1984). This can be understood by noting that all islands are nucleated at almost the same time (at the very beginning of growth). The second difference is that the size distributions are sensitive to the actual coverage of the substrate, in contrast with previous cases. In other

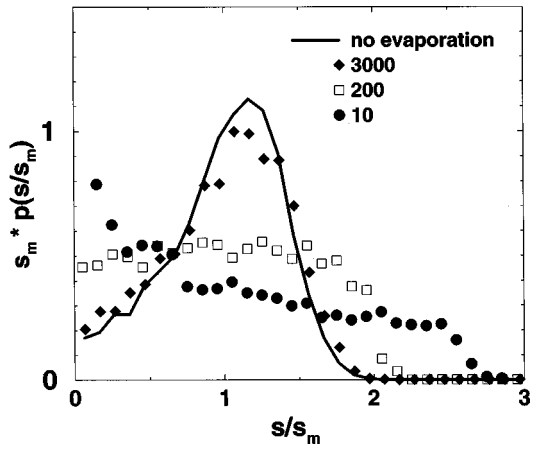

FIG. 14. Normalized island size distributions obtained for $F=10^{-8}$, $\tau=1$ and different values of the evaporation time τ_e for islands formed by total coalescence. The size distributions were obtained for different coverages θ between 0.05 and 0.2. The solid line shows the size distribution obtained without evaporation. The number next to each symbol corresponds to τ_e.

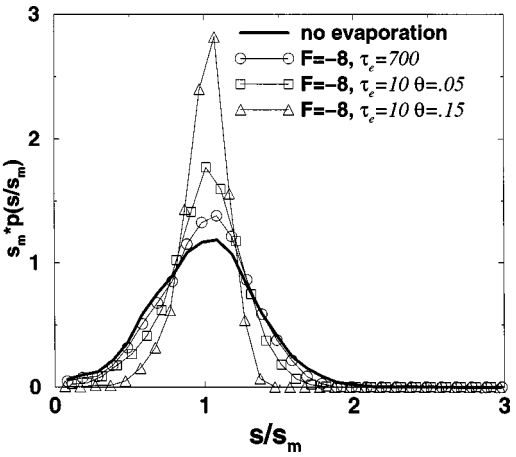

FIG. 15. Effect of the presence of defects on the island size distribution. The rescaled island size distributions are obtained for $F=10^{-8}$ and different values of the evaporation time τ_e ($\tau=1$) for islands formed by total coalescence by nucleation on defects. The size distributions were obtained for different coverages θ between 0.05 and 0.15. Contrary to what is observed for homogeneous nucleation (i.e., without defects), the histograms do depend on the coverage for nucleation on defects. The heavy solid line shows the size distribution obtained without evaporation.

words, there is no perfect rescaling of the data obtained at different coverages, even if rescaling for different fluxes or diffusion times has been checked.

C. Other growth situations

Other processes that have not been analyzed here include the following: A possible (but difficult to study) process is a long-range interaction between particles (electrostatical or through the substrate). There is some experimental evidence of this kind of interaction for the system Au/KCl(100) (Zanghi *et al.*, 1975), but to my knowledge it has never been incorporated in growth models. Chemical impurities adsorbed on the substrate can change the growth in a conventional vacuum, and these effects are extremely difficult to understand and control (Liu *et al.*, 1995b; Haug *et al.*, 1997; Xiao *et al.*, 1997). Of course, many other possible processes have not been addressed in this review, such as the influence of strain, of extended defects as steps or vacancy islands, etc.

V. HOW TO ANALYZE EXPERIMENTAL DATA

Figures 10 and 13 constitute in some sense ''abacuses'' from which one can determine the value of the microscopic parameters (diffusion, evaporation) if the saturation island density is known. The problem is, does the measured island density correspond to the defect concentration of the surface or to homogeneous nucleation? If the latter is true, which curve should be used to interpret the data? In other words, is evaporation present in the experiments and what is the magnitude of τ_e? I shall now give some tricks, first for finding out which processes are relevant and then for quantifying them.

Let us concentrate first on the presence of defects. One possibility is to look at the evolution of N_{sat} with the flux. As already explained, if this leaves unaffected the saturation density, nucleation is occurring on defects. A similar test can be performed by changing the substrate temperature, but there is the nagging possibility that this changes the defect concentration on the surface. It is also possible to study the kinetics of island nucleation, i.e., look at the island concentration as a function of thickness or coverage. The presence of defects can be detected by the fact that the maximum island density is reached at very low coverages (typically less than 1%; see Fig. 11) and/or by the fact that the nucleation rate (i.e., the derivative of the island density) scales as the flux and not as the square flux (see Sec. 3 of Stoyanov and Kaschiev, 1981 for more details). One should be careful, however, to check that all the islands, even those containing a few particles, are visible in the microscope images. This is a delicate point for atomic deposition (Henry *et al.*, 1976) but should be less restrictive for clusters, since each cluster already has a diameter typically larger than a nanometer. Of course, this discussion assumes that the defects are of the ''ideal'' kind studied here, i.e., perfect traps. If atoms can escape from the defects after some time, the situation is changed, but I am unaware of studies on this question.

The question of evaporation is more delicate. First, one should check whether particle reevaporation is important. In principle, this can be done by measuring the condensation coefficient, i.e., the amount of matter present on the surface as a function of the amount of matter brought by the beam. If possible, this measure leaves no ambiguity. Otherwise, the kinetics of island creation is helpful. If the saturation is reached at low thicknesses ($e_{sat} \leqslant 0.5$ ML), this means that evaporation is not important. Another way of detecting particle evaporation is by studying the evolution of the saturation island density with the flux; in the case of 2D growth (Fig. 10), the exponent is 0.36 when evaporation is negligible, but roughly 0.66 when evaporation significantly affects the growth (Jensen *et al.*, 1997). There are similar differences for 3D islands: the exponent changes from 0.29 to 0.66 (Jensen *et al.*, 1998; Fig. 13). Suppose now that one finds that evaporation is indeed important; before being able to use Fig. 10 or Fig. 13, one has to know the precise value of τ_e. One way to find out is to make a precise fit of the kinetic evolution of the island density or the condensation coefficient (see Sec. VI. B. 2 for an example). Below, I show how to find τ_e if one knows only the saturation values of the island density and the thickness.

As a summary, here is a possible experimental strategy for analyzing the growth. First, get a series of micrographs of submonolayer films as a function of the thickness. The distinction between the pure juxtaposition and total coalescence cases can be easily made by comparing

the size of the supported islands to the (supposedly known) size of the incident clusters. Also, if the islands are spherical, this means that coalescence has taken place, whereas if they are ramified that clusters only juxtapose upon contact. Of course, all the intermediate cases are possible (see the case of gold clusters below). One can calculate the ratio of deposited thickness over the coverage; if this ratio is close to 1, the islands are flat (i.e., one cluster thick), otherwise they are three dimensional (unless there is evaporation).

From these micrographs, it is possible to measure the island density as a function of the thickness. Figure 11 should now be helpful to distinguish between the different growth mechanisms. For example, if the saturation island density is obtained for large thicknesses (typically more than 1 ML), then evaporation is certainly relevant and trying to measure the condensation coefficient is important to confirm this point. It is clear from Figs. 10 and 13 that the knowledge of N_{sat} alone cannot determine τ_e, since many values of τ and τ_e can lead to the same N_{sat}. In the 2D case, the values of the microscopic parameters can be obtained by noting that the higher the evaporation rate, the higher the amount of matter "wasted" for film growth (i.e., reevaporated). One therefore expects that the smaller τ_e, the higher e_{sat}, which is confirmed by Fig. 16(a). Therefore, from the (known) value of e_{sat}, one can determine the value of the evaporation parameter $\eta = F\tau X_S^6$ [Fig. 16(a)]. Once η is known, X_S is determined from Fig. 16(b), since N_{sat} is known. $F\tau$ can afterwards be determined (from X_S and η). This is only valid for $X_S \gg 1$ (Jensen *et al.*, 1997), a condition always fulfilled in experiments.

The 3D case is more difficult since the same strategy (measuring N_{sat} and e_{sat}) fails. The reason is that in the limit of high evaporation, e_{sat} goes as $e_{sat} \sim {N_{sat}}^{-1/2}$, thus bringing no independent information on the parameters (Jensen *et al.*, 1998). The same is true for the condensation coefficient at saturation C_{sat}, which is a constant, i.e., independent of the value of τ_e or the normalized flux [see Fig. 17(b)]. This counterintuitive result (one would think that the higher the evaporation rate, the smaller the condensation coefficient at saturation) can be understood by noting that *in this limit*, islands only grow by direct impingement of particles within them (Jensen *et al.*, 1998) and therefore X_S (or τ_e) has no effect on the growth. Fortunately, in many experimental situations, the limit of high evaporation is not reached and one "benefits" from (mathematical) crossover regimes where these quantities do depend on the precise values of τ_e. Figure 17 gives the evolutions of C_{sat} and e_{sat} as a function of N_{sat} for different values of τ_e and F. Then, knowing e_{sat} and N_{sat} leads to an estimate of τ_e from Fig. 17(a), which can be confirmed with Fig. 17(b) provided C_{sat} is known.

To conclude, one should be aware that a saturation thickness much smaller than 1 ML can also be attributed to island mobility. This is a subtle process and it is difficult to obtain any information on its importance. We note that interpreting data as not affected by island diffusion when it is actually present leads to errors on diffusion coefficients of one order of magnitude or more, depending on the value of $F\tau$ (see Fig. 10). Finally, one should be careful in interpreting the N_t vs thickness curves, since most observations are not made in real time (as in the computer simulations) and there can be post-deposition evolutions (see, for example, Brune *et al.*, 1994 for such complications in the case of atomic deposition).

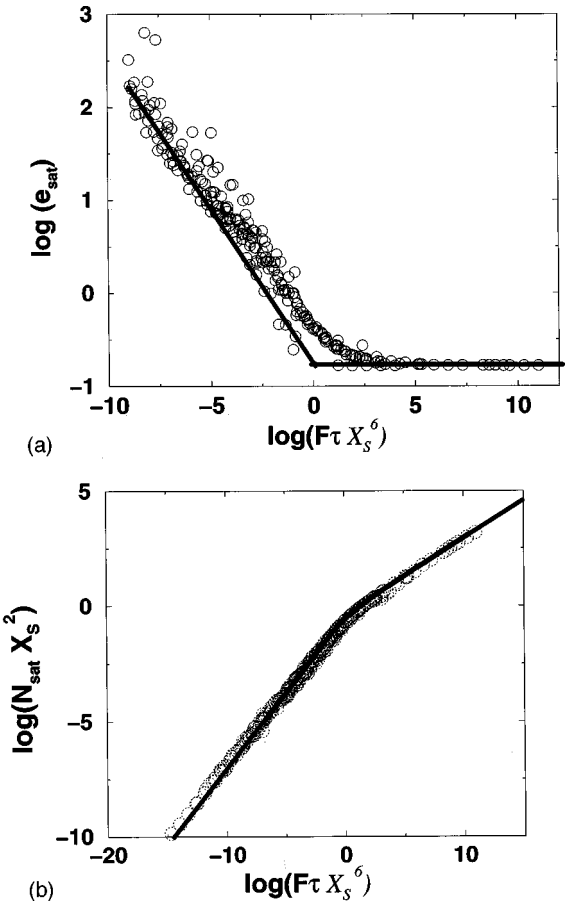

FIG. 16. Values of (a) the thickness e_{sat} and (b) island density N_{sat} at the *saturation* of island density as a function of the evaporation parameter $\eta = F\tau X_S^6$ for growth with pure juxtaposition (Jensen *et al.*, 1997). The solid lines represent theoretical predictions (Jensen *et al.*, 1997).

VI. EXPERIMENTAL RESULTS

I review in this section the experimental results obtained in recent years for low-energy cluster deposition, mainly in the submonolayer regime. The aim is double: first, to give some examples of the analysis of experiments (as indicated in Sec. V) and second, to show that from a comparison of experiments and models one can deduce important physical quantities characterizing the interaction of a cluster with a surface (cluster diffusivity) and with another cluster (coalescence). The following can be read with profit by those interested only in atomic deposition as examples of interpretation, since these elementary processes are relevant for some cases of atomic deposition. The reader is cautioned some

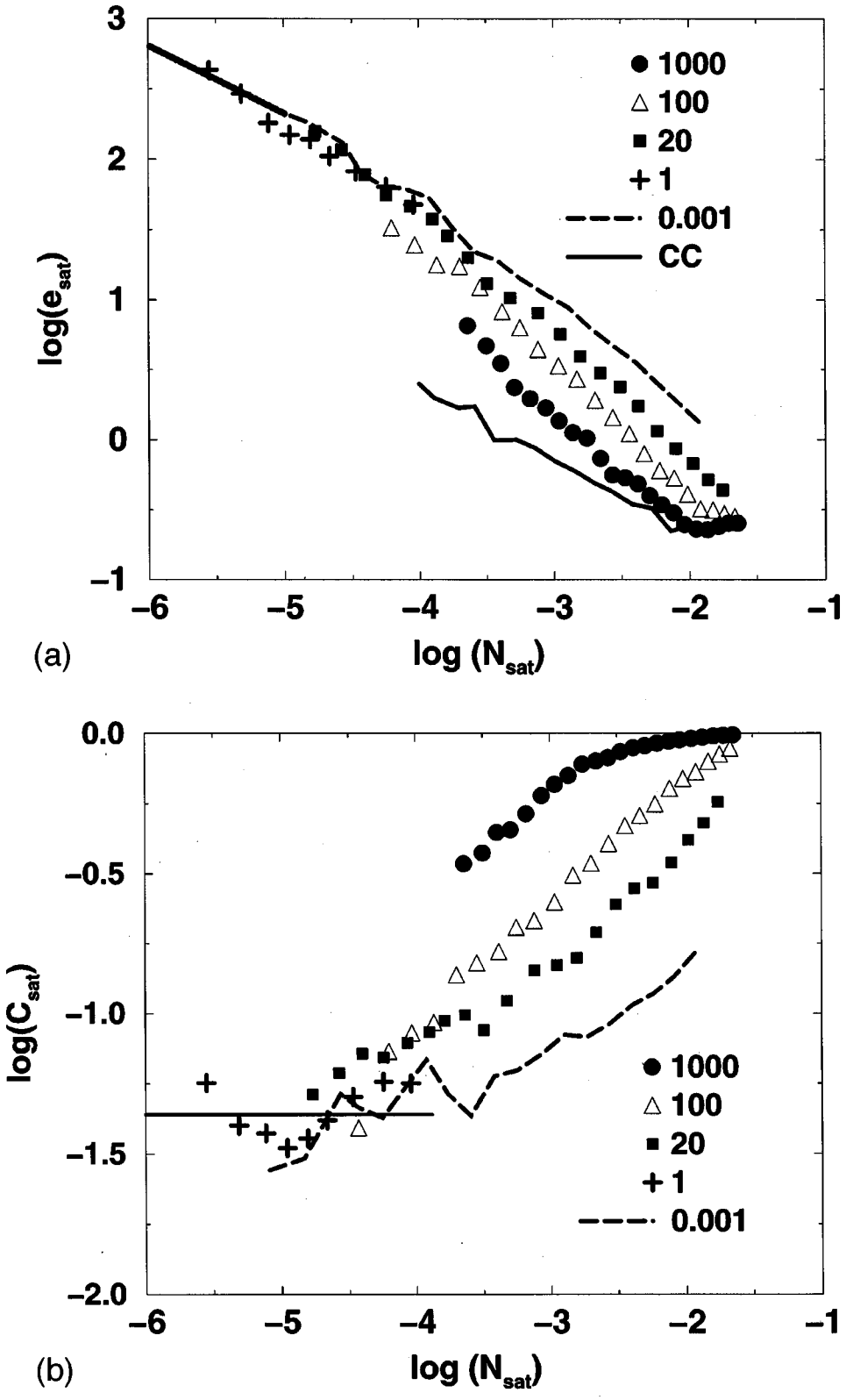

FIG. 17. Values of the thickness e_{sat} (a) and the condensation coefficient C_{sat} (b) at the *saturation* of island density in the total coalescence limit (3D growth for atomic deposition). In the limit of low island densities (i.e., high evaporation rates), C_{sat} is a *constant* (see Jensen *et al.*, 1998; this regime is indicated by the solid line). However, there are crossover regimes that depend on the precise τ_e, and that are shown here. Then, from a measure of C_{sat} and N_{sat} one can get an estimate for τ_e for the not too low island densities which correspond to many experimental cases. In the same spirit, (a) shows the evolution of e_{sat} as a function of N_{sat} in the crossover regime. The numbers correspond to the different τ_e/τ used for the simulations and CC refers to the case of complete condensation (no evaporation). The dotted line in the upper left shows the limiting regime $e_{sat} \sim N_{sat}^{-1/2}$.

mechanisms specific to atomic deposition (transient mobility, funnelling, etc.) are not discussed here (see Chang and Thiel, 1994). Also, growth without cluster diffusion has to be interpreted in the framework of the percolation model, as indicated above (Melinon *et al.*, 1991).

Before analyzing experimental data, it is important to know how to make the connection between the units used in the programs and the experimental ones (see also the List of Symbols). In the program, the unit length is the diameter of a cluster. In the experiments, it is therefore convenient to use as a surface unit the *site*, which is the projected surface of a cluster $\pi d^2/4$ where d is the mean incident cluster diameter. The flux is then expressed as the number of clusters reaching the surface per second per site (which is the same as ML/s) and the island density is given per site. The thickness is usually computed in cluster monolayers (ML), obtained by multiplying the flux by the deposition time. The coverage—the ratio of the area covered by the supported islands over the total area—has to be measured on the micrographs.

A. A simple case: Sb_{2300} clusters on pyrolitic graphite

Let us begin with the case of antimony clusters containing 2300 (± 600) atoms deposited on pyrolitic graphite, since here the growth has been thoroughly investigated (Bardotti *et al.*, 1995, 1996). I first briefly present the experimental procedure and then the results and their interpretation in terms of elementary processes.

1. Experimental procedure

As suggested in the preceding section, various samples are prepared for several film thicknesses, incident fluxes, and the substrate temperatures. For films grown on highly oriented pyrolitic graphite (HOPG), before deposition at room temperature, freshly cleaved graphite samples are annealed at 500 °C for five hours in the deposition chamber (where the pressure is $\simeq 10^{-7}$ Torr) in order to clean the surface. The main advantage of HOPG, conveniently annealed, is that its surfaces consist mainly of defect-free large terraces ($\simeq 1\,\mu$m) between steps. It is also relatively easy to observe these surfaces by electron or tunneling microscopy (Bardotti *et al.*, 1995, 1996). Therefore deposition on HOPG is a good choice to illustrate the interplay between the different elementary processes that combine to lead to the growth. After transfer in air, the films are observed by transmission electron microscopy (TEM) (with JEOL 200CX or TOP CON electron microscopes operating at 100 kV in order to improve the contrast of the micrographs).

2. Results

Figure 18(a) shows a general view of the morphology of the antimony submonolayer film for $e = 0.14$ ML and $T_s = 353\,K$. A detailed analysis (Bardotti *et al.*, 1995, 1996) of this kind of micrographs shows that the ramified islands are formed by the juxtaposition of particles

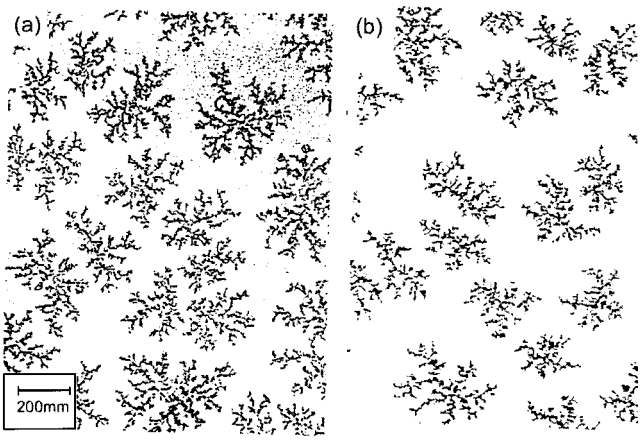

FIG. 18. Typical island morphologies obtained experimentally (a) by TEM and (b) from the computer simulations at the same coverage. (a) Sb_{2300} deposition on graphite HOPG at $T_s = 353$ K and $f = 610^{-3}\,\mathrm{nms}^{-1}$, corresponding to $F = 1.710^{-3}$ ML/s. The deposited thickness is 0.5 nm or $e = 0.14$ ML (b) model including only deposition, diffusion, and pure juxtaposition of the incident clusters, $F\tau = 9 \times 10^{-11}$.

that have the same size distribution as the free clusters of the beam. From this, we can infer two important results. First, clusters do not fragment upon landing on the substrate as indicated in the introduction. Second, antimony clusters remain juxtaposed upon contact and do not coalesce to form larger particles [option (a) of Fig. 6].

From a qualitative point of view, Fig. 18(a) also shows that the clusters are able to move on the surface. Indeed, since the free clusters are deposited at random positions on the substrate, it is clear that, in order to explain the aggregation of the clusters in those ramified islands, one has to admit that the clusters move on the surface. How can this motion be quantified? Can we admit that diffusion and pure juxtaposition are the only important physical phenomena at work here?

Figure 19(a) shows the evolution of the island density as a function of the deposited thickness. We see that the saturation island density N_{sat} is reached for $e \simeq 0.15$ ML. This indicates that evaporation or island diffusion are not important in this case. Therefore we guess that the growth should be described by a simple combination of deposition, diffusion of the incident clusters, and juxtaposition. This has been confirmed in several ways. I give only two different confirmations, directing the reader to Bardotti *et al.* (1995, 1996) for further details. First, a comparison of the experimental morphology and that predicted by models including only deposition, diffusion, and pure juxtaposition shows a very good agreement [Fig. 18(b)]. Second, Fig. 19(b) shows that the saturation island density accurately follows the prediction of the model when the flux is varied. Recall that if the islands were nucleated on defects of the surface, the density would not be significantly affected by the flux.

Having carefully checked that the experiments are well described by the simplest of the models (no evapo-

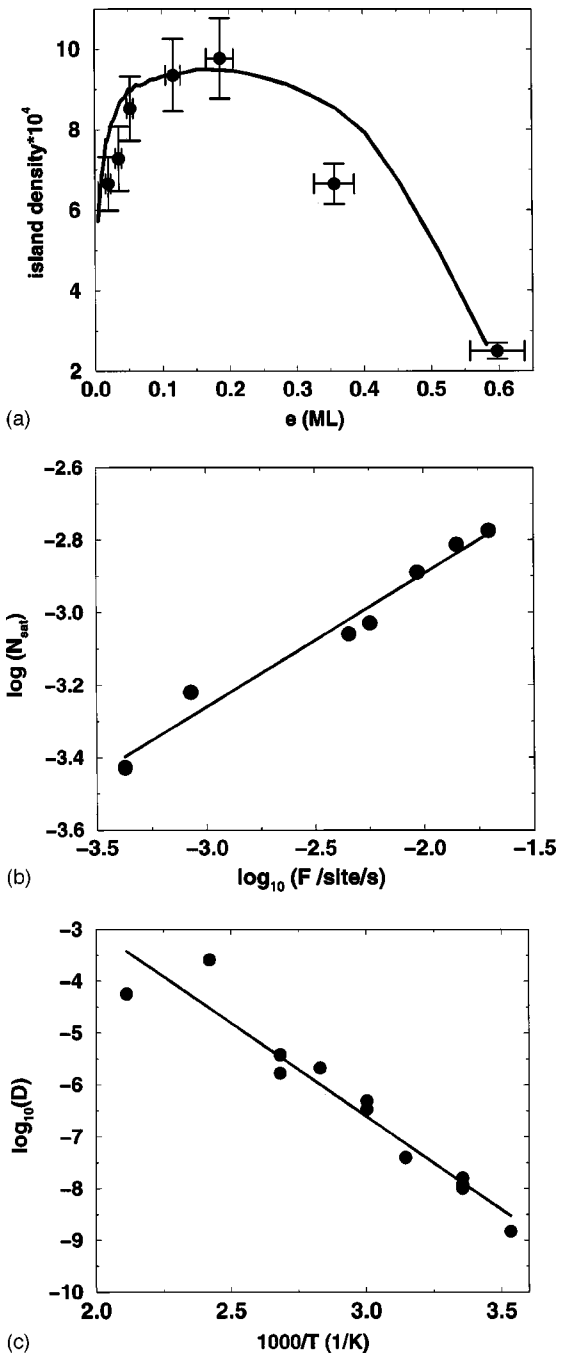

FIG. 19. Main experimental results of Sb_{2300} cluster deposition on HOPG. (a) Evolution of island density: as a function of the deposited thickness. The solid line is a fit to the experimental data with $F\tau = 1.75 \times 10^{-8}$. (b) Evolution of the maximum island density (N_{sat}) as a function of the incident flux F at room temperature. The solid line is a fit to the experimental data: we find $N_{sat} = aF^{0.37 \pm 0.03}$. (c) Dependence of the diffusion coefficient on the temperature. From a fit on the experimental data (solid line), one finds $D = D_0 \exp(-E_a/kT)$, with $E_a = 0.7 \pm 0.1$ eV and $D_0 = 10^4\ \mathrm{cm^2\,s^{-1}}$. The island densities are expressed *per site*, a site occupying the projected surface of a cluster, equivalent to $2.08 \times 10^{-13}\ \mathrm{cm^2}$.

ration, no defects), I can confidently use Fig. 10 to quantify the diffusion of the clusters. As detailed in Bardotti *et al.* (1995, 1996), one first measures the saturation island density for different substrate temperatures. The normalized fluxes ($F\tau$) are obtained from Fig. 10. Knowing the experimental fluxes, one can derive the diffusion times and coefficients. The result is a surprisingly high mobility of Sb_{2300} on graphite, with diffusion coefficients of the same order of magnitude as the atomic ones, i.e., $10^{-8}\ \mathrm{cm^2\,s^{-1}}$, at room temperature [Fig. 19(c)]. Moreover, the prefactor D_0 of the Arrhenius equation $D = D_0 \exp(-E_a/kT)$ is unexpectedly high: $D_0 = 10^4\ \mathrm{cm^2\,s^{-1}}$. The canonical value for atomic diffusion (Gomer, 1990; Ratsch and Scheffler, 1998) is instead $D_0 = 10^{-3}\ \mathrm{cm^2\,s^{-1}}$, seven orders of magnitude lower. We have no explanation of this huge difference at the moment, although it is interesting to note that Wang *et al.* (1998) have also found high prefactors for cluster diffusion when the cluster moves by gliding as a whole on the surface (see also Sec. VII. A.3).

The magnitude of the diffusion coefficient is so high that we wondered whether there was any problem in the interpretation of the data, despite the very good agreement between experiments and growth models described above. For example, one could think of a linear diffusion of the incoming clusters, induced by the incident kinetic energy of the cluster in the beam (the cluster could "slide" on the graphite surface). This seems unrealistic for two reasons: first, in order to explain the low island density obtained in the experiments (see above), it should be assumed that the cluster, which has a low kinetic energy (less than 10 eV), can travel at least several thousand nanometers before being stopped by friction with the substrate. This would imply that the diffusion is just barely influenced by the substrate, which only slows down the cluster. In this case, it is difficult to explain the large changes observed in the island density when the substrate temperature varies. Second, we have deposited antimony clusters on a graphite substrate tilted to 30° from its usual position (i.e., perpendicular to the beam axis). Then, a linear diffusion of the antimony clusters arising from their incident kinetic energy would lead to anisotropic islands (they would grow differently in the direction of tilt and its perpendicular). Experiments (Bardotti *et al.*, 1995, 1996) show that there is no difference between ordinary and tilted deposits. Therefore we can confidently believe that Sb_{2300} clusters perform a very rapid Brownian motion on graphite surfaces. A similar study has been carried out for Sb_{250} on graphite, showing the same order of magnitude for the mobility of the clusters (Bardotti *et al.*, 1995, 1996). The microscopic mechanisms that could explain such a motion will be presented in Sec. VII.

B. Other experiments

In this subsection, I try to analyze data obtained in earlier studies (Dos Santos Aires, 1990; Francis *et al.*, 1996). I provide *possible* (i.e., not in contradiction with any of the data) explanations, with the respective values of the microscopic processes. I stress that the idea here is not to make precise fits of the data, but rather to identify the microscopic processes at work and obtain good guesses about their respective values.

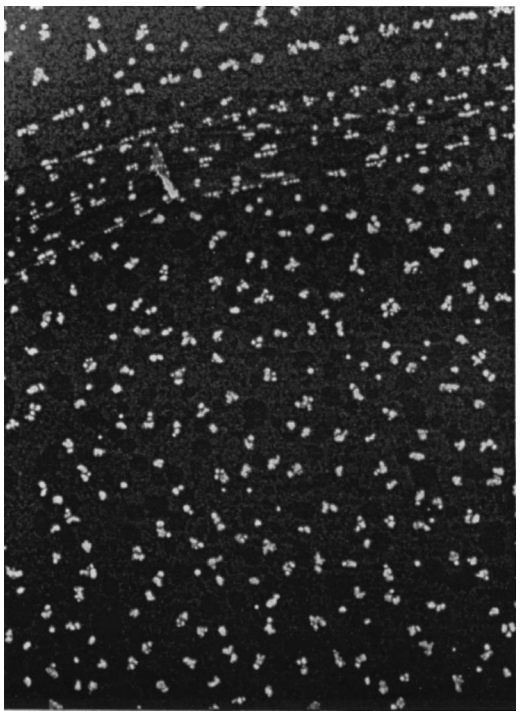

FIG. 20. Scanning electron microscopy of a submonolayer deposit of Ag_{160} slightly accelerated (50 eV) clusters on HOPG. From Francis *et al.*, 1996.

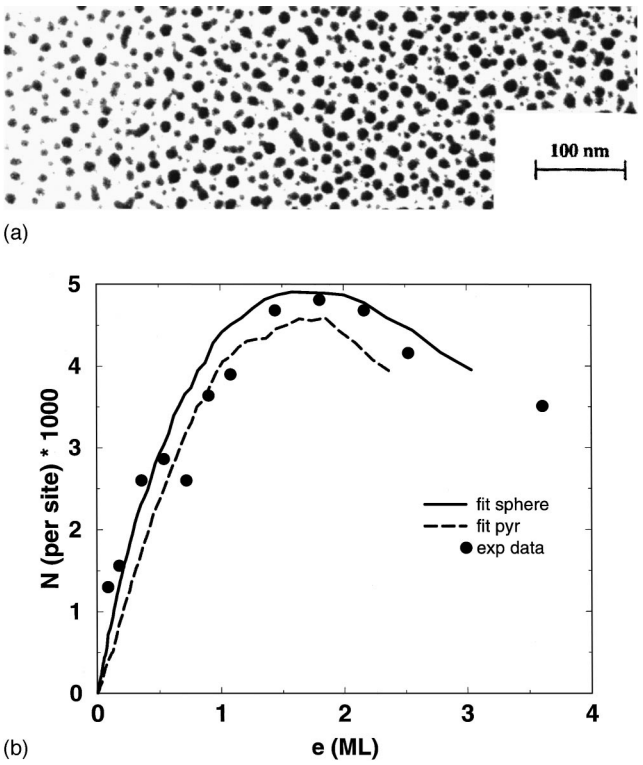

FIG. 21. Experimental results for Sb_{36} deposition on morphous carbon. (a) Morphology of a Sb_{36} film at $e=1.8$ ML. (b) Evolution of the island density (per site) as a function of thickness (ML). The dashed line represents a fit of the data with $F\tau=10^{-5}$ assuming a pyramidal (half-sphere) shape for the supported islands, while the solid line assumes that islands are spherical and $F\tau=3\times10^{-6}$.

1. Slightly accelerated Ag_{160} clusters on HOPG

Palmer's group (Francis *et al.*, 1996) has investigated the growth of films by Ag_{160} cluster deposition. Figure 20 shows the ramified morphology of a submonolayer deposit. Although no precise fit is possible given the limited experimental data, the island density and size show that Ag_{160} clusters are mobile on HOPG.

2. Sb_{36} on a-C

Small antimony clusters are able to move on amorphous carbon, as demonstrated by Fig. 21 and by the fact that the films are dramatically affected by changes in the incident flux (Dos Santos Aires, 1990).

Figure 21(a) shows that these small clusters gather in large islands and coalesce upon contact. The island density is shown in Fig. 21(b). The maximum is reached for a very high thickness ($e\simeq1.8$ ML), which can only be explained by supposing that there is significant reevaporation of Sb_{36} clusters from the surface. Evaporation of small antimony clusters (Sb_n with $n\leqslant100$) from a-C substrates has also been suggested by other authors (Bréchignac *et al.*, 1997, 1998; Yoon, 1997). A fit using $\tau_e=20$, deduced from Fig. 17(a), gives, with $F\tau=10^{-5}$ for $F=6\times10^{-3}$ clusters site^{-1}s^{-1}, leading to $\tau\sim2\times10^{-3}$ s, $D=2\,10^{-12}$ cm^2/s, $\tau_e=0.04$ s and $X_S\sim6$ nm before evaporation, and a condensation coefficient of 0.2 when the maximum island density is reached. However, some authors have argued (Fuchs *et al.*, 1991) that the condensation coefficient is not so low. It is interesting to try a different fit of the data—in better agreement with this indication—to give an idea of the uncertainties of the fits. For this, I assume that the deposited islands are spherical [solid line of Fig. 21(b)] by the procedure described in Sec. IV. Here I have taken $F\tau=3\times10^{-6}f$ or $f=6\times10^{-3}$ clusters site^{-1}s^{-1}, leading to $\tau\sim5\times10^{-4}$ s, $\tau_e=0.04$ s, corresponding to $D=8\times10^{-12}$ cm^2/s, and $X_S\sim11$ nm before evaporation, and a condensation coefficient of 0.5 when the maximum island density is reached. Note that the condensation coefficient is, as expected, higher than in the previous fit and that the agreement with the experimental island densities for the lowest thicknesses is better. Comparing the two fits, it can be seen that the difference in the diffusion coefficient is a factor of 4, and a factor of 2 in the X_S. This means that the orders of magnitude of the values for the microscopic mechanisms can be trusted despite a lack of comprehensive experimental investigation.

Similar studies (Jensen, 1998b) have allowed the diffusion and evaporation characteristic times for other clusters deposited on amorphous carbon to be obtained. For Bi_{90}, one finds $D\sim3\times10^{-13}$ cm^2 s^{-1} and $X_S\sim8$ nm and for In_{100}: $D\simeq4\times10^{-15}$ cm^2 s^{-1} and strong coalescence (the incident clusters are liquid).

3. Au_{250} on graphite

Figure 22 shows the morphology of a gold submonolayer film obtained by deposition of Au_{250} (±100) clus-

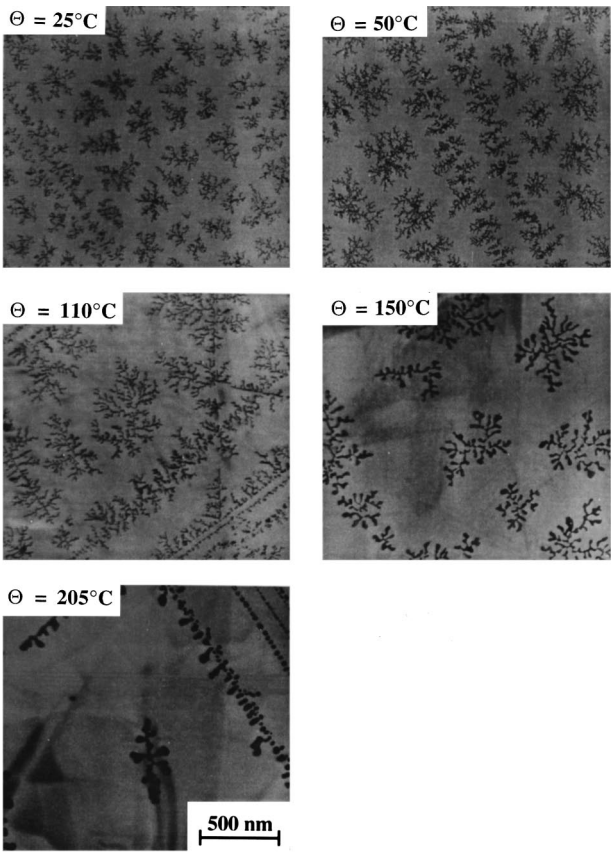

FIG. 22. Morphologies of a Au_{250} films at $e=0.12$ ML and increasing temperatures as indicated in the micrographs. There are fewer and fewer islands as the substrate temperature is raised and the islands become more and more compact.

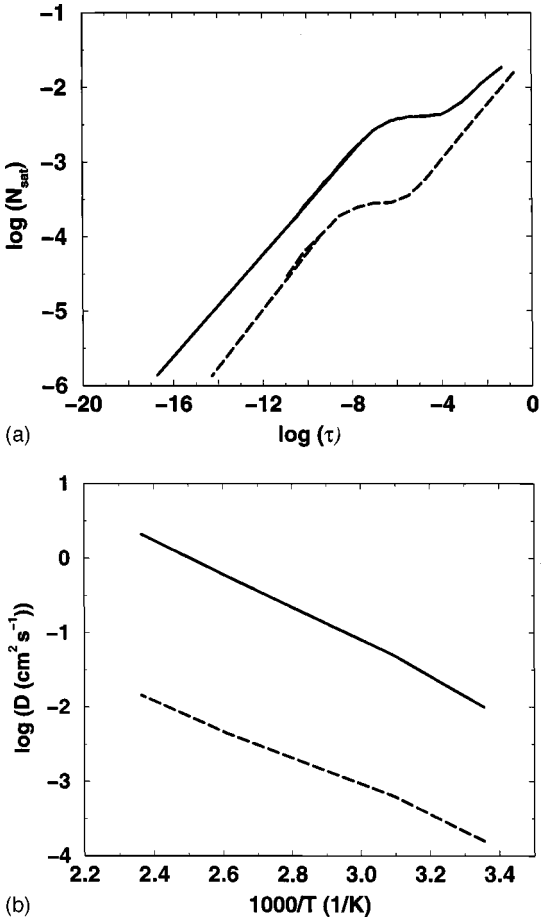

FIG. 23. Effect of a chopped flux on the growth of a film. (a) Saturation island density as a function of the diffusion time τ ($F_i=6$ ML/s) for two hypotheses: only the monomers move (solid line) or islands up to the pentamer move too (dashed line). The lowest island densities have been extrapolated. (b) Temperature dependence of diffusion coefficient as derived from (a) and Fig. 22 in the two hypotheses: solid line, only the monomers move; dashed line, islands up to the pentamer move too.

ters prepared by a laser source on graphite in a UHV chamber for different substrate temperatures.

The structures are strikingly similar to those obtained in the Sb_{2300} case: large, ramified islands. We can conclude that Au_{250} clusters do move on graphite and that they do not completely coalesce. A more careful examination of the island morphology indicates that the size of the branches is not the same as the size of the incident clusters, as was the case for Sb_{2300}. Here the branches are larger, meaning that there is a partial coalescence, limited by the kinetics of the growth. This is a very interesting experimental test for coalescence models that are presented later. I first try to estimate the diffusion coefficient of the gold clusters. We have to be careful here because the incident flux is chopped with the laser frequency, roughly 10 Hz. The active portion of the period (i.e., when the flux is "on") is $\simeq 100\,\mu$s.

An analysis of growth in the presence of a chopped flux has been reported elsewhere (Jensen and Niemeyer, 1997; Combe and Jensen, 1998). Figure 23(a) shows the values of N_{sat} as a function of the diffusion time τ under the experimental condition $F_i=6$ ML/s for two hypotheses: (a) only the monomers move or (b) islands up to the pentamer move too (island mobility is supposed to be inversely proportional to its mass). Note that there is a range of diffusion times (up to two orders of magnitude) that leads to the same island saturation value, a strange situation in homogeneous nucleation (see Jensen and Niemeyer, 1997, and Combe and Jensen, 1998 for details).

Given the experimental island density, the diffusion coefficients in both hypotheses are shown in Fig. 23(b). The values of the diffusion coefficient seem too high, especially in the case of exclusive monomer diffusion, but there is no experimental evidence of island mobility for the moment. Note, however, that since the incident clusters do significantly coalesce, it is not unreasonable to assume that the smallest islands (which are spherical as the incident clusters) can move too. We are at present running additional tests (on cluster reevaporation or non-Brownian cluster diffusion) to confirm the observation of such high diffusion coefficients (see Lewis *et al.*, 1999).

4. Au_{250} on NaCl

Given the surprisingly high mobility of Au_{250} (± 100) on HOPG, it seemed worth testing gold cluster mobility

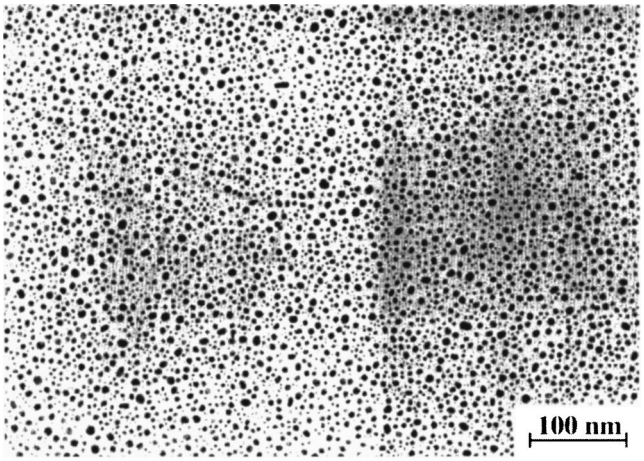

(a)

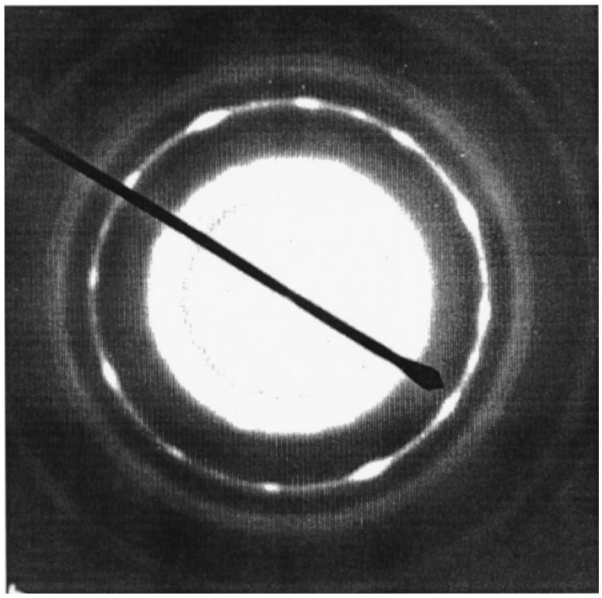

(b)

FIG. 24. A Au_{250} submonolayer deposit on NaCl at $e=0.12$ ML (a) morphology (b) diffraction pattern. The supported islands are small (mean diameter $\simeq$5 nm) and in epitaxy with the substrate, as shown by the diffraction pattern.

on other substrates. I present here recent results obtained by depositing Au_{250} clusters on NaCl (Treilleux, 1999). The high island density [Fig. 24(a)] shows that gold clusters are not very mobile on this substrate, with an upper limit on the diffusion coefficient of $D \simeq 10^{-15}\,cm^2/s$. This is in agreement with the low mobilities observed by other authors in the 1970s. The diffraction pattern [Fig. 24(b)] is similar to that obtained in Figs. 15(c) and 15(d) of Masson, Métois, and Kern (1971). The authors interpreted their results by the presence of multi-twinned Au particles with two epitaxial orientations: Au(111)/NaCl(100) and Au(100)/NaCl(100). This is reasonable taking into account the interatomic distances for these orientations: $d_{AuAu(111)} = 0.289\,nm$, $d_{NaCl(100)} = 0.282\,nm$ and $d_{AuAu(100)} = 0.408\,nm$, $1/2 d_{NaCl(100)} = 0.398\,nm$ (along the face diagonal). These preliminary results suggest that epitaxy may prevent clusters from moving rapidly on a surface, a result that has also been observed by other groups (see next section). They also show that, at least in this case, forming the clusters on the surface by atomic aggregation or depositing preformed clusters changes neither the orientation nor the diffusion of the clusters on the surface. Work is in progress to determine the precise atomic structure of the clusters, their orientation on the substrate, and their diffusion at higher temperatures (Treilleux, 1999).

VII. TOWARDS A PICTURE OF CLUSTER DIFFUSION AND COALESCENCE AT THE ATOMIC SCALE

In the preceding sections I have tried to analyze the growth of nanostructures with the help of two main ingredients: diffusion of the clusters on the surface and their interactions. I have taken the diffusion as just one number quantifying the cluster motion, without worrying about the microscopic mechanisms that could explain it. For atomic diffusion, these mechanisms have been extensively studied (Gomer, 1990; Lagally, 1993; Chang and Thiel, 1994) and are relatively well known. In the (simplest) case of compact (111) flat surfaces, diffusion occurs by site-to-site jumps over bridge sites (the transition state). Therefore diffusion is an activated process and plotting the diffusion constant vs the temperature yields the height of the barrier, which gives information about the microscopics of diffusion. This kind of simple interpretation is not valid for cluster diffusion. It is always possible to infer an ''activation'' energy from an Arrhenius plot [see Fig. 19(c)] but the meaning of this energy is not clear, since the precise microscopic diffusion mechanism is unknown.

Similarly, cluster-cluster coalescence (Fig. 6) has been supposed to be total or null (i.e., pure juxtaposition) but without considering the kinetics or the intermediate cases that can arise (see the experimental results for gold on graphite, for example).

In this section, I describe some preliminary results that can shed some light on the microscopic mechanisms leading to cluster diffusion or coalescence.

A. Diffusion of the clusters

Before turning to the possible microscopic mechanisms, one must investigate whether cluster diffusion is indeed such a general phenomenon. Let us review now the available experimental data concerning the diffusion of three-dimensional (3D) clusters. I have already presented in the previous section several examples of high cluster mobilities over surfaces. In the case of Sb_{2300} on graphite, mobilities as high as $D = 10^{-8}\,cm^2\,s^{-1}$ are obtained at room temperature, and similar values can be inferred for Ag cluster deposition (Francis *et al.*, 1996; Goldby *et al.*, 1996). On a-C substrates, diffusion is not that rapid, but has to be taken into account to understand the growth. More than 20 years ago, the Marseille group (Masson, 1971; Zanghi *et al.*, 1975; Métois *et al.*, 1977; Kern *et al.*, 1979) carefully studied the mobility of

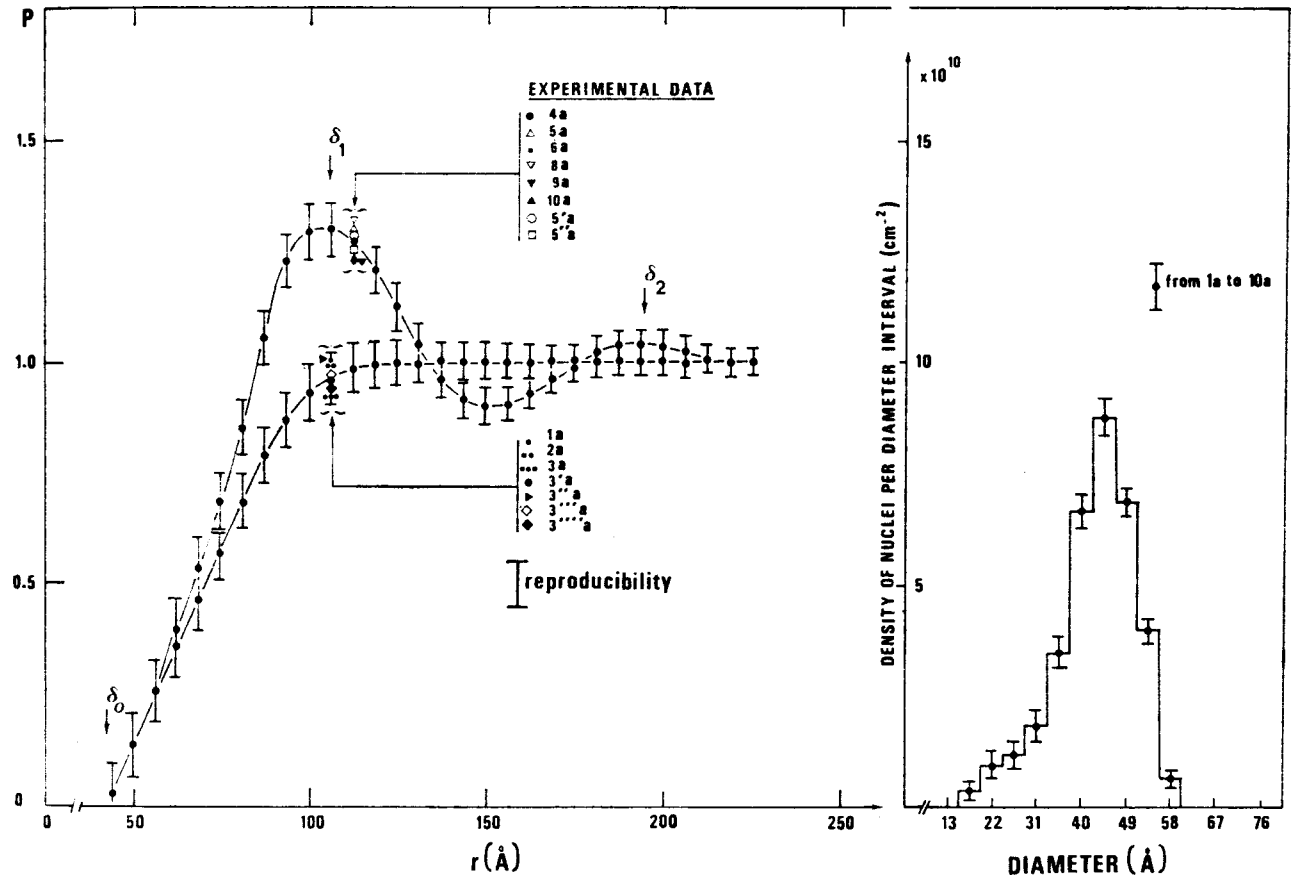

FIG. 25. Radial distribution functions for gold clusters grown at 293 K by atomic deposition before and after annealing at 390 K for several minutes. The right inset shows the size distribution of the clusters, which does not change, demonstrating that no particle-particle coalescence via atomic evaporation takes place. From Zanghi *et al.*, 1975.

nanometer-size gold crystallites on ionic substrates (MgO, KCl, NaCl). By three different methods, they proved that these 3D clusters—grown by atomic deposition at room temperature—are significantly mobile at moderately high temperatures ($T \sim 350$ K). The three different methods were direct observation under the electron microscope beam (Métois *et al.*, 1977), comparison of abrupt concentration profiles (Masson, 1971), and the radial distribution functions (Zanghi *et al.*, 1975) before and after annealing. All these results are carefully reviewed by Kern *et al.* (1979). I shall focus here on the last method (Zanghi *et al.*, 1975). Figure 25 shows the radial distribution functions of the gold clusters obtained just after deposition (the flat curve) and after annealing (the oscillating curve) a similar deposit for a few minutes at 350 K [Fig. 4 of Zanghi *et al.* (1975)]. The flat curve is a standard as-grown radial distribution function (see, for example, Evans and Bartelt, 1997). The other curve is significantly different from the first, although the cluster size distribution remains identical (Fig. 25). This shows that gold clusters move as an entity on KCl(100) at 350 K, since the conservation of the size distribution rules out atomic exchange between islands (the evaporation-condensation mechanism presented below in Sec. VII. A.1). From the shape of the radial distribution function some features of the cluster-cluster interaction can be derived, mainly that it is a repulsive interaction. The detailed interaction mechanisms are not clear (Kern *et al.*, 1979). A different study (Masson, 1971), showed that the clusters were mobile only for a limited amount of time (several minutes), and then stopped. It turns out that clusters stop as soon as they reach epitaxial orientation on the substrate. Indeed, the gold(111) planes can orient on the KCl(100) surface, reaching a stable, minimum energy configuration (for more details on the epitaxial orientations of gold clusters on NaCl, see Matthews and Grünbaum, 1966 and Kuo and Shen, 1997). Therefore 3D cluster diffusion might be quite a common phenomenon, at least when there is no epitaxy between the clusters and the substrate.

What are the possible microscopic mechanisms for this behavior? Unfortunately for the field of cluster deposition, recent theoretical and experimental work has focused mainly on one-atom-thick, two-dimensional islands, whose diffusion mechanisms might be different from those of 3D islands. The focus on 2D islands is due to the technological impetus provided by applications of atomic deposition—notably molecular-beam epitaxy, for which one wants to achieve flat layers. Let us briefly review the current state of the understanding of 2D island diffusion to see what inspiration we can draw for 3D cluster diffusion.

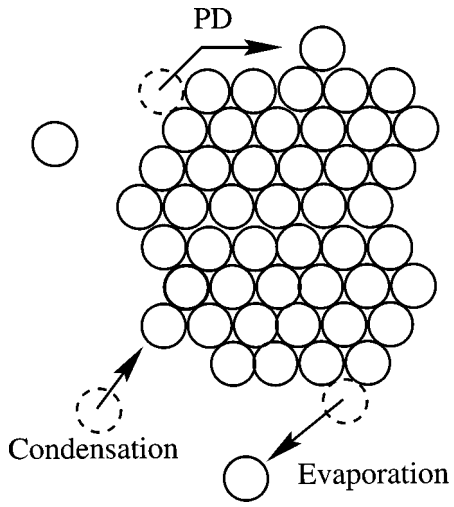

FIG. 26. Individual atomic mechanisms leading to island diffusion. PD refers to diffusion of atoms on the periphery of the island, while the exchange of atoms between the island and the atomic 2D gas is shown by the condensation and evaporation labels: dashed circles, old positions of the atoms; continuous circles, new positions, after the elementary process.

1. 2D island ddiffusion mechanisms

There are two main types of mechanisms proposed to account for 2D island diffusion: single adatom motion and collective (simultaneous) atom motion. It should be noted that small islands (fewer than ~ 15 atoms) are likely to move by specific mechanisms, depending on the details of the island geometry and atomic energy barriers (Kellogg, 1994a, 1994b; Liu *et al.*, 1994). Therefore I concentrate here on larger 2D islands.

a. Individual mechanisms

The most common mechanism invoked to account for 2D island diffusion has been that of individual atomic motion. By individual, I mean that the movement of the whole island can be decomposed into the motion of uncorrelated single atoms. There are two main examples of such diffusion: evaporation-condensation (EC) and periphery diffusion (PD). Theoretical investigations on these individual mechanisms have generated much interest since it was conjectured that the diffusion constant D_{ind} is proportional to the number of atoms (island mass) to some power that depends on the precise mechanism (EC or PD) causing island diffusion, but not on temperature or the chemical nature of the system. If true, this conjecture would prove very useful, for it would allow us to determine experimentally the mechanism causing island migration by measuring the exponent and some details of the atom-diffusion energetics by measuring how D_{ind} depends on temperature. Unfortunately, recent studies have shown that this prediction is too simplistic, as I show now for the two different mechanisms.

(i) Periphery diffusion. Figure 26 shows the elementary mechanism leading to island diffusion via atomic motion on the edge of the island (label PD). Assuming, as did Bogicevic *et al.* (1998), that

- each atomic jump displaces the center of mass of the island by a distance of order $1/N$ (where N is the number of atoms of the island),
- each edge atom (density n_s) jumps with a rate $k \sim \exp(-E_{ed}/k_BT)$ where E_{ed} is the activation energy for jumping from site to site along the border and k_B is the Boltzmann constant.

One obtains (Bogicevic *et al.*, 1998)

$$D_{ind} \sim k n_s 1/N^2 \sim \exp(-E_{ed}/k_BT) N^{-3/2} \tag{7.1}$$

if one postulates that n_s, the mean concentration of edge atoms, is proportional to the perimeter of the island (i.e., to $N^{1/2}$). This equation allows us, in principle, to determine the edge activation energy by measuring the temperature dependence of D_{ind}.

However, recent experiments (Pai *et al.*, 1997) and kinetic Monte Carlo simulations (Voter, 1986; Sholl and Skodje, 1995; Shao *et al.*, 1996; Bogicevic *et al.*, 1998) have suggested that Eq. (7.1) is wrong. First, the size exponent is not universal but depends on the precise energy barriers for atomic motion (and therefore on the chemical nature of the material) and, second, the measured activation energy does not correspond to the atomic edge diffusion energy. The point is that the limiting mechanism for island diffusion is corner breaking, for islands would not move over long distances simply by edge diffusion of the outer atoms (Bogicevic *et al.*, 1998). Further studies are needed to fully understand and quantify the periphery diffusion mechanism.

(ii) Evaporation-condensation. An alternative route to diffusion is by exchange of atoms between the island and a 2D atomic gas. This is the usual mechanism leading to Ostwald ripening (Zinke-Allmang *et al.*, 1992). Atoms can randomly evaporate from the island and atoms belonging to the 2D gas can condense on it (Fig. 26). This leads to fluctuations in the position of the island center of mass, which are difficult to quantify because of the possible correlations in the atomic evaporation and condensation. Indeed, an atom that has just evaporated from an island is likely to condense on it again, which cannot be accounted for by a mean-field theory of island-gas exchange of atoms (Van Siclen, 1995; Soler, 1996). The mean-field theory leads to a diffusion coefficient scaling as the inverse radius of the island (Wen *et al.*, 1994, 1996), while correlations cause a slowing down of diffusion, which scales as the inverse square radius of the island (Sholl and Skodje, 1995; Van Siclen, 1995; Khare and Einstein, 1996; Soler, 1996).

Experimentally, Wen *et al.* (1994, 1996) have observed by STM the movement of Ag 2D islands on Ag(100) surfaces. They measured a diffusivity almost independent of the island size, which rules out the periphery-diffusion mechanism and roughly agrees with their (Wen *et al.*, 1994, 1996) calculation of the size dependence of the evaporation-condensation mechanism. Since this calculation has been shown to be only approximate, further theoretical and experimental work is needed to clarify the role of evaporation-condensation

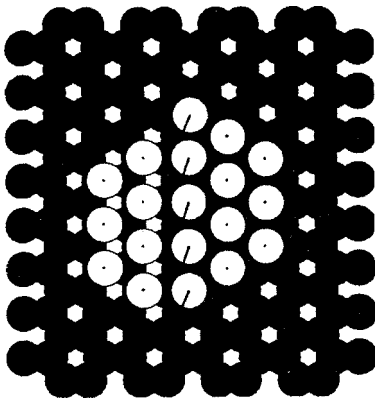

FIG. 27. Principle of island motion by dislocation propagation. The atomic column in the middle of the island jumps from fcc to hcp sites, moving the island center of mass. From Hamilton *et al.* (1995).

in 2D island diffusion. However, the work by Wen *et al.* (1994, 1996) has convincingly shown that these islands move significantly and that, for silver, island diffusion is the main route to the evolution of the island size distribution, contrary to what was usually assumed (Ostwald ripening exclusively due to atom exchange between islands, via atom diffusion on the substrate).

b. Collective diffusion mechanisms

These individual mechanisms lead, in general, to relatively slow diffusion of the islands [of order $10^{-17}\,\mathrm{cm}^2/\mathrm{s}$ at room temperature (Wen *et al.*, 1994, Wen *et al.*, 1996)]. For small clusters, different (and faster) mechanisms, such as dimer shearing, involving the simultaneous displacement of a dimer, have been proposed (Shi *et al.*, 1996). More generally, Hamilton *et al.* (1995) have proposed a different mechanism, also involving collective motions of the atoms, which leads to fast island motion. By collective, I mean that island motion is due to a simultaneous (correlated) motion of at least several atoms of the island.

Specifically, Hamilton *et al.* (1995) proposed that dislocation motion could cause rapid diffusion of relatively small (5 to 50 atoms) homoepitaxial islands on fcc(111) surfaces. Figure 27 shows the basic idea: a row of atoms move simultaneously from fcc to hcp sites, thus allowing the motion of the dislocation and consequently of the island center of mass. Alternative possibilities suggested by Hamilton *et al.* for dislocation-mediated island motion are the ''kink'' mechanism (the same atomic row moves by sequential but correlated atomic motion) or the ''gliding'' mechanism studied below, where all the atoms of the island move simultaneously. Molecular-dynamics simulations, together with a simple analytical approach (Hamilton *et al.*, 1995) suggest that for the smallest islands ($N<20$) the gliding mechanism is favored, for intermediate sizes ($20<N<100$) the dislocation motion has the lowest activation energy, while for the largest studied islands ($N>100$) the preferential mechanism is that of ''kink'' dislocation motion. We mention at this point recent direct observations of cluster motion by field ion microscopy (Wang and Ehrlich, 1997). Figure 28 shows successive images of a compact Ir_{19} cluster moving on Ir(111). By a careful study, the authors ruled out the individual atomic mechanisms discussed above, as well as the dislocation mechanism. Instead, they suggest that gliding of the cluster as a whole is likely to explain the observed motion (Wang and Ehrlich, 1997; Wang *et al.* 1998).

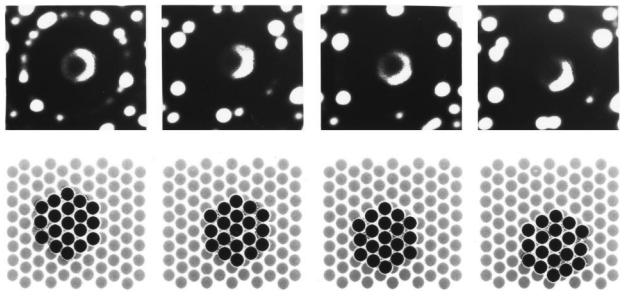

FIG. 28. Successive positions of an Ir_{19} 2D cluster on an Ir(111) surface observed by field ion microscopy at low temperature. The motion takes place at $T\sim690$ K and the figures correspond to 6, 10, and 14 heating intervals of 10 seconds each. From Wang and Ehrlich, 1997.

Hamilton later studied the case of heteroepitaxial, strained islands (Hamilton, 1996). He showed that—due to the misfit between the substrate and the island structures—there can exist islands for which introducing a dislocation does not cost too much extra energy. These metastable misfit dislocations would propagate easily within the islands, leading to ''magic'' island sizes with a very high mobility (Hamilton, 1996).

2. 3D island diffusion mechanisms

For 3D clusters, the three microscopic mechanisms presented above are possible in principle. However, as noted above, the individual atom mechanisms lead to a diffusivity smaller than the diffusion of Sb_{2300} on graphite by several orders of magnitude. These mechanisms have also been ruled out for the diffusion of gold crystallites on ionic substrates (Kern *et al.*, 1979). Several tentative explanations based on the gliding of the cluster as a whole over the substrate have been proposed (Kern *et al.*, 1979). Reiss (1968) showed that, for a rigid crystallite that is not in epitaxy on the substrate, the activation energy for rotations might be weak, simply because during a rotation, the energy needed by atoms that have to climb up a barrier is partially offset by the atoms going into more stable positions. Therefore the barrier for island diffusion is of the same order as that for an atom, as long as the island does not reach an epitaxial orientation. Masson *et al.*, 1971, and Kern *et al.*, 1979 allowed for a partial rearrangement of the interface between the island and the substrate when there is a misfit. The interface would be composed of periodically disposed zones in registry with the substrate, surrounded with perturbed (''amorphous'') zones, weakly bound to the substrate. This theory—similar in spirit to the dislocation theory proposed by Hamilton (Hamilton *et al.*,

1995; Hamilton, 1996) for 2D islands—leads to reasonable predictions (Kern *et al.*, 1979) but is difficult to test quantitatively.

To clarify the microscopic mechanisms of 3D cluster diffusion, I now present in detail molecular-dynamics (MD) studies carried out recently (Deltour *et al.*, 1997). These simulations aimed at clarifying the generic aspects of the question rather than modeling a particular case. Both the cluster and the substrate are made up of Lennard-Jones atoms (Lennard-Jones, 1924), interacting through potentials of the form

$$V(r)=4\epsilon\left[\left(\frac{\sigma}{r}\right)^{12}-\left(\frac{\sigma}{r}\right)^{6}\right].$$

Empirical potentials of this type, originally developed for the description of inert gases, are now commonly used to model generic properties of condensed systems. Lennard-Jones potentials include only atom-atom pair interaction and ensure a repulsive interaction at small atomic distances and an attractive interaction at longer distances, the distance scale being fixed by σ and the energy scale by ϵ. For a more detailed discussion of the different interatomic potentials available for MD simulations and their respective advantages and limitations, see (Mater. Res. Soc. Bulletin, 1996a). The substrate is modeled by a single layer of atoms on a triangular lattice, attached to their equilibrium sites by weak harmonic springs that preserve surface cohesion. The Lennard-Jones parameters for cluster atoms, substrate atoms, and the interaction between them are, respectively, $(\epsilon_{cc},\sigma_{cc})$, $(\epsilon_{ss},\sigma_{ss})$, and $(\epsilon_{sc},\sigma_{sc})$. ϵ_{cc} and σ_{cc} are used as units of energy and length. ϵ_{sc}, σ_{ss}, and T, the temperature of the substrate, are the control parameters of the simulation. The last two parameters are then constructed by following the standard combination rules: $\epsilon_{ss}=\sigma_{ss}^{6}$ and $\sigma_{sc}=\frac{1}{2}(\sigma_{cc}+\sigma_{ss})$. Finally, the unit of time is defined as $\tau=(M\sigma_{cc}^{2}/\epsilon_{cc})^{1/2}$, where M is the mass of the atoms, which is identical for cluster and substrate atoms. The simulation uses a standard molecular-dynamics technique with thermostatting of the surface temperature (Allen and Tidesley, 1987).

In these simulations, the clusters take the spherical cap shape of a solid droplet (Fig. 29) partially wetting the substrate. The contact angle, which can be defined following Hautman and Klein (1991), is roughly independent of the cluster size (characterized by its number of atoms n, for $50<n<500$). This angle can be tuned by changing the cluster-substrate interaction. For large enough ϵ_{sc}, total wetting is observed. The results presented below have been obtained at a reduced temperature of 0.3 for which the cluster is solid. This is clearly visible in Fig. 29, where the upper and lower halves of the cluster, (in the top view) colored white and gray at the beginning of the run, clearly retain their identity after the cluster center of mass has moved over three lattice parameters. Hence the cluster motion appears to be controlled by collective motions of the cluster as a whole rather than by single atomic jumps.

The MD simulations have confirmed that one of the most important parameters for determining the cluster

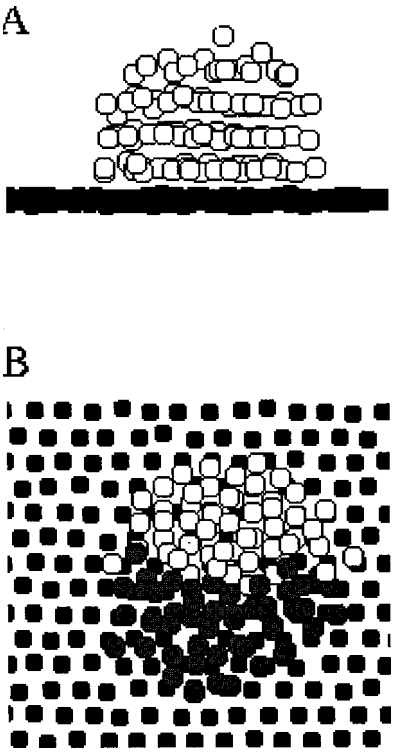

FIG. 29. Configuration of a Lennard-Jones cluster on the crystalline surface. (A) Side view—The cluster is partially wetting the surface. (B) Top view—The two halves of the cluster have been colored at the beginning of the run. After the cluster center of mass has moved by roughly three substrate lattice constants from its original position, the two parts of the cluster are still well distinct. Then the cluster diffusion cannot be explained in terms of single-atom mechanisms ($n=100$, $\sigma_{ss}=0.7$, $\epsilon_{sc}=0.4$, $T=0.3$).

diffusion constant is the ratio of the cluster lattice parameter to the substrate lattice parameter. The results for the diffusion coefficient are shown in Fig. 30(a). When the substrate and cluster are commensurate ($\sigma_{ss}=\sigma_{cc}\equiv 1$), the cluster can lock into a low-energy epitaxial configuration. A global translation of the cluster would imply overcoming an energy barrier scaling as $n^{2/3}$, the contact area between the cluster and the substrate. In that case diffusion will be very slow, unobservable on the time scale of the MD simulations. What is interesting to note is that even small deviations from this commensurate case lead to a measurable diffusion on the time scale of the MD runs. This can be understood from the fact that the effective potential in which the center of mass moves is much weaker, as the cluster atoms, constrained to their lattice sites inside the rigid solid cluster, are unable to adjust to the substrate potential [see above, Reiss model (Reiss, 1968)]. The effect is rather spectacular: a 10% change on the lattice parameter induces an increase in the diffusion coefficient by several orders of magnitude.

Finally, I show in Fig. 30(b) the effect of cluster size on the diffusion constant for different lattice parameter values. As the number n of atoms in the cluster is varied between $n=10$ and $n=500$, the diffusion constant de-

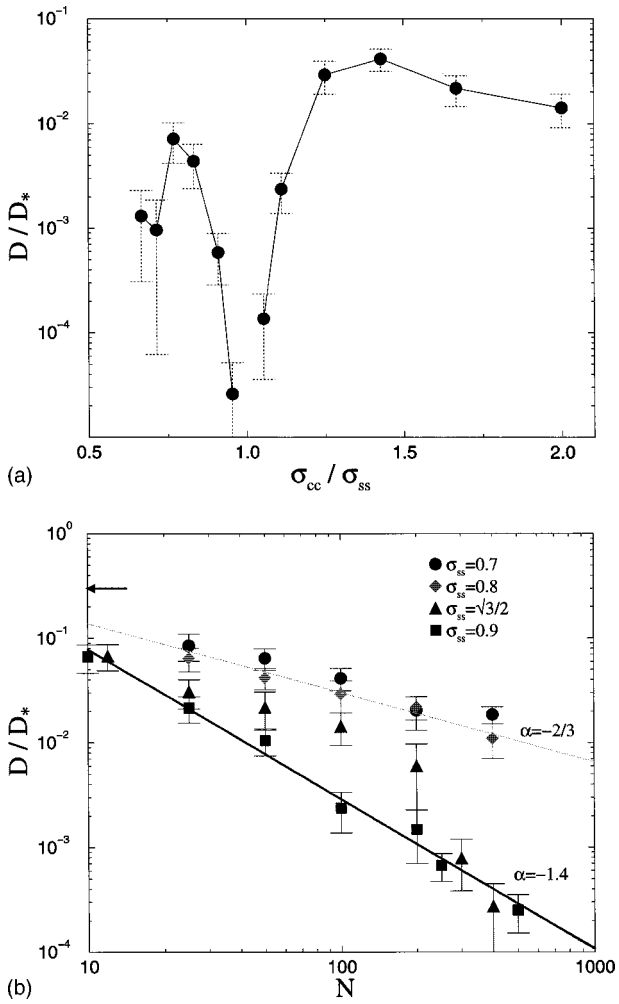

FIG. 30. MD simulations of cluster diffusion. (a) Dependence of the diffusion coefficient on the mismatch between the lattice parameter of the substrate and the cluster. A small change in the lattice parameter of the cluster leads to a huge change in the diffusivity ($n=100$, $\epsilon_{sc}=0.4$, $T=0.3$, Run Length $=12\,500\ \tau$); (b) dependence of the diffusion coefficient of a cluster on number of atoms. Data correspond to different mismatches between the cluster and the substrate lattice parameters. The diffusion coefficient decreases as a power law with exponent α. The two different slopes correspond to different diffusion regimes: the weaker dependence corresponds to a Brownian trajectory; the stronger corresponds to a "hopping-like" diffusion. For comparison, the arrow indicates the diffusion coefficient of a single adatom with $\sigma_{ss}=0.9$.

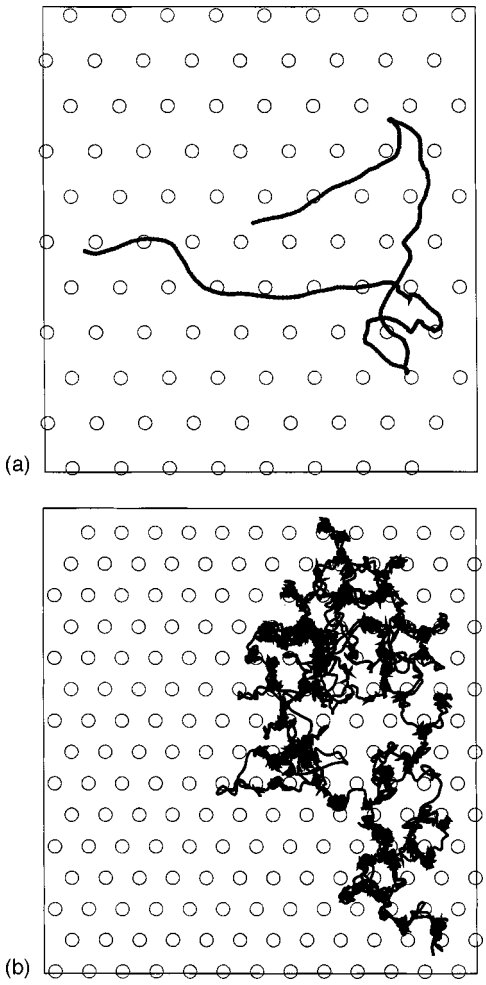

FIG. 31. Trajectory of a cluster center of mass diffusing on a substrate. The solid line represents the trajectory and the circles, the equilibrium position of the surface atoms. (a) Large mismatch: the motion is "Brownian-like," i.e., the cluster does not "see" the structure of the surface. The values of the parameters are $\epsilon_{sc}=0.4$, $\sigma_{ss}=0.7$, $T=0.3$, and $n=100$; (b) small mismatch: the cluster center of mass jumps from one hexagon center to a nearest-neighbor one. The values of the parameters are the same as for (a), except for $\sigma_{ss}=0.9$.

creases, roughly following a power law $D\sim n^{\alpha}$. This power-law exponent α depends significantly on the mismatch between the cluster and the substrate lattice parameters. For high mismatches ($\sigma_{ss}=0.7,0.8$), α is close to -0.66. As the diffusion constant is inversely proportional to the cluster-substrate friction coefficient, this result is in agreement with a simple "surface of contact" argument yielding $D\sim n^{-2/3}$. On the other hand, when the lattice mismatch is equal to 0.9, one obtains $\alpha\approx -1.4$, although the shape of the cluster, characterized by the contact angle, does not appreciably change. It is instructive to follow the trajectory followed by the cluster center of mass (Fig. 31). In the runs with a large mismatch [Fig. 31(a)], this trajectory is "Brownian-like," with no apparent influence of the substrate. This is consistent with the simple "surface of contact" argument. However, when the mismatch is small [Fig. 31(b)], the center of mass of the cluster follows a "hopping-like" trajectory, jumping from site to site on the honeycomb lattice defined by the substrate. When $\sigma_{ss}=\sqrt{3}/2$, there seems to be a transition between the two regimes around $n=200$.

It is interesting to consider the interpretation of cluster motion in terms of dislocation displacement within the cluster, a mechanism that has been proposed to explain rapid 2D cluster diffusion (Hamilton *et al.*, 1995; Hamilton, 1996; see the discussion in Sec. VII. A.1). For this, one can "freeze" the internal degrees of freedom of the cluster deposited on a thermalized substrate. The center-of-mass trajectory is integrated using the quaternion algorithm (Allen and Tidesley, 1987; Deltour *et al.*,

1997). Surprisingly, the diffusion constant follows the same power law as in the free-cluster case (Deltour *et al.*, 1997). This result proves that the diffusion mechanism in this case cannot be simply explained in terms of dislocation migration within the cluster, as proposed by Hamilton *et al.* (1995) and Hamilton (1996) to explain the diffusion of 2D islands. As the substrate atoms are tethered to their lattice site, strong elastic deformations or dislocations within the lattice are also excluded. Hence the motor for diffusion is here the vibrational motion of the substrate, and its efficiency appears to be comparable to that of the internal cluster modes.

Very recently, Luedtke and Landmann (1999) performed MD simulations of the diffusion of large gold clusters on HOPG substrates. They found high cluster mobility, in agreement with the preceding simulations. Their studies suggest that cluster diffusion in this case proceeds by two different mechanisms: long (several cluster diameters) linear ''flights'' separated by relatively slow diffusive motion, as observed in the preceding simulations. Further work is needed to ascertain the atomic mechanisms leading to this kind of motion.

3. Discussion

What are the (partial) conclusions that can be drawn from these studies of cluster diffusion? I think that the main parameter determining the mobility of 3D islands on a substrate is the possible epitaxy of the cluster on the substrate. Indeed, if the island reaches an epitaxial orientation, it is likely to have a mobility limited by the individual atomic movements, which give a small diffusion constant (of order $10^{-17}\,\mathrm{cm}^2\,\mathrm{s}^{-1}$ at room temperature). Diffusivities of this magnitude will not affect the growth of cluster films during typical deposition times, and clusters can be considered immobile. The effect of these kinds of diffusion rates can only be seen by annealing the substrates at higher temperatures or for long times. According to Hamilton (Hamilton *et al.*, 1995), dislocations could propagate even for epitaxial islands, but it is likely that this mechanism is more important in the case of heteroepitaxial islands, which I now proceed to discuss. Indeed, if the island is not in epitaxy on the substrate, high mobilities can be observed because the cluster sees a potential profile that is not very different from that seen by a single atom. It should be noted that this nonepitaxy can be obtained when the two lattice parameters (of the substrate and the island) are very different, or also when they are compatible if there is relative misorientation. The latter has been observed for gold on ionic substrates (Kern *et al.*, 1979) and mobility is relatively high until the crystallites reach epitaxy.

The MD simulations presented above show that, for Lennard-Jones (LJ) potentials, only homoepitaxy prevents clusters from moving rapidly on a surface. It should be noted that relaxation of the cluster or the substrate—which would favor a locking of the cluster in an energetically favorable position at the expense of some elastic energy—has not been observed in these LJ simulations, nor has dislocation propagation. This is probably realistic for the low interaction energies that correspond to metal clusters on graphite. It could also be argued that dislocation motion is more difficult in 3D clusters than in 2D islands, since the upper part of the particle (absent in 2D islands) tends to keep a fixed structure.

Another important parameter is the cluster-substrate interaction: one would think that a large attractive interaction (for metal-on-metal systems, for example) could induce an epitaxial orientation and prevent the cluster from diffusing, even in the heteroepitaxial case. The differences between the diffusion of clusters grown on a substrate by atom deposition and aggregation and those previously formed in a beam and deposited must also be investigated. One could anticipate that islands formed by atom aggregation *on* the substrate would accommodate easily to the substrate geometry, whereas preformed clusters might keep their (metastable) configuration. However, it is not at all clear that island nucleation and epitaxy are simultaneous phenomena, for it has been observed that islands can form in a somewhat arbitrary configuration and subsequently orient on the substrate after diffusion and rotation (see Kern *et al.*, 1979).

B. Cluster-cluster coalescence

What happens now when two clusters meet? If they remain simply juxtaposed, morphologies similar to Fig. 18(a) are observed. In this case, the incident clusters have retained their original morphology, and the supported particles are identical to them, even if they are in contact with many others after cluster diffusion. It is clear, by looking, for example, at Fig. 22 that this is not always the case. Sometimes, the supported islands are clearly larger than the incident clusters: some coalescence has taken place. How can one understand and predict the size of the supported particles? Which are the relevant microscopic parameters? This section tries to answer these questions, which are of dramatic interest for catalysis, since the activity of the deposits crucially depends on specific area and therefore on the sintering process (see, for example, Ruckenstein and Pulvermacher, 1973; Dadybujor *et al.*, 1986; Stevenson *et al.*, 1987).

We shall first briefly examine the classical theory for sphere-sphere coalescence (i.e., ignoring the effect of the substrate) and then review recent molecular-dynamics simulations that suggest that this classical theory may not be entirely satisfactory for nanoparticles.

1. Continuum theory of coalescence

The standard analysis of the kinetics of sintering is due to Mullins and Nichols (Mullins, 1957; Nichols and Mullins, 1965; Nichols, 1966). The ''motor'' of the coalescence is the diffusion of atoms of the cluster (or island) surface from the regions of high curvature (where they have fewer neighbors and therefore are less bound)

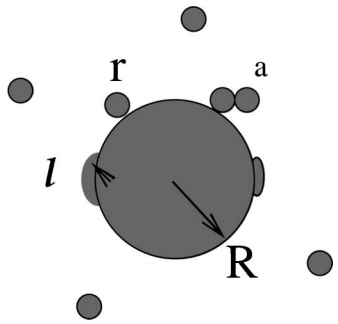

FIG. 32. Schematic illustration of the competition between coalescence and kinetic ramification. R is the radius of the largest island, r that of the incident clusters, and l stands for the typical length of a coalescing cluster. The label "a" refers to the ramification process when a cluster is touched by another one before coalescence can take place.

towards the regions of lower curvature. The precise equation for the atom flux is (Nichols and Mullins, 1965; Nichols, 1966)

$$\vec{J}_s = -\frac{D_s \gamma \Omega \nu}{k_B T} \overrightarrow{\nabla_s K}, \tag{7.2}$$

where D_s is the surface diffusion constant (supposed to be isotropic), γ the surface energy (supposed to be isotropic too), Ω the atomic volume, ν the number of atoms per unit surface area, k_B Boltzmann's constant, T the temperature, and K the surface curvature ($K = 1/R_1 + 1/R_2$) where R_1 and R_2 are the principal radii of curvature. For sphere-sphere coalescence, an order-of-magnitude estimate of the shape changes induced by this flux is (Nichols and Mullins, 1965; Nichols, 1966)

$$\frac{\partial n}{\partial t} \sim 2B \frac{\partial^2 K}{\partial s^2}(y = s = 0), \tag{7.3}$$

where dn is the normal outward distance traveled by a surface element during dt, s the arc length, and $B = D_s \gamma \Omega^2 \nu / k_B T$ (the z axis is taken as the axis of revolution). For this geometry, Eq. (7.3) becomes (Fig. 32)

$$\frac{\partial l}{\partial t} \sim \frac{B}{l^3}\left(1 - \frac{l}{R}\right), \tag{7.4}$$

where I have made an order-of-magnitude estimate of the second derivative of the curvature: $\partial K/\partial s \sim (K(R) - K(l))/l$ and similarly $\partial^2 K/\partial s^2 \sim (1 - l/R)/l^3$ (see Fig. 32). Integrating Eq. (7.4) leads to

$$l \sim (r^4 + 4Bt)^{1/4} \quad \text{for} \quad l \ll R. \tag{7.5}$$

Equation (7.5) gives an estimate of the coalescence kinetics for two spheres of radius r and R.

Despite its plausibility, Eq. (7.5) has to be used with care. First, the calculation leading to it from the expression of the flux [Eq. (7.2)] is only approximate. More importantly, Eq. (7.2) assumes isotropic surface tension and diffusion coefficients. While this approximation may be fruitful for large particles [in the μm range (Heyraud *et al.*, 1989)], it is clearly wrong for clusters in the nanometer range. These are generally faceted (Buffat and Borel, 1976; Flüelli *et al.*, 1988; Lewis *et al.*, 1997) as a result of anisotropic surface energies. This has two important consequences: First, since the particles are not spherical, the atoms do not feel a uniform curvature. For those located on the planar facets, the curvature is even 0, meaning that they will not tend to move away spontaneously. This effect should significantly reduce the atomic flux. This point has recently been confirmed by KMC simulation (Jensen *et al.*, 1999). Second, the diffusion is hampered by the edges between the facets (Valkealahti and Manninen, 1998), which induce a kind of Schwoebel effect (Schwoebel and Shipsey, 1966; Schwoebel, 1969; Villain, 1991). Then the effective mass transfer from one end of the cluster to the other may be significantly lower than expected from the isotropic curvatures used in Eq. (7.2). For these anisotropic surfaces, a more general formula that takes into account the dependence of γ on the crystallographic orientation should be used [see, for example, Villain and Pimpinelli (1995)]. However, this formula is of limited practical interest for two reasons. First, the precise dependence of the surface energy on the crystallographic orientation is difficult to obtain. Second, as a system of two touching faceted clusters does not, in general, show any symmetry, the solution to the differential equation is hard to find. One possibility currently being explored (Combe *et al.*, 1998) is to assume a simple analytical equation for the anisotropy of 2D islands and integrate numerically the full (anisotropic) Mullins' equations.

2. Molecular-dynamics simulations of coalescence

Since continuum theories face difficulties in characterizing the evolution of nanoparticle coalescence, it might be useful to perform molecular-dynamics (MD) studies of this problem. Several studies (Yu and Duxbury, 1995; Zhu and Averback, 1996; Lewis *et al.*, 1997) have been performed, showing that two distinct and generally sequential processes lead to coalescence for particles in the nanometer range: plastic deformation (Zhu and Averback, 1996) and slow surface diffusion (Yu and Duxbury, 1995; Lewis *et al.*, 1997).

Zhu and Averback (1996) studied the first stages (up to 160 ps) of the coalescence of two single-crystal copper nanoparticles (diameter 4.8 nm). Figure 33 presents four stages of the coalescence process, demonstrating that plastic deformation takes place (see the arrows indicating the sliding planes) and that a relative rotation of the particles occurs during this plastic deformation [(c) and (d)]. During the first 5 ps, the deformation is elastic, until the elastic limit [roughly 0.8 nm (Zhu and Averback, 1996)] is reached: after this, since the shear stress (Fig. 34) is very high, dislocations are formed and glide on (111) planes in the $\langle 110 \rangle$ direction, as usually seen in fcc systems. Figure 34 also shows that after 40 ps [i.e., Fig. 33(c)] the stress on the glide plane is much smaller and dislocation motion is less important: the two particles rotate until a low-energy grain boundary is found [Fig. 33(d)]. This initial stage of the coalescence, where the two particles reorient and find a low-energy configuration, is very rapid, but does not lead in general to

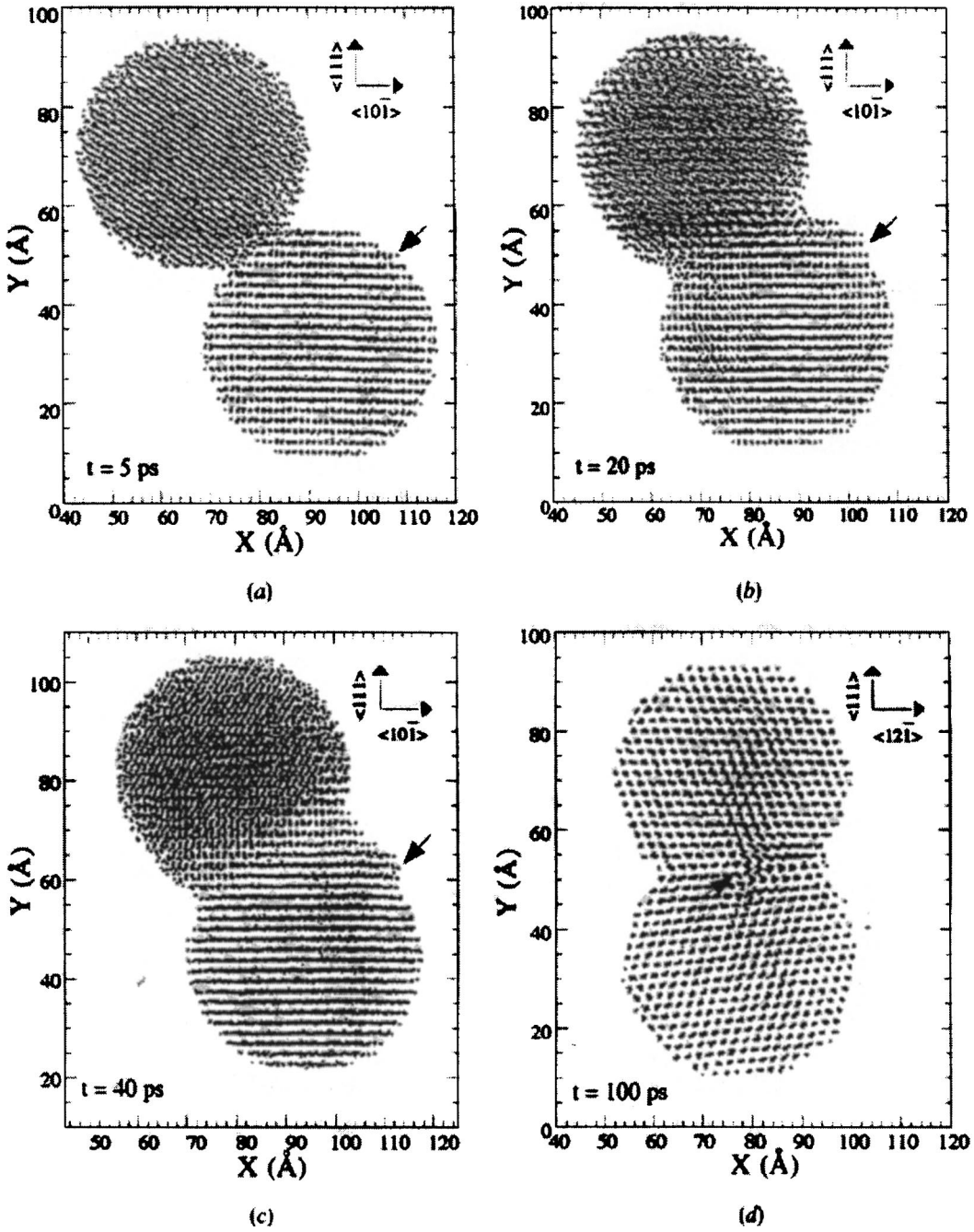

FIG. 33. Atomic positions at four different times during partial coalescence of Cu clusters (4.8-nm diameter each). The atomic positions are projected onto the $(12\bar{1})$ plane of the bottom sphere for (a) to (c) and onto the $(10\bar{1})$ plane for (d). The arrows indicate the sliding plane [(a) to (c)] and the grain-boundary dislocation (d). From Zhu and Averback (1996).

thorough coalescence. An interesting exception may have been found by Yu and Duxbury (1995): their MD simulations showed that for very small clusters (typically less than 200 atoms) coalescence is abrupt provided the temperature is sufficiently close to the melting temperature. They argue that this is due to a (not specified) ''nucleation process'': plastic deformation is a tempting possibility.

For larger clusters, the subsequent stages are much slower and imply a different mechanism: atom diffusion on the surface of the particles. The intial stages of this diffusion-mediated coalescence have been studied by Lewis *et al.* (1997). Their aim was to determine whether Mullins' (continuum) predictions were useful in this size domain. In Lewis *et al.*'s simulations, the embedded-atom method (Foiles *et al.*, 1986) was used to simulate the behavior of unsupported gold clusters for relatively long times ($\sim$10 ns). Evidently, an important role of the substrate in the actual coalescence of supported clusters is to ensure thermalization, which is taken care of here by coupling the system to a fictitious ''thermostat'' (Allen and Tildesley, 1987; Frenkel and Smit, 1996). One therefore expects these coalescence events to be relevant to the study of supported clusters when they are

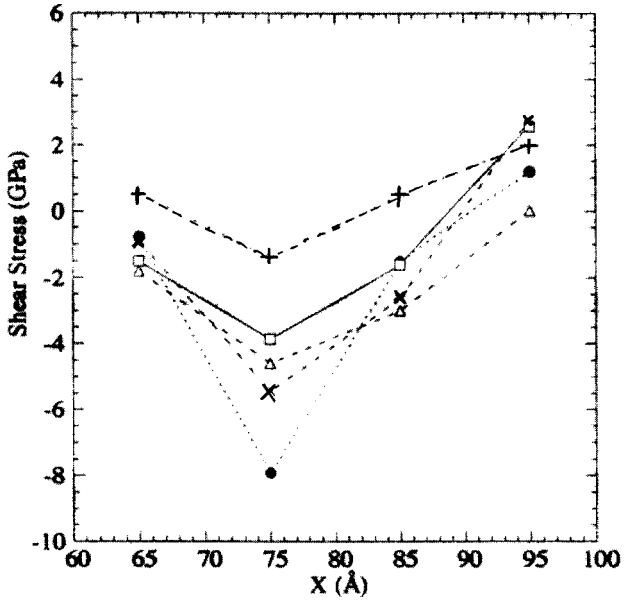

FIG. 34. Distribution of shear stress in a sliding plane at different times during the coalescence shown in Fig. 33: ●, 5 ps; □, 10 ps; △, 20 ps; ×, 30 ps; +, 40 ps. From Zhu and Averback (1996).

loosely bound to the substrate, e.g., for gold clusters on a graphite substrate. Strong interaction of the clusters with the substrate may be complicated and lead to cluster deformation even for clusters deposited at low energies, for example, if the cluster wets the substrate (Luedtke and Landman, 1994; Hou, 1998).

Figure 35 shows the evolution of the ratio x/R, where x is the radius of the neck between the two particles. After an extremely rapid approach of the two clusters due to the mechanisms studied above (plastic deformation), a slow relaxation to a spherical shape begins (Fig. 36). The time scale for the slow sphericization process is difficult to estimate from Fig. 35, but it would appear to

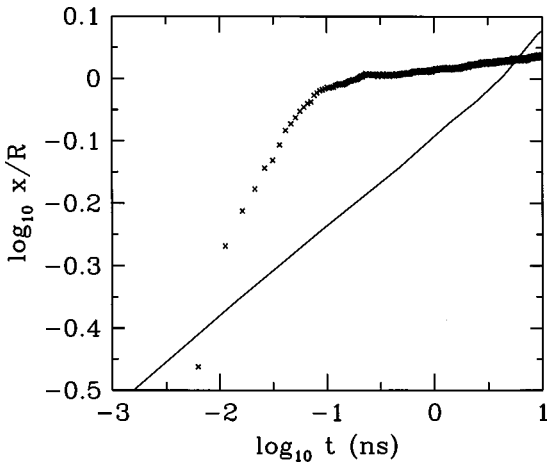

FIG. 35. Evolution in time of the ratio of the neck radius x to the cluster radius R. The solid line represents the numerical solution obtained by Nichols (1966) with an arbitrary time scale, while the crosses are the results of Lewis *et al.*'s (1997) simulations.

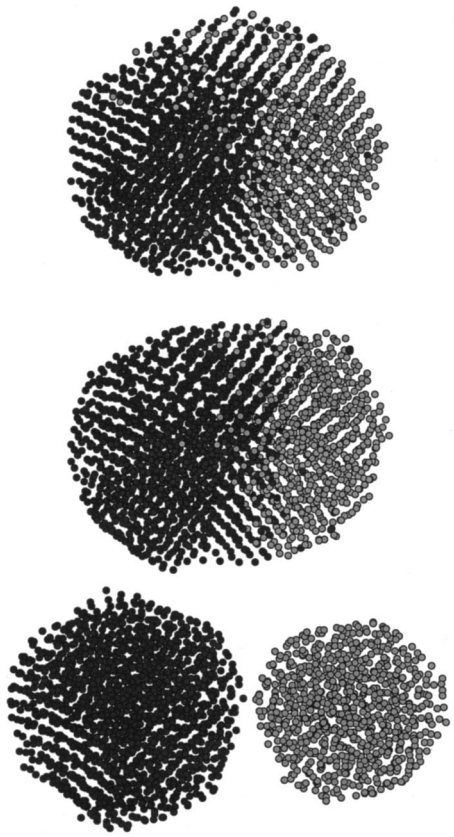

FIG. 36. Successive cluster morphologies during the coalescence of a gold 767-atom liquid cluster with another gold 1505-atom solid cluster. The figures represent three stages of the coalescence process after 0, 1, and 10 ns, i.e., times much longer than those studied by Zhu and Averback (1996).

be of the order of a few hundred ns or more. This number is substantially larger than one would expect on the basis of phenomenological theories of the coalescence of two soft spheres. Indeed, Nichols and Mullins (1965; Nichols, 1966) predict a coalescence time for two identical spheres $\tau_c = k_B T R^4/(C D_s \gamma a^4)$, where D_s is again the surface diffusion constant, a the atomic size, γ the surface energy, R the initial cluster radius, and C a numerical constant [$C=25$ according to Nichols and Mullins (1965) and Nichols (1966)]. Taking $D_s \sim 5 \times 10^{-10}\,\mathrm{m^2\,s^{-1}}$ (the average value found in the simulations; see Lewis *et al.*, 1997), $R=30$ Å, $\gamma \approx 1\,\mathrm{J\,m^{-2}}$, and $a=3$ Å, yields a coalescence time τ_c of the order of 40 ns. The same theories, in addition, make definite predictions on the evolution of the shape of the system with time. In particular, in the tangent-sphere model, the evolution of the ratio x/R is found to vary (Nichols and Mullins, 1965; Nichols, 1966) as $x/R \sim (t/\tau_c)^{1/6}$ for values of x/R smaller than the limiting value $2^{1/3}$. In Fig. 35, the prediction of this simple model (solid line) is compared with the results of the present simulations. There is no agreement between model and simulations. The much longer coalescence time observed has been attributed (Lewis *et al.*, 1997) to the presence of facets on the initial clusters, which persist (and rearrange) during coalescence. The facets can be seen in the initial and interme-

diate configurations of the system in Fig. 36; the final configuration of Fig. 36 shows that the cluster is more spherical (at least from this viewpoint), and that new facets are forming. That diffusion is slow can in fact be seen from Fig. 36: even after 10 ns, at a temperature only about 200 degrees below melting for a cluster of this size, very few atoms have managed to diffuse a significant distance away from the contact region.

The precise role of the facets in the coalescence process is a subject of current interest. Experiments have shown that shape evolution is very slow in the presence of facets for 3D crystallites (see, for example, Dreschler *et al.*, 1981; Métois and Heyraud, 1981; Meunier, 1995). Recent experiments (Stoldt *et al.*, 1998) and computer simulations (Jensen *et al.*, 1999) on 2D islands suggest that the presence of facets can be effective in slowing down the coalescence process. Clearly, more work is needed to get a quantitative understanding of the coalescence, of nanoparticles and to evaluate the usefulness of Mullins' approach, especially if one manages to include the crystalline anisotropy (see also Selke and Duxbury, 1994; Adam *et al.*, 1997).

C. Island morphology

We turn now to the prediction of one of the essential characteristics of cluster films the size of the supported particles. As I have already mentioned in the introduction, the size of the nanoparticles controls many interesting properties of the films. Therefore even an approximate result may be useful, and this is what I obtain in this section.

The experiments shown above demonstrate that the supported particles can have a variety of sizes, from that of the incident clusters (Sb_{2300}/HOPG, Sec. VI. A) up to many times this size (for example, Au_{250}/HOPG, Sec. VI. B.3). To understand how the size of the supported particles is determined, one can look at a large circular island to which clusters are arriving by diffusion on the substrate (Fig. 32). There are two opposing effects at work here. One is the thermodynamic tendency of the system to minimize its surface (free) energy. Therefore one expects the clusters touching an island to coalesce with it, leading to compact (spherical) domains. The other process, driving the system away from this minimization, is the continuous arrival of clusters on the island edge. This kinetic effect tends to form ramified islands. What is the result of this competition? Since there is a kinetically driven ramification process, it is essential to take into account the kinetics of cluster-cluster coalescence, as sketched in the previous section. I shall use Eq. (7.5), even if it is only approximate, to derive an upper limit for the size of the compact domains grown by cluster deposition. This will be an upper limit since, as pointed out in the previous section, coalescence for faceted particles could be slower than predicted by Eq. (7.5), hence diminishing the actual size of these domains.

We first need an estimate of the kinetics of the second process: the impinging of clusters on the large island. A very simple argument is used here [see also Pimpinelli *et al.*, (1993) and Bales and Chrzan (1995) for a similar analysis for atomic growth]: since the number of clusters reaching the surface is F per unit surface per second and the total number of islands is N_t per unit surface, each island receives on average a cluster every $t_r = N_t/F$.

We are now in a position to quantify the degree of coalescence in a given growth experiment. Let us suppose that a cluster touches a large island at $t=0$. If no cluster impinges on the island before this cluster completely coalesces [in a time τ_c according to Eq. (7.5)], then the islands are compact (circular). But, if a cluster touches the previous cluster before its total coalescence has taken place, it will almost freeze up the coalescence of the previous cluster. This is because now the atoms on the (formerly) outer surface of the first cluster do not feel curvature since they have neighbors on the second cluster. The mobile atoms are now those of the second cluster [see Fig. 32(a)] and the coalescence takes a longer time to proceed (the atoms are farther form the large island). Then, if $t_r \ll \tau_c$, the islands formed on the surface are ramified. For intermediate cases, the size R_c of the compact domains can be estimated from Eq. (7.5) as $R_c = x(\tilde{t}_r)$, where $\tilde{t}_r$ takes into account the fact that, to freeze the coalescence of a previous cluster, one cluster has to touch the island at roughly the same point: $\tilde{t}_r \simeq t_r 2\pi R/r$ and

$$R_c^4 = r^4 + 4B\frac{2\pi R_c}{r}\frac{N_t}{F}. \tag{7.6}$$

Equation (7.6) describes the limiting cases ($B \sim \infty$ or $B \sim 0$) correctly. The challenge with the intermediate cases is to obtain a reliable estimate of the (average) atomic surface self-diffusion. For gold, Chang and Thiel (1994) give values that vary between 0.02 eV on compact facets and 0.8 eV on more open surfaces. One solution is to go the other way around and estimate D_s from the experimental data and Eq. (7.6). From Fig. 22, estimating R_c from the thickness of the island arms, and using the experimental values for r (0.85 nm) and the fact that since the flux is pulsed (see Sec. VI. B.3), the time between two successive arrivals of clusters is approximately the time between two pulses (0.1 s), and not N_t/F, one obtains $D_s \simeq 3\times 10^{-3}$ cm^2 s^{-1} exp$(-0.69$ eV$/(k_B T))$, which seems a sensible value.

Despite the difficulty of defining average diffusion coefficients, one can use Eq. (7.6) to obtain a reasonable guess for the size of the compact domains by assuming that D_s is thermally activated: $D_s(T) = D_0 \exp(-E_a/(k_B T))$ with a prefactor $D_0 = 10^{-3}$ cm^2 s^{-1} and an activation energy E_a taken as a fraction of the bonding energy between atoms (proportional to $k_B T_f$). One obtains (Jensen, 1998b)

$$B = 10^{11} \exp(-4.6 T_f/T) \text{ nm}^4/\text{s}. \tag{7.7}$$

Inserting this value in Eq. (7.6) leads to Fig. 37, where the size of the compact domains is plotted as a function of T/T_f. The important feature is that as long as $T/T_f \leqslant 1/4$, the incident particles do not merge. Note that this 1/4 is sensitive to the assumed value of D^*, but only via

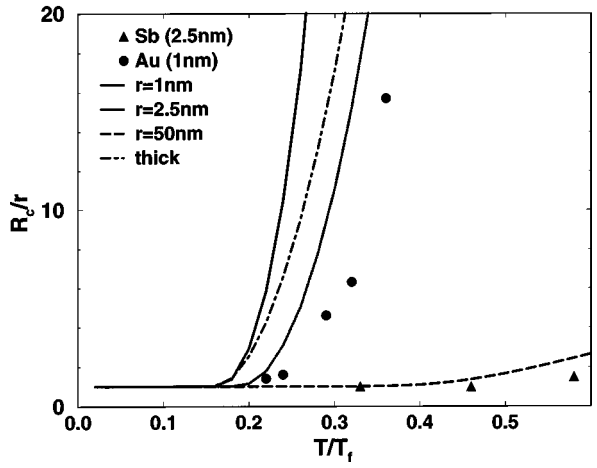

FIG. 37. Approximate dependence of the radius of the supported particles R_c as a function of the substrate temperature for submonolayer and thick films. Lines refer to predictions from Eq. (7.6) with different incident cluster radii, while symbols represent experimental results. The theoretical predictions for the submonolayer regime were obtained by taking $N_t/F=0.1$ and using Eq. (7.7). For the thick-film limit, I used $F=10^{-3}$ ML/s and $r=2.5$ nm [Eq. (7.8)]. One should consider these theoretical R_c values as an upper limit, since coalescence may be much slower at these (nano)scales (see the text). As a consequence, it is no surprise that the predicted values are clearly larger than the experimental ones. Concerning Sb, the huge difference could come from a partial oxidation of the clusters on the substrate because of the relatively bad vacuum conditions (pressure $\sim 10^{-7}$ Torr). Even a thin oxide layer can significantly decrease atomic surface diffusion and transport, thus slowing the coalescence process.

its logarithm. Again, this estimate of R_c/r is an upper limit, since coalescence could be slower than predicted by Eq. (7.5).

What would happen now if the incident clusters were liquid? An experimental example of this liquid coalescence is given by the deposition of In_{100} on a-C (see above). A rough guess of the coalescence time is given by a hydrodynamics argument (Barrat, 1998): the driving force of the deformation is the surface curvature γ/R^2 where γ is the liquid surface tension and R the cluster radius. This creates a velocity field that one can estimate using the Navier-Stokes equation: $\eta\Delta v=\gamma/R^2$ where η is the viscosity and v is the velocity of the fluid. This leads to $\tau_c(liquid)\sim R/v\sim \eta R/\gamma$. Inserting reasonable values for both η (0.01 Pa s) and γ (1 J m^{-2}) leads to $\tau_c(liquid)\sim 0.01R$, which gives $\tau_c(liquid)=10$ ps for $R\sim 1$ nm. This is the good order of magnitude of the coalescence times found in simulations of liquid gold clusters [$\tau_c(liquid)\sim 80$ ps (Lewis *et al.*, 1997)]. Now, since $\tau_c(liquid)\ll t_r$ ($t_r\sim 0.1$ s, see above), cluster-cluster coalescence is almost instantaneous, which would lead to $R_c\sim\infty$. In fact, R_c is limited in this case by static coalescence between the large islands formed during the growth. The reason is that the large islands may be solid or pinned by defects, leading to a slow coalescence. The analysis is similar here to what has been done for atomic deposition (Jeffers *et al.*, 1994).

D. Thick films

The preceding section has studied the first stages of the growth, the submonolayer regime, which interests researchers trying to build nanostructures on the surface. I attempt here a shorter study of the growth of thick films, which are known to be very different from the bulk material in some cases (Siegel,1991, 1996; Melinon *et al.*, 1995; Edelstein and Cammarata, 1996; Perez *et al.*, 1997). The main reason for this is their microstructure, as a random stacking of nanometer-size crystallites. Therefore it is interesting to understand how the size of these crystallites is determined and how stable the nanostructured film is. One can anticipate that the physical mechanism for cluster-size evolution is, as in the submonolayer case, sintering by atomic diffusion. For thick films, however, surface diffusion can only be effective before a given cluster has been "buried" by the subsequent deposited clusters. Thus most of the size evolution takes place during growth, for later the physical routes to coalescence (bulk or grain boundary diffusion) are expected to be much slower. Studies of compacted nanopowders (Nieman *et al.* 1991; Siegel 1991, 1996) have shown that nanoparticles are very stable against grain growth. Siegel (1991, 1996) explains this phenomenon in the following way. The two factors affecting the chemical potential of the atoms, and potentially leading to structure evolutions, are local differences in cluster size or in curvature. However, for the relatively uniform grain size distributions and flat grain boundaries observed for cluster assembled materials (Siegel, 1991, 1996), these two factors are not active, and there is nothing locally telling the atoms in which direction to migrate to reduce the global energy. Therefore the whole structure is likely to be in a deep local (metastable) minimum in energy, as observed in closed-cell foams. The stability of such structures has been confirmed by several computer simulations (Celino *et al.*, 1993, 1995; Zhu and Averback, 1995), which have indicated a possible mechanism of grain growth at very high ($T/T_f\sim 0.8$) temperatures: grain boundary amorphization or melting (Zhu and Averback, 1995).

What determines the size of the supported particles during the growth? For thick films, a reasonable assumption is that a cluster impinging on a surface already covered by a layer of clusters does not diffuse, because it forms strong bonds with the layer of deposited clusters. This hypothesis has been checked for the growth of Sb_{2300} on graphite (Bardotti *et al.* 1995, 1996). The process differs from submonolayer growth in two main ways: first, an impinging cluster has more than one neighbor and the sphere-sphere kinetics are not very realistic; second, the time for ramification that was used in the preceding section is no longer useful here, since clusters do not move. As a first approximation, to get an upper limit on the size of the domains, we can use the same coalescence kinetics and take a different "ramification" time. The average time for the arrival of a cluster touching another is roughly $t_f\sim 1/(Fd^2)$, where d

$=2r$ is the diameter of the cluster. If the same formula [Eq. (7.5)] is used, one finds

$$R_c^4 = r^4 + \frac{B}{Fr^2}. \tag{7.8}$$

The results obtained using the same approximation as in the preceding section for B [Eq. (7.7)] are shown in Fig. 37.

The deposition of Ni and Co clusters has been experimentally observed (Tuaillon, 1995; Tuaillon *et al.*, 1997). The size of the crystallites is comparable to the size of the incident (free) clusters. This is compatible with Eq. (7.8) since the T_f of these elements is very high ($\simeq 1800\,K$). Therefore Eq. (7.8) predicts that films grown at $T=300K$, ($T/T_f \sim 0.17$) should keep a microstructure with $R_c \simeq r$, as is observed experimentally (Tuaillon, 1995; Tuaillon *et al.*, 1997). I stress again that a structure obtained with cluster deposition with this characteristic size is not likely to recrystallize in the bulk phase (thereby losing its nanophase properties) unless brought to temperatures close to T_f (Siegel, 1991, 1996; Celino *et al.* 1993, 1995; Zhu and Averback, 1995).

VIII. CONCLUSIONS AND PERSPECTIVES

What are the principal ideas presented in this paper?

First, useful models for analyzing the first stages of thin-film growth by cluster deposition have been presented in detail (Sec. III). These models are useful at a fundamental level (meaning, in carefully controlled experimental conditions), and I have shown in Sec. VI how many experimental results concerning submonolayer growth can be interpreted by combining these few simple processes (deposition, diffusion, evaporation, etc.). Specifically, the experimental evolution of the island density as a function of the number of deposited particles can be compared to the predictions of computer simulations, giving quantitative information about the relevant elementary processes.

Second, the quantitative information on diffusion has shown that large clusters can move rapidly on the surface, with diffusion constants comparable to the atomic ones. A first attempt to understand this high diffusivity at the atomic level is given in Sec. VII: the conclusion is that rapid cluster diffusion might be quite common, provided the cluster and the substrate do not find an epitaxial arrangement. Concerning cluster-cluster coalescence, it has been suggested that this process might be much slower than predicted by the usual sintering theories (Nichols and Mullins, 1965; Nichols, 1966), probably because of the cluster facets.

Third, despite all the approximations involved in its derivation, Fig. 37 gives important information on the morphology of the film: an upper limit for the ratio of the size of the compact domains over the size of the incident clusters. This helps us to understand why cluster deposition leads to nanostructured films provided the deposition temperature is low compared to the fusion temperature of the material deposited ($T_s \leqslant T_f/4$). Clearly, further experimental and theoretical work is needed in order to confirm (or invalidate) Fig. 37.

It is clear that we still need to understand many aspects of the physics of cluster deposition. Possible investigation directions include the following, given in an arbitrary order. First, the coalescence of nanoparticles has yet to be understood and quantified. This is a basic question for both submonolayer and thick materials. Second, one has to characterize better the interactions between clusters and the substrate, and especially the influence of these interactions on cluster diffusion. It is also important to investigate the possible interactions between the clusters, which could dramatically affect growth. Obtaining ordered arrays of nanoparticles is a hot topic at this moment. One possibility is the pinning of clusters on surface ''defects,'' which calls for a better understanding of cluster interaction with defects. Another idea is to use the self-organization of some living organism such as bacteria to produce an ordered array on which one could arrange the clusters (see Mann, 1996, especially Chap. 5). Clearly, investigating the interaction of clusters with biological substrates is not an easy task, but it is known that practical results are not always linked to a clear understanding of the underlying mechanisms.

ACKNOWLEDGMENTS

This article could never have been written without all the experimental and theoretical work carried out in our group in Lyon and in collaboration with other groups. On the experimental side, the Center for the Study of Small Clusters (Centre pour l'Etude des Petits Agrégats) gathers researchers from solid-state physics (Département de Physique des Matériaux, DPM), the gas phase (Laboratoire de Spectrométrie Ionique et Moléculaire, LASIM), and catalysts (Institut de Recherche sur la Catalyse, IRC). I therefore acknowledge all their researchers for their help, and especially those who have done part of the research presented here: Laurent Bardotti, Michel Broyer, Bernard Cabaud, Francisco J. Cadete Santos Aires, Véronique Dupuis, Alain Hoareau, Michel Pellarin, Brigitte Prével, Alain Perez, Michel Treilleux, and Juliette Tuaillon. A post-doc year at Boston University, under the direction of Professor Stanley, gave the initial impetus for the growth models. I want to thank Gene for his warm hospitality in Boston. The theoretical work was carried out in collaboration with Jean-Louis Barrat, Pierre Deltour, and Muriel Meunier (DPM, Lyon), my friend Hernán Larralde (Instituto de Física de Cuernavaca, Mexico), Laurent Lewis (Université de Montréal, P.Q., Canada), and Alberto Pimpinelli (Université Blaise Pascal, Clermont-2, France). I am happy to thank Claude Henry (CRMC2, Marseille) and Horia Metiu (University of California) for a careful reading of the manuscript, Jean-Jacques Métois (CRMC2, Marseille) for interesting discussions, and Leo Maslíah (Instituto Uruguayo de DepreRisa) for continuous inspiration.

APPENDIX A: GROWTH OF 2D ISLANDS: REGIMES AND EXPONENTS

Regimes are predicted by rate-equation calculations for the growth of 2D islands with evaporation. These predictions agree with the computer simulations presented in this paper and are relevant for both cluster and atomic deposition (see Jensen *et al.*, 1997 for more details).

I shall here briefly review how the rate equations can be written (Jensen *et al.*, 1997), and then turn to the different regimes that can be derived from them.

The rate equation describing the time evolution of the density ρ of monomers on the surface is, to lowest relevant orders in F,

$$\frac{d\rho}{dt}=F(1-\theta)-\frac{\rho}{\tau_e}-F\rho-2\sigma_o\rho-\sigma_i N_t. \tag{A1}$$

The first term on the right-hand side denotes the flux of monomers onto the island-free surface (θ is the island coverage discussed below). The second term represents the effect of evaporation, i.e., monomers evaporate after an average time τ_e. The third term is due to the possibility of losing monomers by direct impingement of a deposited monomer right beside a monomer still on the surface, to form an island. This ''direct-impingement'' term is usually negligible and indeed will turn out to be very small in this particular equation, but the effect of direct impingement plays a crucial role in the kinetics of the system in the high-evaporation regimes. The last two terms represent the loss of monomers by aggregation with other monomers and with islands, respectively. The factors σ_o and σ_i are the ''cross sections'' for encounters and are calculated in the literature (Venables, 1973; Bales and Chrzan, 1994; Jensen *et al.*, 1997).

The number N_t of islands will be given by

$$\frac{dN_t}{dt}=F\rho+\sigma_o\rho, \tag{A2}$$

where the first term represents the formation of islands due to direct impingement of deposited monomers next to monomers already on the surface, and the second term accounts for the formation of islands by the encounter of monomers diffusing on the surface.

For the island coverage θ, i.e., the area covered by all the islands per unit area, one has

$$\frac{d\theta}{dt}=2[F\rho+\sigma_o\rho]+\sigma_i N_t+JN_t. \tag{A3}$$

The term in brackets represents the increase of coverage due to formation of islands of size 2 (i.e., formed by two monomers) either by direct impingement or by monomer-monomer aggregation. The next term gives the increase of coverage due to the growth of the islands as a result of monomers aggregating onto them by diffusion, and the last term represents the growth of the islands due to direct impingement of deposited monomers onto their boundary or directly on the island. This last term depends on X_S^*, the desorption length of monomers diffusing on top of the islands (Jensen *et al.*, 1997). In all the simulations presented in Sec. III, I have taken $X_S^*=0$. The total surface coverage is given by $\theta+\rho\sim\theta$ except at very short times.

The cross sections can be evaluated in the quasistatic approximation, which consists in assuming that R does not vary in time and that the system is at a steady state. One finds (Venables, 1973; Bales and Chrzan, 1994; Jensen *et al.*, 1997)

$$\sigma_i=2\pi RD\left(\frac{dP}{dr}\right)_{r=R}=2\pi D\rho\left(\frac{R}{X_S}\right)\frac{K_1(R/X_S)}{K_0(R/X_S)}. \tag{A4}$$

The cross section for monomer-monomer encounters σ_o is obtained from the same formula, replacing R by the monomer radius, and D by $2D$ as corresponds to relative diffusion.

After some additional approximations, one finds (Jensen *et al.*, 1997) three principal regimes, which are spanned as the evaporation time τ_e decreases. They have been called (a) the *complete condensation regime*, where evaporation is not important, (b) the *diffusion regime*, where islands grow mainly by diffusive capture of monomers, and finally, (c) the *direct-impingement regime*, where evaporation is so important that islands can grow only by capturing monomers directly from the vapor. Within each of these regimes, there are several subregimes characterized by the value of X_S^*. I use $l_{CC}\equiv(F\tau)^{-1/6}$, the island-island distance at saturation when there is no evaporation, and R_{sat} as the maximum island radius, reached at the onset of coalescence.

(1) For *complete condensation*, $X_S\gg l_{CC}$,

$$N_{sat}\sim F^{1/3}\tau^{1/3} \text{ for any } X_S^*. \tag{A5}$$

(2) For *diffusive growth*, $1\ll X_S\ll l_{CC}$,

$$N_{sat}\sim\begin{cases}(FX_S^2\tau_e)^{2/3}(X_S+X_S^*)^{-2/3} & \text{if } X_S^*\ll R_{sat} \text{ (a)}\\ F\tau_e X_S^2 & \text{if } X_S^*\gg R_{sat} \text{ (b)},\end{cases} \tag{A6}$$

with $R_{sat}\sim(X_S+X_S^*)^{1/3}(FX_S^2\tau_e)^{-1/3}$, which gives for the crossover between regimes (a) and (b): $X_S^*(crossover)\sim(FX_S^2\tau_e)^{-1/2}$.

(3) For *direct-impingement growth*, $X_S\ll 1$,

$$N_{sat}\sim\begin{cases}(F\tau_e)^{2/3} & \text{if } X_S^*\ll 1 \text{ (a)}\\ (F\tau_e)^{2/3}X_S^{*-2/3} & \text{if } 1\ll X_S^*\ll R_{sat} \text{ (b)}\\ F\tau_e & \text{if } X_S^*\gg R_{sat} \text{ (c)},\end{cases} \tag{A7}$$

with $R_{sat}\sim(F\tau_e)^{-1/3}X_S^{*1/3}$, which gives for the crossover between regimes (a) and (b): $X_S^*(crossover)\sim(F\tau_e)^{-1/2}$. As pointed out before, it is worth noting that these regimes are different from those predicted in the ''classical'' (Venables *et al.*, 1984) papers (see Jensen *et al.*, 1997).

APPENDIX B: GROWTH OF 3D ISLANDS: REGIMES AND EXPONENTS

I present here a summary of the different limits of growth of 3D islands in the presence of evaporation

and/or defects. These results are derived in detail in Jensen *et al.* (1998) from the resolution of rate equations similar to those presented in Appendix A. For each regime, I give, in order, the saturation island density N_{sat}, the thickness at saturation e_{sat} (i.e., the thickness when the island density first reaches its saturation value), the thickness at coalescence e_c (i.e., the thickness when the island density starts to decrease due to island-island coalescence), and the scaling kinetics of the mean island radius as a function of time before the saturation island density is reached. I use $l_{CC}=(F\tau)^{1/7}$ for 3D islands (Jensen *et al.*, 1998) (no defects).

(1) For high evaporation: $X_S \ll l_{CC} \ll l_{def}$,

$$N_{sat} \sim [F\tau_e(1+X_s^2)]^{2/3},$$

$$e_{sat} \sim e_c \sim [F\tau_e(1+X_s^2)]^{-1/3},$$

$$R \sim Ft.$$

(2) For low evaporation: $l_{CC} \ll X_S \ll l_{def}$ or $l_{CC} \ll l_{def} \ll X_S$,

$$N_{sat} \sim \left(\frac{F}{D}\right)^{2/7},$$

$$e_{sat} \sim e_c \sim \left(\frac{D}{F}\right)^{1/7},$$

$$R \sim (FDt^2)^{1/9} \sim t^{2/9}.$$

In the case of a dirty substrate, i.e., one with many defects,

(1) For high evaporation: $X_S \ll l_{def} \ll l_{CC}$,

$$N_{sat} \sim c,$$

$$e_{sat} \sim \frac{1}{[1+X_s^2]},$$

$$e_c \sim \frac{1}{c^{1/2}},$$

$$R \sim Ft.$$

(2) For low evaporation: $l_{def} \ll X_S \ll l_{CC}$ or $l_{def} \ll l_{CC} \ll X_S$,

$$N_{sat} \sim c,$$

$$e_{sat} \sim c,$$

$$e_c \sim \frac{1}{c^{1/2}}.$$

$R \sim (Ft/c)$ for $t \leq c/F$, i.e., before saturation.

$R \sim (Ft/c)^{1/3}$ between saturation and coalescence ($c/F \leq t \leq 1/Fc^{1/2}$).

LIST OF SYMBOLS

Principal symbols and terms used in this paper. The natural length unit in the model corresponds to the mean diameter of an incident cluster.

C_{sat}	condensation coefficient (ratio of matter actually present on the substrate over the thickness) at saturation
d	cluster diameter in nm, $d=d_0 n^{1/3}$ where d_0 depends on the element
D	Diffusion coefficient expressed in $cm^2 s^{-1}$ ($D=site/4\tau$)
e	mean thickness of the film, $e=Ft$ where t is the deposition time
F	impinging flux expressed in monolayers (or clusters per site) per second
island	structure formed on the surface by aggregation of cluster
l_{CC}	the island-island distance at saturation when there is no evaporation
ML	monolayer: the amount of matter needed to cover uniformly the substrate with one layer of cluster (1 cluster per site)
N_{sat}	saturation (maximum) island density on the surface, expressed per site
N_t	island density on the surface, expressed per site
site	area occupied by a cluster on the surface: site $=\pi d^2/4$
n	number of atoms of the cluster
X_S	mean diffusion length on the substrate before desorption: $X_S=\sqrt{D\tau_e}$
θ	coverage; fraction of the substrate covered by the clusters
ρ	density of isolated clusters on the surface, expressed per site
τ	diffusion time: mean time needed for a cluster to make a "jump" between two sites (in seconds)
τ_e	evaporation time: mean time before a monomer evaporates from the surface
ϕ	normalized flux ($\phi=F\tau$) expressed in clusters per site

REFERENCES

Adam, E., A. Chame, F. Lançon, and J. Villain, 1997, J. Phys. I **7**, 1455.

Alivisiatos, A. P., 1996, Science **271**, 933.

Allen, M. P., and D. J. Tildesley, 1987, *Computer Simulation of Liquids* (Clarendon, Oxford).

Anderson, H. H., 1997, Ed. *Small Particles and Inorganic Clusters*, Proceedings of ISSPIC 8 Copenhagen, (Springer-Verlag, Berlin).

Andres, R. P., J. D. Bielefeld, J. I. Henderson, D. B. Janes, V. R. Kolagunta, C. P. Kubiak, W. J. Mahoney, and R. G. Osifchin, 1996, Science **273**, 1690.

Arthur, J. R., 1997, in *Encyclopedia of Applied Physics*, edited by G. L. Trigg (Wiley-VCH, Weinheim, Germany), Vol 21, p. 409, and references therein. This is a short and clear introduction to this enormous field.

Averback, R. S., 1991, Ed. *Cluster and Cluster-Assembled Materials*, MRS Proceedings, Vol. 206.

Bales, G. S., and D. C. Chrzan, 1994, Phys. Rev. B **50**, 6057.

Bales, G. S., and D. C. Chrzan, 1995, Phys. Rev. Lett. **74**, 4879.

Banyai, L., and S. W. Koch, 1993, *Semiconductor Quantum Dots* (World Scientific, Singapore).

Barabási, A.-L., and H. E. Stanley, 1995, *Fractal Concepts in Surface Growth* (Cambridge University Press, Cambridge).
Bardotti, L., P. Jensen, M. Treilleux, A. Hoareau, and B. Cabaud, 1995, Phys. Rev. Lett. **74**, 4694.
Bardotti, L., P. Jensen, M. Treilleux, A. Hoareau, and B. Cabaud, 1996, Surf. Sci. **367**, 276.
Barrat, J. L., 1998 (private communication).
Bartelt, M. C., L. S. Perkins, and J. W. Evans, 1995, Surf. Sci. Lett. **344**, L1193.
Besenbacher, F., , B. S. Clausen, B. Hammer, A. Molenbroek, J. K. Noerskov, and I. Steensgaard, 1998, Science **279**, 1913.
Binder, K. 1986, Ed., *Monte Carlo Methods in Statistical Physics* (Springer, Berlin).
Binder, K., 1994, *Mechanics: Classical to Monte Carlo Methods*, in *Encyclopedia of Applied Physics* **10**, edited by G. L. Trigg (Wiley, London).
Binder, K., 1997, Rep. Prog. Phys. **60**, 487.
Biswas, R., G. S. Grest, and C. M. Soukoulis, 1988, Phys. Rev. B **38**, 8154.
Bogicevic, A., S. Liu, J. Jacobsen, B. Lundqvist, and H. Metiu, 1998, Phys. Rev. B **57**, R9459.
Bortz, A. B., M. H. Kalos, and J. L. Lebowitz, 1975, J. Comput. Phys. **17**, 10.
Bréchignac, C., Ph. Cahuzac, F. Carlier, M. de Frutos, A. Masson, C. Colliex, C. Mory, and B. Yoon, 1997, Z. Phys. D **40**, 515.
Bréchignac, C., Ph. Cahuzac, F. Carlier, C. Colliex, C. Mory, M. de Frutos, A. Masson, and B. Yoon, 1998, Phys. Rev. B **57**, R2084.
Brune, H., and K. Kern, 1997, "Heteroepitaxial metal growth: the effects of strain" in *Growth and Properties of Ultrathin Epitaxial Layers*, edited by D. A. King and D. P. Woodruff, The Chemical Physics of Solid Surfaces, Vol. 8 (Elsevier, Amsterdam), p.149.
Brune, H., H. Röder, C. Boragno, and K. Kern, 1994, Phys. Rev. Lett. **73**, 1955.
Brune, H., *et al.*, 1995, Phys. Rev. B **52**, R14 380.
Brune, H., 1998, Surf. Sci. Rep. **31**, 121.
Buffat, Ph., and J-P. Borel, 1976, Phys. Rev. A **13**, 2287.
Bunshah, R. F., 1994, *Handbook of Deposition Technologies for Films and Coatings*, 2nd ed., (Noyes, Park Ridge, New Jersey).
Canning, A., G. Galli, and J. Kim, 1997, Phys. Rev. Lett. **78**, 4442.
Carroll, S. J., S. G. Hall, R. E. Palmer, and R. Smith, 1998, Phys. Rev. Lett. **81**, 3715.
Celino, M., G. D'Agostino, and V. Rosato, 1993, Phys. Rev. B **48**, 22.
Celino, M., G. D'Agostino, and V. Rosato, 1995, Mater. Sci. Eng., A **204**, 101.
Chang, S.-L., and P. A. Thiel, 1994, Crit. Rev. Surf. Chem. **3**, 239.
Che, M., and C. O. Benett, 1989, Adv. Catal. **36**, 55.
Cheng, H.-P., and U. Landman, 1993, Science **260**, 1304.
Cho, A. Y., 1994, *Molecular Beam Epitaxy* (American Institute of Physics, New York).
Chrzan, D. C., and M. S. Daw, 1997, Phys. Rev. B **55**, 798.
Combe, N., and P. Jensen, 1998, Phys. Rev. B **57**, 15 553.
Combe, N., P. Jensen, A. Pimpinelli, and C. Misbah, 1998, unpublished.
Dadybujor, D. B., S. P. Marsh, and M. E. Glicksman, 1986, J. Catal. **99**, 358.
de Heer, W., 1993, Rev. Mod. Phys. **65**, 611.
Deltour, P., P. Jensen, and J-L. Barrat, 1997, Phys. Rev. Lett. **78**, 4597.
Dos Santos Aires, F., 1990, Ph.D. thesis (University of Lyon).
Dreschler, M., J. J. Métois, and J. C. Heyraud, 1981, Surf. Sci. **108**, 549.
Eaglesham, D. J., and M. Cerullo, 1990, Phys. Rev. Lett. **64**, 1943.
Edelstein, A. S., and R. C. Cammarata, 1996, Eds., *Nanomaterials: Synthesis, Properties and Applications*, (IOP, Bristol).
Evans, J. W., and M. C. Bartelt, 1994, J. Vac. Sci. Technol. A **12**, 1800.
Evans, J. W., and M. C. Bartelt, 1996, Phys. Rev. B **54**, R17 359.
Evans, J. W., and M. C. Bartelt, 1997, in *Directions in Condensed Matter Physics*, edited by Z. Zhang and M. Lagally (World Scientific, New York).
Fecht, H. J., 1997, Europhys. News **28**(3), 89.
Fendler, J. H., 1998, Ed., *Nanoparticles and Nanostructured Films* (Wiley-VCH, Weinheim, Germany,).
Flüelli, M., P. A. Buffat, and J. P. Borel, 1988, Surf. Sci. **202**, 343.
Foiles, S. M., M. I. Baskes, and M. S. Daw, 1986, Phys. Rev. B **33**, 7983.
Francis, G. M., I. M. Goldby, L. Kuipers, B. von Issendorff, and R. E. Palmer, 1996, J. Chem. Soc. Dalton Trans. **1**, 665.
Frenkel, D., and B. Smit, 1996, *Understanding Molecular Simulation* (Academic, New York).
Frenkel, J., and T. Kontorova, 1938, Phys. Z. Sowjetunion **13**, 1.
Freund, H. J., 1997, Angew. Chem. Int. Ed. **36**, 452.
Fuchs, G., P. Melinon, F. Dos Santos Aires, M. Treilleux, B. Cabaud, and A. Hoareau, 1991, Phys. Rev. B **44**, 3926.
Furman, I., and O. Biham, 1997, Phys. Rev. B **55**, 7917.
Ganz, E., K. Sattler, and J. Clarke, 1989, Surf. Sci. **219**, 33.
Gleiter, H., 1992, Nanostruct. Mater. **1**, 1.
Glocker, D. A., 1995, *Handbook of Thin Film Process Technology* (IOP, Bristol/Philadelphia).
Goldby, I. M., L. Kuipers, B. von Issendorff, and R. E. Palmer, 1996, Appl. Phys. Lett. **69**, 2819.
Gomer, R., 1990, Rep. Prog. Phys. **53**, 917.
Granqvist, C. G., and R. A. Buhrman, 1976, J. Appl. Phys. **47**, 2200.
Gunter, P. L. J., J. W. H. Niemantsverdriet, T. H. Ribeiro, and G. A. Somorjai, 1997, Catal. Rev. Sci. Eng. **39**, 77.
Haberland, H., M. Karrais, M. Mall, and Y. Thurner, 1992, J. Vac. Sci. Technol. A **10**, 3266.
Haberland, H., Z. Insepov, and M. Moseler, 1995, Phys. Rev. B **51**, 11 061.
Hadjiapanayis, C., and R. W. Siegel, 1994, Eds., *Nanophase Materials: Synthesis-Properties-Applications*, NATO Adv. Study Inst. Ser., Ser. E **260** (Nijhoff, Dordrecht).
Hagena, O. F., 1992, Rev. Sci. Instrum. **63**, 2374.
Hagena, O. F., G. Knop, R. Fromknecht, and G. Linker, 1994, J. Vac. Sci. Technol. A **12**, 282.
Hamilton, J. C., 1996, Phys. Rev. Lett. **77**, 885.
Hamilton, J. C., M. S. Daw, and S. M. Foiles, 1995, Phys. Rev. Lett. **74**, 2760.
Hamilton, J. C., 1997, Phys. Rev. B **55**, R7402.
Harsdorff, M., 1984, Thin Solid Films **116**, 55.
Haug, K., Z. Zhang, D. John, C. F. Walters, D. M. Zehner, and W. E. Plummer, 1997, Phys. Rev. B **55**, R10 233.
Hautman, J., and M. L. Klein, 1991, Phys. Rev. Lett. **67**, 1763.

Henry, C. R., C. Chapon, and B. Mutaftschiev, 1976, Thin Solid Films **33**, 1.
Henry, C. R., and M. Meunier, 1996, Mater. Sci. Eng., A **217/218**, 239.
Henry, C. R., C. Chapon, S. Giorgio, and C. Goyhenex, 1997, in *Chemistry and Reactivity of Clusters and Thin Films*, edited by R. M. Lambert and G. Pacchioni, NATO Adv. Study Inst. Ser., Ser. E (Kluwer, Boston), **31**, 117.
Henry, C. R., 1998, Surf. Sci. Rep. **31**, 231.
Herman, M. A., and H. Sitter, 1989, *Molecular Beam Epitaxy* (Springer, Berlin).
Herrmann, H. J., 1986, Phys. Rep. **136**, 153.
Heyraud, J. C., J. J. Métois, and J. M. Bermond, 1989, J. Cryst. Growth **98**, 355.
Hou, M., 1998, Nucl. Instrum. Methods Phys. Res. B **135**, 501.
Ibach, H., 1997, Surf. Sci. Rep. **29**, 193.
Insepov, Z., and I. Yamada, 1995, Nucl. Instrum. Methods Phys. Res. B **99**, 248.
Jacobs, P. W., S. J. Wind, F. H. Ribeiro, and G. A. Somorjai, 1997, Surf. Sci. **372**, L249.
Jeffers, G., M. A. Dubson, and P. M. Duxbury, 1994, J. Appl. Phys. **75**, 5016.
Jena, P. *et al.*, 1996, in *Cluster Assembled Materials*, edited by K. Sattler, Materials Science Forum **232** (Trans Tech Publications Zurich, Switzerland), p. 1.
Jena, P., and S. N. Khanna, 1996, Mater. Sci. Eng., A **217/218**, 218.
Jensen, P., A.-L. Barabási, H. Larralde, S. Havlin, and H. E. Stanley, 1994a, Nature (London) **368**, 22.
Jensen, P., A.-L. Barabási, H. Larralde, S. Havlin, and H. E. Stanley, 1994b, Phys. Rev. B **50**, 15 316.
Jensen, P., A.-L. Barabási, H. Larralde, S. Havlin, and H. E. Stanley, 1994c, Physica A **207**, 219.
Jensen, P., L. Bardotti, A.-L. Barabási, H. Larralde, S. Havlin, and H. E. Stanley, 1995, *Disordered Materials and Interfaces*, Proc. Symposium of Materials Research Society, edited by H. Z. Cummins, D. J. Durian, D. L. Johnson, and H. E. Stanley (Materials Research Society, Pittsburgh), p. 391.
Jensen, P., A.-L. Barabási, H. Larralde, S. Havlin, and H. E. Stanley, 1996, Fractals **4**, 321.
Jensen, P., 1996, La Recherche **283**, 42.
Jensen, P., and B. Niemeyer, 1997, Surf. Sci. Lett. **384**, 823.
Jensen, P., H. Larralde, and A. Pimpinelli, 1997, Phys. Rev. B **55**, 2556. Note that in this paper, a mistake was made in the normalization of the island size distributions (Fig. 9).
Jensen, P., 1998a, Comments At. Mol. Phys. **34**(3–6), 297.
Jensen, P., 1998b (unpublished).
Jensen, P., M. Meunier, H. Larralde, and A. Pimpinelli, 1998, Surf. Sci. **412-413**, 458.
Jensen, P., N. Combe, H. Larralde, J. L. Barrat, C. Misbah, and A. Pimpinelli, 1999, Eur. J. Phys. B **11**, 497.
Joyes, P., 1990, *Les agrégats inorganiques élémentaires* (Ed. de Physique, Paris).
Kalff, M., G. Comsa, and T. Michely, 1998, Phys. Rev. Lett. **81**, 1255.
Kang, H. C., and W. H. Weinberg, 1989, J. Chem. Phys. **90**, 2824.
Kay, E., 1986, Z. Phys. D **3**, 251.
Kelchner, C. L., and A. E. De Pristo, 1997, Nanostruct. Mater. **8**, 253.
Kellogg, G. L., 1994a, Phys. Rev. Lett. **73**, 1833.
Kellogg, G. L., 1994b, Surf. Sci. Rep. **21**, 1.
Kern, R., G. Le Laye, and J. J. Métois, 1979, *Current Topics in Materials Science* (North Holland, New York), Vol. 3, Chap. 3.
Khare, S. V., and T. L. Einstein, 1996, Phys. Rev. B **54**, 11 752.
Khare, S. V., N. C. Bartelt, and T. L. Einstein, 1995, Phys. Rev. Lett. **75**, 2148.
Koch, C. C., 1991, in *Materials Science and Technology*, edited by R. W. Cahn (VCH, Weinheim, Germany), Vol. 15, p. 584.
Kolb, M., R. Botet, and R. Jullien, 1983, Phys. Rev. Lett. **51**, 1123.
Kuipers, L., and R. E. Palmer, 1996, Phys. Rev. B **53**, R7646.
Kuo, L. Y., and P. Shen, 1997, Surf. Sci. Lett. **373**, L350.
Lagally, M., 1993, Phys. Today **46**(11), 24, and references therein.
Larralde, H., P. Jensen, M. Meunier, and A. Pimpinelli, 1997, in *Proceedings of the Materials Research Society, Fall Meeting*, Boston, 1996.
Lennard-Jones, J. E., 1924, Proc. R. Soc. London, Ser. A **106**, 463.
Leonard, D., M. Krishnamurthy, C. M. Reaves, S. P. Denbaars, and P. M. Petroff, 1993, Appl. Phys. Lett. **63**, 23.
Lewis, B., and J. C. Anderson, 1978, in *Nucleation and Growth of Thin Films* (Academic, New York).
Lewis, L., P. Jensen, and J-L. Barrat, 1997, Phys. Rev. B **56**, 2248.
Lewis, L., P. Jensen, and J-L. Barrat, 1999 (unpublished).
Linderoth, T. R., J. J. Mortensen, K. W. Jacobsen, E. Laegsgaard, I. Stensgaard, and F. Besenbacher, 1996, Phys. Rev. Lett. **77**, 87.
Liu, S., Z. Zhang, J. Norskov, and H. Metiu, 1994, Surf. Sci. **321**, 161.
Liu, S., L. Bönig, and H. Metiu, 1995a, Phys. Rev. B **52**, 2907.
Liu, S., L. Bönig, J. Detch, and H. Metiu, 1995b, Phys. Rev. Lett. **74**, 4495, and references therein.
Luedtke, W. D., and U. Landman, 1991, J. Vac. Sci. Technol. B **9**, 414.
Luedtke, W. D., and U. Landman, 1994, Phys. Rev. Lett. **73**, 569.
Luedtke, W. D. and U. Landman, 1999, Phys. Rev. Lett. **82**, 3835.
Ma, J. X., M. Han, H. Q. Zhang, Y. C. Gong, and G. H. Wang, 1994, Appl. Phys. Lett. **65**, 1513.
Mann, S., 1996, Ed., *Biomimetic Materials Chemistry* (VCH Publishers, New York).
Massobrio, C., and B. Nacer, 1997, Z. Phys. D **40**, 526, and references therein.
Masson, A., J. J. Métois, and R. Kern, 1971, Surf. Sci. **27**, 463.
Mater. Res. Soc. Bulletin, 1996a, **21** (2), special edition on interatomic potentials for atomistic simulations.
Mater. Res. Soc. Bulletin, 1996b, **21**(4), special edition on heteroepitaxy and strain.
Mater. Res. Soc. Bulletin, 1998, **23**(2), special edition on semiconductor quantum dots.
Matthews, J. W., and E. Grünbaum, 1966, J. Vac. Sci. Technol. **3**, 133.
McEachern, R. L., W. L. Brown, M. F. Jarrold, M. Sosnowski, G. Takaoka, H. Usui, and I. Yamada, 1991, J. Vac. Sci. Technol. A **9**, 3105.
Meakin, P., 1983, Phys. Rev. Lett. **51**, 1119.
Melinon, P., P. Jensen, J. Hu, A. Hoareau, B. Cabaud, and D. Guillot, 1991, Phys. Rev. B **44**, 12 562.

Melinon, P., V. Paillard, V. Dupuis, A. Perez, P. Jensen, A. Hoareau, J. P. Perez, J. Tuaillon, M. Broyer, J. L. Vialle, M. Pellarin, B. Baguenard, and J. Lerme, 1995, Int. J. Mod. Phys. B **9**, 339.

Métois, J. J., K. Heinemann, and H. Poppa, 1977, Philos. Mag. **35**, 1413.

Métois, J. J., and J. C. Heyraud, 1981, Thin Solid Films **75**, 1.

Metropolis, N., A. W. Rosenbluth, M. N. Rosenbluth, A. H. Teller, and E. Teller, 1953, J. Chem. Phys. **21**, 1087.

Meunier, M., and C. R. Henry, 1994, Surf. Sci. **307**, 514.

Meunier, M., 1995, Ph.D. thesis (Université Aix-Marseille).

Michely, T., M. Hohage, M. Bott, and G. Comsa, 1993, Phys. Rev. Lett. **70**, 3943.

Milani, P., and W. A. deHeer, 1990, Rev. Sci. Instrum. **61**, 147.

Moison, J. M., F. Houzay, F. Barthe, L. Leprince, E. Andre, and O. Vatel, 1994, Appl. Phys. Lett. **64**, 196.

Mottet, C., R. Ferrando, F. Hontinfinde, and A. C. Levi, 1998, Surf. Sci. **417**, 220.

Mullins, W. W., 1957, J. Appl. Phys. **28**, 333.

Nichols, F. A., and W. W. Mullins, 1965, J. Appl. Phys. **36**, 1826.

Nichols, F. A., 1966, J. Appl. Phys. **37**, 2805.

Nieman, G. W., J. R. Weertman, and R. W. Siegel, 1991, J. Mater. Res. **6**, 1012.

Nosho, B. Z., V. Bressler-Hill, S. Varma, and W. H. Weinberg, 1996, Surf. Sci. **364**, 164.

Pacchioni, G., and N. Roesch, 1994, Surf. Sci. **306**, 169.

Pai, W. W., A. K. Swan, Z. Zhang, and J. F. Wendelken, 1997, Phys. Rev. Lett. **79**, 3210.

Paillard, V., P. Melinon, J. P. Perez, V. Dupuis, A. Perez, and B. Champagnon, 1993, Phys. Rev. Lett. **71**, 4170.

Palmer, R. E., 1997 New Sci. **2070**, 38.

Palpant, B., B. Prevel, J. L. Lerme, E. Cottencin, M. Pellarin, M. Treilleux, A. Perez, J. L. Vialle, and M. Broyer, 1998, Phys. Rev. B **57**, 1963.

Pascual, J. J., J. Méndez, J. Gomez-Herrero, A. M. Baro, N. Garcia, and V. T. Binh, 1993, Phys. Rev. Lett. **71**, 1852.

Perez, J. P., V. Dupuis, J. Tuaillon, A. Perez, V. Paillard, P. Melinon, M. Treilleux, L. Thomas, B. Barbara, and B. Bouchet-Fabre, 1995, J. Magn. Magn. Mater. **145**, 74.

Perez, A., P. Melinon, V. Dupuis, P. Jensen, B. Prevel, J. Tuaillon, L. Bardotti, C. Martet, M. Treilleux, M. Broyer, M. Pellarin, J.l. Vialle, and B. Palpant, 1997, J. Phys. D **30**, 709.

Phys. Today (Special edition), 1990 (February), special edition on Optics of nanostructures.

Phys. Today (Special edition), 1993 (June), special edition on nanoscale and ultrafast devices.

Pimpinelli, A., J. Villain, and D. E. Wolf, 1993, J. Phys. I **3**, 447.

Pimpinelli, A., P. Peyla, P. Jensen, and H. Larralde, 1997, in *Directions in Condensed Matter Physics* edited by Z. Zhang and M. Lagally (World Scientific, Singapore).

Pimpinelli, A., and J. Villain, 1998, *Physics of Crystal Growth* (Cambridge University Press, Cambridge).

Ratsch, C., A. Zangwill, and P. Smilauer, 1994, Surf. Sci. **314**, L937.

Ratsch, C., P. Smilauer, A. Zangwill, and D. D. Vvedensky, 1995, Surf. Sci. Lett. **329**, L599.

Ratsch, C., and M. Scheffler, 1998, Phys. Rev. B **58**, 13 163.

Ray, C., M. Pellarin, J. L. Lermé, J. L. Vialle, M. Broyer, X. Blase, P. Melinon, P. Kéghélian, and A. Perez, 1998, Phys. Rev. Lett. **80**, 5365.

Rayane, D., P. Melinon, B. Tribollet, B. Cabaud, A. Hoareau, and M. Broyer, 1989, J. Chem. Phys. **91**, 3100.

Reiss, H., 1968, J. Appl. Phys. **39**, 5045.

Robins, J. L., and T. N. Rhodin, 1964, Surf. Sci. **2**, 346.

Rousset, J. L., A. M. Cadrot, F. J. Cadete Santos Aires, A. Renouprez, P. Melinon, A. Perez, M. Pellarin, J. L. Vialle, and M. Broyer, 1995, J. Chem. Phys. **102**, 8574.

Rousset, J. L., B. C. Khanra, A. M. Cadrot, F. J. Cadete Santos Aires, A. Renouprez, and M. Pellarin, 1996, Surf. Sci. **352–354**, 583.

Roux, J. F., B. Cabaud, G. Fuchs, D. Guillot, A. Hoareau, and P. Melinon, 1994, Appl. Phys. Lett. **64**, 1212.

Roux, J. F., L. Bardotti, B. Cabaud, M. Treilleux, P. Jensen, and A. Hoareau, 1997, Mater. Sci. Eng., B **49**, 110.

Rubinstein, E., 1996, Ed., Science **271**, 920.

Ruckenstein, E., and B. Pulvermacher, 1973, J. Catal. **29**, 224.

Samy El-Shall, M., and A. S. Edelstein, in *Nanomaterials: Synthesis, Properties, and Applications*, edited by A. S. Edelstein and R. C. Cammarata (IOP, Bristol), Chap. 2.

Sattler, K., J. Muhlbach, and E. Recknagel, 1980, Phys. Rev. Lett. **45**, 821.

Sattler, K., 1996, Ed., *Cluster Assembled Materials*, Mater. Sci. Forum **232** (Trans Tech Publications, Zurich, Switzerland).

Schaefer, D. M., A. Patil, R. P. Andres, and R. Reifenberger, 1995, Phys. Rev. B **51**, 5322.

Schiotz, J., T. Rasmussen, K. W. Jacobsen, and O. H. Nielsen, 1996, Philos. Mag. Lett. **74**, 339.

Schiotz, J., F. D. Di Tolla, and K. W. Jacobsen, 1998, Nature (London) **391**, 561.

Schroeder, M., and D. E. Wolf, 1997, Surf. Sci. **375**, 129.

Schroeder, M., P. Smilauer, and D. E. Wolf, 1997, Phys. Rev. B **55**, 10 814.

Schweber, S. S., 1993, Physics Today (November), p. 34.

Schwoebel, R. L., and E. J. Shipsey, 1966, J. Appl. Phys. **37**, 3682.

Schwoebel, R. L., 1969, J. Appl. Phys. **40**, 614.

Science, 1996, Special issue on clusters, Science **271**, 920.

Selke, W., and P. M. Duxbury, 1994, Z. Phys. B **94**, 311.

Shalaev, V. M., and M. Moskovits, 1997, Eds., *Nanostructured Materials: Clusters, Composites and Thin Films*, ACS Symposium series **679** (American Chemical Society Editions, Washington DC).

Shao, H., P. C. Weakliem, and H. Metiu, 1996, Phys. Rev. B **53**, 16 041.

Shi, Z. P., A. K. Swan, Z. Zhang, and J. F. Wendelken, 1996, Phys. Rev. Lett. **76**, 4927.

Shitara, T., D. D. Vvedensky, M. R. Wilby, J. Zhang, J. H. Neave, and B. A. Joyce, 1992, Phys. Rev. B **46**, 6825.

Sholl, D. S., and R. T. Skodje, 1995, Phys. Rev. Lett. **75**, 3158.

Siegel, R. W., 1991, in *Materials Science and Technology*, edited by R. W. Cahn (VCH, Weinheim, Germany), Vol. 15, p. 584.

Siegel, R. W., 1996, in *Nanomaterials: Synthesis, Properties, and Applications*, edited by A. S. Edelstein and R. C. Cammarata (IOP, Bristol).

Smoluchovsky, M., 1916, Phys. Z. **17**, 557; 585.

Soler, J. M., 1996, Phys. Rev. B **53**, R10 540.

Springholz, G., V. Holy, M. Pinczoltis, and G. Bauer, 1998, Science **282**, 734.

Stauffer, D., and A. Aharony, 1992, *Introduction to Percolation Theory*, 2nd edition, (Taylor and Francis, London).

Stevenson, S. A., J. A. Dumesic, R. T. K. Baker, and E. Ruckenstein, 1987, *Metal-Support Interactions in Catalysis, Sitering and Redispersion* (Van Nostrand Reinhold, New York).
Stoldt, C. R., A. M. Cadilhe, C. J. Jenks, J.-M. Wen, J. W. Evans, and P. A. Thiel, 1998, Phys. Rev. Lett. **81**, 2950.
Stoyanov, S., and D. Kaschiev, 1981, in *Current Topics in Materials Science*, edited by E. Kaldis (North-Holland, Amstudam), Vol. 7, p. 69.
Stroscio, J. A., and D. T. Pierce, 1994, J. Vac. Sci. Technol. B **12**, 1783.
Sugano, S., Y. Nishina, and S. Ohnishi, 1987, Eds. *Microclusters*, Springer Series in Materials Science **4** (Springer, Berlin).
Suzuki, K., Y. Nishina, A. Kasuya, and K. Sumiyama, 1996, Eds., Mater. Sci. Eng., A **217/218** (Proceedings of the International Conference on Nanoclusters and Granular Materials).
Tang, L.-H., 1993, J. Phys. I **3**, 935.
Treilleux, M., 1999 (in preparation).
Tuaillon, J., 1995 Ph.D. thesis (Université de Lyon).
Tuaillon, J., V. Dupuis, P. Melinon, B. Prevel, M. Treilleux, A. Perez, M. Pellarin, J. L. Vialle, and M. Broyer, 1997, Philos. Mag. A **76**, 493.
Turner, D., and H. Shanks, 1991, J. Appl. Phys. **70**, 5385.
Turton, R., 1995, *The Quantum Dot* (Freeman, San Francisco).
Valkealahti, S., and M. Manninen, 1998, Phys. Rev. B **57**, 15 533.
Van Siclen, C. deW., 1995, Phys. Rev. Lett. **75**, 1574.
Vandoni, G., C. Felix, R. Monot, J. Buttet, and W. Harbich, 1994, Chem. Phys. Lett. **229**, 51.
Venables, J. A., 1973, Philos. Mag. **27**, 697.
Venables, J. A., G. D. T. Spiller, and M. Hanbucken, 1984, Rep. Prog. Phys. **47**, 399.
Vialle, J. L., B. Baguenard, A. Bourgey, E. Cottancin, J. Lerme, B. Palpant, M. Pellarin, F. Valadier, and M. Broyer, 1997, Rev. Sci. Instrum. **68**, 2312.
Villain, J., 1991, J. Phys. I **1**, 19.
Villain, J., A. Pimpinelli, L.-H. Tang, and D. E. Wolf, 1992, J. Phys. I **2**, 2107.
Villain, J., A. Pimpinelli, and D. E. Wolf, 1992, Comments Condens. Matter Phys. **16**, 1.
Villain, J., and A. Pimpinelli, 1995, *Physique de la Croissance Cristalline* (Eyrolles, Saclay) (for the English edition with many additions, see Pimpinelli and Villain, 1998).
Vitomirov, I. M., C. M. Aldao, G. D. Waddill, C. Capasso, and J. H. Weaver, 1990, Phys. Rev. B **41**, 8465.
Voter, A. F., 1986, Phys. Rev. B **34**, 6819.
Wang, G. H., H. Q. Zhang, M. Han, J. X. Ma, and Q. Wang, 1994, Phys. Lett. A **189**, 218.
Wang, S. C., and G. Ehrlich, 1997, Phys. Rev. Lett. **79**, 4234.
Wang, S. C., U. Kürpick, and G. Ehrlich, 1998, Phys. Rev. Lett. **81**, 4923.
Wawro, A., R. Czajka, A. Kasuya, and Y. Nishina, 1996, Surf. Sci. **365**, 503.
Weertman, J. R., and R. S. Averback, 1996, in *Nanomaterals; Synthesis Properties and Applications*, edited by A. S. Edelstem and R. C. Cammarata (IOP, Bristol).
Weisbuch, C., and B. Binter, 1991, *Quantum Semiconductor Structures* (Academic Press, New York).
Wen, J. M., S. L. Chang, J. W. Burnett, J. W. Evans, and P. A. Thiel, 1994, Phys. Rev. Lett. **73**, 2591.
Wen, J. M., S. L. Chang, J. W. Burnett, J. W. Evans, and P. A. Thiel, 1996, Phys. Rev. Lett. **76**, 562.
Xiao, X., Y. Xie, C. Jakobsen, and Y. R. Shen, 1997, Phys. Rev. B **56**, 12 529, and references therein.
Yamada, I., H. Inokawa, and T. Takagi, 1984, J. Appl. Phys., Part 1 **56**, 2746.
Yamada, I., and G. H. Takaoka, 1993, Jpn. J. Appl. Phys., Part 1 **32**, 2121, and references therein.
Yamada, I., 1996, Mater. Sci. Eng., A **217/218**, 82.
Yoon, B., 1997, Ph.D. thesis (University of Orsay).
Yu, X., and P. M. Duxbury, 1995, Phys. Rev. B **52**, 2102.
Zanghi, J. C., J. J. Métois, and R. Kern, 1975, Philos. Mag. **31**, 743.
Zhang, Z., and M. G. Lagally, 1997, Science **276**, 377.
Zhdanov, V. P., and P. R. Norton, 1994, Appl. Surf. Sci. **81**, 109.
Zhu, H., and R. S. Averback, 1995, Mater. Sci. Eng., A **204**, 96.
Zhu, H., and R. S. Averback, 1996, Philos. Mag. Lett. **73**, 27.
Zinke-Allmang, M., L. C. Feldman, and M. H. Grabow, 1992, Surf. Sci. Rep. **16**, 377.
Zinsmeister, G., 1966, Vacuum **16**, 529.
Zinsmeister, G., 1968, Thin Solid Films **2**, 497.
Zinsmeister, G., 1969, Thin Solid Films **4**, 363.
Zinsmeister, G., 1971, Thin Solid Films **7**, 51.